

For Reference

NOT TO BE TAKEN FROM THIS ROOM

Ex libris
UNIVERSITATIS
ALBERTAENSIS



T H E U N I V E R S I T Y O F A L B E R T A

RELEASE FORM

NAME OF AUTHOR Abdelazim A. Soliman
TITLE OF THESIS Sputtered Thin Film Semiconducting Photoelectrodes
..... for Solar/Hydrogen Energy Conversion
.....
DEGREE FOR WHICH THESIS WAS PRESENTED Doctor of Philosophy
YEAR THIS DEGREE GRANTED Fall 1981

Permission is hereby granted to THE UNIVERSITY OF
ALBERTA LIBRARY to reproduce single copies of this thesis
and to lend or sell such copies for private, scholarly
or scientific research purposes only.

The author reserves other publication rights, and
neither the thesis nor extensive extracts from it may be
printed or otherwise reproduced without the author's written
permission.

THE UNIVERSITY OF ALBERTA

SPUTTERED THIN FILM SEMICONDUCTING PHOTOELECTRODES
FOR SOLAR/HYDROGEN ENERGY CONVERSION

by



ABDELAZIM A. SOLIMAN

A THESIS

SUBMITTED TO THE FACULTY OF GRADUATE STUDIES AND RESEARCH
IN PARTIAL FULFILLMENT OF THE REQUIREMENTS FOR THE DEGREE
OF DOCTOR OF PHILOSOPHY

DEPARTMENT OF ELECTRICAL ENGINEERING

EDMONTON, ALBERTA

FALL, 1981

THE UNIVERSITY OF ALBERTA
FACULTY OF GRADUATE STUDIES AND RESEARCH

The undersigned certify that they have read, and recommend to the Faculty of Graduate Studies and Research, for acceptance, a thesis entitled SPUTTERED THIN FILM SEMICONDUCTING PHOTOELECTRODES FOR SOLAR/HYDROGEN ENERGY CONVERSION submitted by ABDELAZIM A. SOLIMAN in partial fulfillment of the requirements for the degree of Doctor of Philosophy.

DEDICATION

To the memory of my mother and my brother.

ABSTRACT

The deposition system and parameters for sputter-depositing crystalline thin film semiconducting TiO_2 electrodes for water photo-electrolysis are described. Also the sputtering target fabrication procedure is briefly explained.

Results of primary investigations on TiO_2 film deposition using dc sputtering, rf sputtering and plasma anodization techniques are presented. In addition, a detailed description of a semiconducting TiO_2 electrode fabrication process is presented. The results of investigating the behavior of these electrodes in photoelectrochemical cells are given.

Kinetics of film growth during reactive sputtering of a Ti metal target are investigated. Results of the effect of oxygen partial pressure on film deposition rate, film crystalline structure, and optical properties are illustrated. A simple procedure for forming an abrupt doping level change in a very narrow region at the back surface of a semiconducting electrode is presented.

A model for the photoexcited semiconductor electrode that shows how the semiconductor is expected to behave as a function of the different physical parameters of the semiconductor is developed. The model lays particular emphasis on the effect of built-in drift fields caused by impurity gradients, takes into account the effect of surface reaction parameters at the semiconductor/electrolyte interface and includes the effect of nonuniform doping on the depletion region width.

Computer simulations of the developed model for the semiconducting TiO_2 electrodes are carried out and the results are presented.

A possibility for improvement of the photoresponse of a TiO_2 electrode utilizing different doping approaches are primarily investigated and absorption spectra for the doped samples are given.

ACKNOWLEDGEMENT

It is very difficult to express in words my gratitude and appreciation to my supervisor, Dr. H.J.J. Seguin. To me, his individual character, his encouraging attitude and sensitivity were the motivating forces behind the achievement of this work. Without his supervision, encouragement and support, especially during some very critical times where his support was most needed, this work could not have been accomplished. I most gratefully acknowledge him.

The encouragement, the enthusiasm, the sincerity and the efforts of my dear friend, Georgina French, throughout the course of this study, along with her excellent typing of the papers and this thesis are greatly appreciated.

I would also like to express my appreciation to the following people.

Dr. F. Weichman for his helpful discussions.

Steven Au for his help in the computer work.

The staff of the machine shop headed by Konrad Doerrbecker for their excellent service and workmanship.

The staff of the glass shop headed by Peter for their excellent work.

Steven Xu, Linda Haswell and the Graphic and Photo Services for their excellent drawings.

Roy Schamus, Jim Radizion, Jim Dow and Barry Arnold for their technical assistance.

The secretarial staff of the Department and in particular, Barbara Galliaford.

I also wish to thank N.S.E.R.C. and the Imperial Oil Corporation for their financial support.

TABLE OF CONTENTS

	PAGE
CHAPTER 1 INTRODUCTION	1
1.1 STIMULUS FOR THE INVESTIGATION	1
1.2 BASIC PROCESSES AT SEMICONDUCTOR ELECTRODES	3
1.2.1 Redox Reactions and Energy Levels	3
1.3 THE SEMICONDUCTOR/ELECTROLYTE INTERFACE	5
1.3.1 The Semiconductor Electrode under Illumination	7
1.4 DRIVING FORCE FOR WATER PHOTOELECTROLYSIS	9
1.5 PHOTODECOMPOSITION OF SEMICONDUCTOR ELECTRODES	10
1.6 CELLS FOR WATER PHOTOELECTROLYSIS	16
1.7 THIN FILM APPROACH	19
1.8 PRESENT WORK	21
CHAPTER 2 THE SPUTTERING TECHNIQUE AND THE FABRICATION SYSTEM	23
2.1 INTRODUCTION	23
2.2 BASIC CONSIDERATIONS	24
2.3 LOW PRESSURE SPUTTERING	25
2.3.1 The Sputtering Process in a Triode Sputtering System	25
2.4 THE DEPOSITION SYSTEM DEVELOPED	29
2.4.1 Gas Introduction System	29
2.4.2 Pressure Measurement	32
2.4.3 Anode	33
2.4.4 Filaments	33
2.4.5 Electromagnets	34
2.4.6 Substrate Table	35
2.4.7 Target Shield	36

	PAGE
2.4.8 Chamber Shields	36
2.4.9 Probe	38
2.4.10 Target Changing Assembly and Procedure	38
2.5 SPUTTERING TARGET PRESS	41
CHAPTER 3 FABRICATION OF SEMICONDUCTING TiO_2 ELECTRODES BY dc SPUTTERING FROM A TiO_2 TARGET	44
3.1 PRIMARY INVESTIGATIONS	44
3.1.1 Deposition Parameters	44
3.1.2 dc Sputtering from a TiO_2 Target	45
3.1.3 rc Sputtering of TiO_2	45
3.1.4 Plasma Anodization of a Predeposited Titanium Layer	46
3.2 ELECTRODE FABRICATION BY SPUTTERING FROM A REDUCED TiO_2 TARGET	48
3.2.1 Introduction	48
3.2.2 Experimental	49
3.2.3 Measurements	51
3.3 RESULTS	51
3.3.1 Cell Photoresponse	56
3.3.2 Effect of Light Intensity	58
3.3.3 Flat Band Potential	61
3.4 CONCLUSION	63
CHAPTER 4 REACTIVE SPUTTERING AND ITS APPLICATION FOR FABRICATING THIN FILM SEMICONDUCTING TiO_2 ELECTRODES	65
4.1 INTRODUCTION	65
PART I	
4.2 MECHANISM OF REACTIVE SPUTTERING	66

	PAGE
4.2.1 Target Oxidation and Deposition Rate	67
4.3 EXPERIMENTAL	68
4.4 RESULTS	69
4.5 DISCUSSION	69
PART II	
4.6 REACTIVELY SPUTTERED LAYERED n^+/n SEMICONDUCTING TiO_2 FILMS FOR WATER PHOTOELECTROLYSIS	76
4.6.1 Cell Fabrication	76
4.7 RESULTS AND DISCUSSION	77
4.7.1 Photoresponse of BSF Reactively Sputtered Electrodes	82
4.7.2 Effect of Light Intensity	85
4.8 CONCLUSION	87
CHAPTER 5 MODELLING OF THE PHOTOEXCITED SEMICONDUCTOR ELECTRODE	89
5.1 INTRODUCTION	89
5.2 THE SEMICONDUCTOR ELECTRODE MODEL	90
5.3 MATHEMATICAL ANALYSIS	92
5.4 VOLTAGE DEPENDENCE OF PHOTOCURRENT	99
5.4.1 Dependence of the Parameter S on the Voltage Drop across the Depletion Region V	99
5.4.2 Dependence of the Depletion Region Width w on V	100
5.5 THEORETICAL PRESENTATION	102
5.6 RESULTS AND DISCUSSION	103
5.6.1 Effect of Surface Reaction Parameters, S_r and S_t	103
5.6.2 Effect of Diffusion Length L_p	109
5.6.3 Effect of Drift Field	113
5.6.4 Effect of Donor Concentration, N_0	117

	PAGE
5.6.5 Effect of the Voltage Drop, V , across the Depletion Region	120
5.7 LIMITATIONS OF THE MODEL	122
5.8 CONCLUSION	122
CHAPTER 6 AN INVESTIGATION OF THE POSSIBILITY FOR IMPROVEMENT OF THE PHOTORESPONSE OF A TiO_2 ELECTRODE	125
6.1 EFFICIENCY CONSIDERATIONS	125
6.2 IMPURITY CENTERS IN SEMICONDUCTORS	130
6.2.1 Impurity Absorption	131
6.2.2 Impurity Sensitization	134
6.2.3 Electron Transfer via Impurity Centers	140
6.3 IMPURITY CENTERS IN TiO_2	140
6.4 EXPERIMENTAL	143
6.5 MEASUREMENTS	145
6.5.1 Film Thickness Measurement	147
6.6 RESULTS AND DISCUSSION	147
6.6.1 Limitations and Sources of Errors	151
6.7 CONCLUSION	152
CHAPTER 7 CONCLUSION	154
REFERENCES	158

LIST OF FIGURES

FIGURE		PAGE
1.1	A Comparison of Energy Levels Distribution in a Semiconductor and a Redox Electrolyte	6
1.2	Energy Band Diagram at a Semiconductor/Electrolyte Interface	8
1.3	Schematics of a Photoelectrolysis Cell Utilizing an <i>n</i> -type Semiconductor	11
1.4	Electron Energy Correlations for an Electrochemical Cell Operating in a Regenerative Mode	13
1.5	Energy Band Diagram for an Electrochemical Cell Operating in a Water Photoelectrolysis Mode	15
1.6	Thermodynamics of Photodecomposition of Semiconductors	17
2.1	Basic Components of a Triode Sputtering System	26
2.2	Schematics of the Triode Sputtering System Developed	30
2.3	Schematics of the Substrate Table Constructed	35
2.4	Pattern Generation Masking Set	37
2.5	A Detailed Structure of the rf/dc Probe	39
2.6	Cross Section of the Target Changing Arm Assembly	40
2.7	Schematic Illustration of the Sputtering Target Press Designed	47

FIGURE		PAGE
3.1	Electrode Configuration	52
3.2	Experimental Setup for Photoresponse Measurements	53
3.3	X-ray Diffraction Photographs of dc Sputtered Reduced TiO_2 Electrodes	57
3.4	Spectral Response of a Sputtered TiO_2 Electrode in a Water Photoelectrolysis Cell	59
3.5	Dependence of Photocurrent on Light Intensity for Sputtered TiO_2 Electrodes at Low Levels of Illumination	60
3.6	Equivalent Circuit of the Semiconductor Electrode in a Photoelectrochemical Cell	62
4.1	Effect of Oxygen Partial Pressure on the Deposition Rate	70
4.2	A UV Spectrograph for TiO_x Thin Films Deposited under Several Oxygen Plasma Conditions	71
4.3	X-ray Diffraction Patterns of TiO_x Thin Films Deposited by Reactive Sputtering of Titanium under Different Oxygen Plasma Conditions ($T_s = 250^\circ\text{C}$)	72
4.4	Primary Cell Configuration	77
4.5	Configuration of a Layered Structured TiO_2 Electrode Fabricated by Reactive Sputtering	80

FIGURE		PAGE
4.6	Energy Band Diagram for an n -type Semiconductor/ Electrolyte Interface with an n^+ Region	81
4.7	X-ray Diffraction for Three Samples Prepared by Reactive Sputtering from a Titanium Metal Target for Different Periods of Time	83
4.8	Spectral Response of BSF Reactively Sputtered TiO_2 Electrodes in a Water Photoelectrolysis Cell	84
4.9	Effect of Light Intensity on the Photocurrent of BSF Reactively Sputtered TiO_2 Electrodes at Low Levels of Illumination	86
5.1	An Energy Band Diagram of an n -type Semiconductor Electrode in a Photoelectrochemical Cell	91
5.2	Algorithm for the General Calculating Procedure Absorption Constant of TiO_2	104 106
5.4	Current Voltage Characteristics with $S_r + S_t$ as a Parameter.	108
5.5a	Spectral Response of a TiO_2 Photoelectrolysis Cell, L_p as a Parameter	110
5.5b	Variation of Quantum Efficiency with λ , L_p as a Parameter	111
5.5c	Effect of the Diffusion Length L_p on the Total Photocurrent Density J_T	112
5.6a	Spectral Response of a TiO_2 Photoelectrolysis Cell, β as a Parameter	114
5.6b	Variation of Quantum Efficiency with λ , β as a Parameter	115

FIGURE		PAGE
5.6c	Effect of the Drift Field β on the Total Photocurrent Density J_T	116
5.7a	Spectral Response of a TiO_2 Photoelectrolysis Cell, N_0 as a Parameter	118
5.7b	Effect of Surface Donor Concentration N_0 on the Total Photocurrent Density J_T	119
5.8	Spectral Response of a TiO_2 Photoelectrolysis Cell, V as a Parameter	121
6.1	An Energy Balance Diagram for a Water Photoelectrolysis Cell using an n -type Semiconductor	127
6.2	Electron Energy Correlations in a Water Photoelectrolysis Cell with an n -type TiO_2 Photoelectrode	128
6.3	Impurity Absorption in Semiconductors	132
6.4	Schematic Outline of Sensitization	135
6.5	Charge Transfer via Surface States at the Semiconductor/Electrolyte Interface	141
6.6	Configuration of a TiO_2 Thin Film, Doped by Diffusion	144
6.7	A Thin Film Quartz Interface	145
6.8	Dependence of the Absorption Coefficient on Wavelengths for Different Doped TiO_2 Thin Films	148

LIST OF SYMBOLS

D_{redox}	probability density function of electron states in the redox electrolyte
D_{ox}, D_{red}	probability density of unoccupied and occupied states respectively
$E_{f,redox}$	Fermi level of a redox electrolyte
V_{redox}	standard redox potential
$\alpha_{red}, \alpha_{ox}$	concentrations of reduced and oxidized species respectively
NHE	normal hydrogen electrode
E_f	equilibrium Fermi level of the semiconductor
V_{FB}	flat band potential
E_{FB}	flat band energy level
V_b	band bending in the semiconductor
V_{ph}	photogenerated voltage
E_{fn}, E_{fp}	quasi Fermi levels of electrons and holes in a semiconductor respectively
$\delta n, \delta p$	excess density of electrons and holes respectively
n_0, p_0	thermal equilibrium of electrons and holes respectively
n_i	intrinsic concentration of free carriers
N_c, N_v	density of states in the conduction and valence bands respectively
E_g	energy gap of the semiconductor
E_c, E_v	conduction and valence band edges respectively
$\Delta E_{fn}, \Delta E_{fp}$	changes in the quasi Fermi energy of electrons and holes respectively
$E_{n,decomp}, E_{p,decomp}$	Fermi energy for decomposition of the semiconductor by electrons and holes respectively

E_{redox}	redox potential
η_a, η_c	anodic and cathodic overpotentials respectively
e^-, h^+	a photogenerated electron/hole pair
eV	electron volt
UV	ultraviolet
q	electronic charge
N_D	donor concentration
H^+/H_2	water reduction level
O_2/H_2O	water oxidation level
δ	penetration depth of light
α	absorption coefficient
w	depletion region width
ϵ	dielectric constant
n^+/n	a layered structure of a lightly doped material deposited on a heavily doped layer of the same material
dc	direct current
rf	radio frequency
θ	Bragg's angle
v_o	oxygen vacancy
$\star Ti$	intersitital titanium atom
T_r	reducing temperature
T_s	substrate temperature
h	Plank's constant
ν	frequency of the incident radiation
K	Boltzman's constant
T	absolute temperature

C_{sc}	depletion region capacitance
V	voltage drop across the depletion region
C_H	capacitance of the Helmholtz double layer
C_M	capacitance of the metal/electrolyte interface
P_{O_2}	partial pressure of oxygen
σ	ratio of oxygen to titanium arrival at the substrate
TiO_x	titanium suboxide
ξ	oxidation rate/sputtering rate
$P_{O_2}^l$	lower critical partial pressure of oxygen
$P_{O_2}^\mu$	upper critical partial pressure of oxygen
$n(z)$	majority carriers concentration in a semiconductor
$\mu_n \quad \mu_p$	mobilities of electrons and holes respectively
D_n, D_p	diffusion coefficients of electrons and holes respectively
E_d	drift field
J	hole current density
J_d, J_p	current density component of holes generated inside and outside the depletion region respectively
$Q'_0(\lambda)$	flux density of the solar spectrum
$P_0(z), \delta P(z)$	spatial distribution of thermal equilibrium and photo-generated holes respectively
$b'(z)$	$\delta P(z)/P_0(z)$
τ_p	hole lifetime
L_p	hole diffusion length $L_p^2 = D_p \tau_p$
N_0	surface donor concentration
β	drift factor
γ	$\alpha - \beta$

Y_1	$\frac{\alpha Q'_0 N_0}{n_i^2 D_p}$
Y_2	$Y_1 / (\gamma^2 - \gamma\beta - 1 / L_p^2)$
A_1, A_2	constants
S	a surface reaction parameter
S_r, S_t	surface recombination and transfer of holes at the semiconductor/electrolyte interface respectively
Y_3	$\alpha / (\alpha^2 - \alpha\beta - 1 / L_p^2)$
J_r	hole recombination current density
J_t	hole transfer current density
$V(z)$	the voltage in the semiconductor as a function of z
$V(0), V(w)$	the voltages at $z = 0$ and at $z = w$ respectively
$N(w)$	donor concentration at $z = w$
w_0	depletion region width for a uniformly doped semiconductor
λ	wavelength
J_T	total photocurrent density for holes
η	quantum efficiency
ΔG	free energy
V_H	voltage drop across the Helmholtz double layer
E_i	ionization energy
X	impurity center
X^+	ionized impurity center
n_{1r}, p_{1r}	density of occupied and unoccupied type I impurity centers respectively
n_{2r}, p_{2r}	density of occupied and unoccupied type II impurity centers respectively
N_{1r}, N_{2r}	density of centers of class I and class II impurities respectively

G	volume rate of generation of free carriers
R_n, R_p	electron and hole recombination rates respectively
v_n, v_p	thermal velocities of electrons and holes respectively
s_{1n}, s_{1p}	capture cross sections of electrons and holes respectively for class I states
s_{2n}, s_{2p}	capture cross sections of electrons and holes respectively for class II states
n_1	refractive index of TiO_2
n_0	refractive index of air
n_2	refractive index of quartz
T_1, R_1	transmittance and reflectance at the n_0/n_1 interface respectively
T_2, R_2	transmittance and reflectance at the n_1/n_2 interface respectively
T_3, R_3	transmittance and reflectance at the n_2/n_0 interface respectively
T	total transmittance
t	film thickness
m	number of peaks
λ_1, λ_2	wavelengths corresponding to two transmittance peaks

CHAPTER 1

INTRODUCTION

1.1 STIMULUS FOR THE INVESTIGATION

Every month the earth receives an amount of solar energy which has been estimated to exceed the energy contained in the world's supply of fossil fuel [1.1, 1.2]. About two-thirds of this energy serves to heat the surface of the land and oceans. Only a tiny fraction is stored as chemical energy by the photosynthesis of green plants, yet this process provides all our food and the fossil fuel we are so rapidly consuming. In the long term, if we are not solely to rely on nuclear power, we have to develop a large scale method for harnessing solar energy.

In principle, solar energy may be utilized in a variety of ways; as a source of heat, as a means of producing electricity or as a means of carrying out chemical reactions and providing chemical fuel. This third category is the subject matter of these investigations. In general, it may be said that the satisfactory long term storage of energy derived from the sun requires the intervention of chemical reactions. This being the case and since the energy conversion in photosynthesis is an electrochemical process, namely a redox reaction of excited chlorophyll molecules, many attempts have been made to develop solar energy converters along the same line [1.3, 1.4]. However, it has been found that the efficiency of artificial systems of this kind is very limited and the prospects of developing more efficient and durable systems of this type

appear to be very low. The only promising alternative, which preserves the advantages of the photosynthesis process regarding the energy conversion efficiency and still exploits a photoredox reaction, is a water photoelectrolytic cell with semiconductor electrodes as energy converters [1.5, 1.6]. This new development suggests that water can be photodecomposed into oxygen and hydrogen utilizing solar energy, without the application of any external bias, if one or both electrodes of a photoelectrolysis cell is an appropriate semiconductor.

In its basic form this system employs an abundant raw material (water) and produces a fuel (hydrogen) which may then be readily stored and/or shipped. This fuel can be used not only to provide heat for industrial or domestic processes, but also to conveniently produce electrical power efficiently, either in a fuel cell or some form of steam or engine driven generator. In addition, hydrogen can be used as a basic raw material for producing other clean fuels and valuable chemicals from various sources such as coal and shale.

From a practical point of view it is necessary to fabricate inexpensive semiconducting electrodes for use in water photoelectrolysis cells, if the photocatalytic production of hydrogen from water on a large scale is to be economically feasible.

The main objective of this research project is to further the achievement of this goal, within the constraints imposed by these practical considerations, by devoting our efforts to sputtered semiconducting thin film electrodes.

In this chapter a brief discussion of the basic processes at the semiconductor/electrolyte interface is presented. The starting point is

the basic concept of energy levels in a redox electrolyte and then the combined energy diagram for the semiconductor in an electrochemical cell is introduced. The physical parameters that determine whether or not a particular combination of a semiconductor and electrolyte is useful in photoelectrolysis are also defined. A brief survey of the subject is then given. It is further shown why some semiconductors require an external voltage to assist the photoelectrolysis while others do not, and why some semiconductors are stable while others are not. Finally, the main features which must be considered in developing a technologically feasible and economically attractive water photoelectrolysis cell are presented.

1.2 BASIC PROCESSES AT SEMICONDUCTOR ELECTRODES

1.2.1 Redox Reactions and Energy Levels.

In a manner similar to metal electrodes, semiconductor electrodes can also perform redox reactions by electron transfer between the electrode and a redox system in a solution. There is, however, a principal difference due to the existence of a band gap in the energy distribution of electronic states in a semiconductor. Electron transfer can only occur within two energy ranges belonging to either the conduction band or the valence band [1.5]. The reason is that electron transfer steps occur between electron energy states of the same level; one being occupied, the other being vacant.

The concept of energy levels for electrons in solids is well known from the band theory of solids, but what an electron level means in a redox electrolyte will be briefly explained.

In the electrolyte, electron energy levels are located at the donors and acceptors, that are the reduced and oxidized components of a redox system. The energy levels of these states can be defined in a fully analogous way to the energy levels in solids; namely, by the energy of electron emission from a donor state or electron attachment to an acceptor state [1.7, 1.8]. This gives the energy of the occupied and the unoccupied states respectively.

Similar to the density of states function in solids, a density of states function D_{redox} for electron states in a redox electrolyte may be defined as the sum of occupied $D_{red}(E)$ and unoccupied $D_{ox}(E)$ [1.8, 1.9] as

$$D_{redox}(E) = D_{red}(E) + D_{ox}(E) .$$

At equilibrium, the occupation of these energy states in the electrolyte follows a Fermi Dirac distribution function. That is

$$D_{red}(E) = D_{redox}(E)f(E-E_{f,redox})$$

$$D_{ox}(E) = D_{redox}(E)f(E_{f,redox}-E) .$$

$E_{f,redox}$ is equivalent to the chemical potential of electrons in a redox electrolyte and is related to the standard redox potential U_{redox} (at equal concentrations of reduced and oxidized species) by [1.10],

$$E_{f,redox} = constant - qU_{redox} + kT \ln \frac{a_{red}}{a_{ox}} , \quad (1.1)$$

where a_{red} and a_{ox} are the concentrations of the reduced and oxidized species in the electrolyte respectively.

The constant in Eqn. 1.1 defines the energy of the electron in a reference electrode. For the standard hydrogen electrode (SHE) this constant has a value between -4.5 and -4.7 [1.11, 1.12] .

A comparison of the distribution of the energy levels in a semiconductor and a redox electrolyte under equilibrium conditions is given in Fig. 1.1.

1.3 THE SEMICONDUCTOR/ELECTROLYTE INTERFACE

When a semiconductor is brought into intimate contact with a redox electrolyte, an equilibrium situation is achieved by electron exchange at the interface. In equilibrium the Fermi level of both sides are adjusted due to the formation of an electric double layer between the semiconductor and the electrolyte. The particular structure of the double layer depends mainly on the concentration of the mobile and immobile charge carriers at both sides of the interface [1.13, 1.14, 1.15]. With free charge carrier concentrations below $10^{19}/\text{cm}^3$ a more or less extended space charge region is formed on the semiconductor, while the ionic charge in the electrolyte can be represented in a good approximation as a plane at a definite distance from the surface (Helmholz plane) [1.9]. As a result of the space charge formation, charge carrier concentrations and energy values of the band edges differ between the bulk and surface of the semiconductor.

The position of the band edges in contact with an electrolyte is an individual property of the particular semiconductor and depends on the composition of the electrolyte. However, if the semiconductor electrode

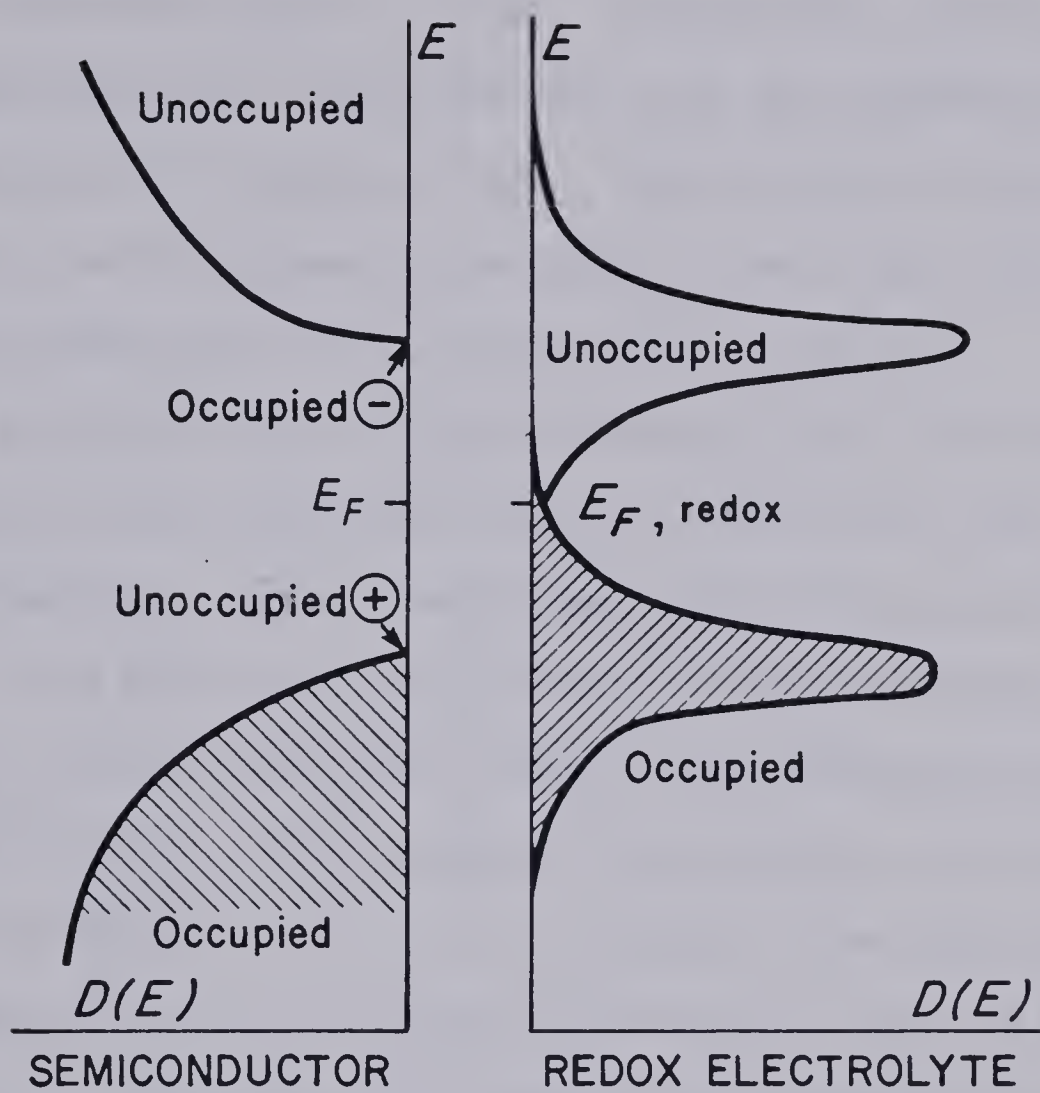


Fig. 1.1 A Comparison of Energy Levels Distribution in a Semiconductor and a Redox Electrolyte.

is polarized in such a direction that an excess charge, with a sign opposite to the majority carriers is collected underneath the electrode surface, a depletion region is formed. Consequently, the energy bands in the semiconductor will be either bent up or down depending on whether the semiconductor is n -type or p -type. This situation is equivalent to a Schottky barrier between a semiconductor and a metal; the redox electrolyte having the function of the metal in this case.

The potential drop (or the band bending) across the space charge region depends on the difference between the equilibrium Fermi level of the semiconductor E_f and the redox Fermi level of the electrolyte $E_{f,redox}$. At a particular redox potential of the electrolyte with $E_f = E_{f,redox}$ there is no excess charge in the semiconductor and therefore no band bending. In the absence of space charge, the bands are flat from the semiconductor bulk to the surface. The redox potential at which there is no band bending is referred to as the flat band potential V_{FB} . The value of V_{FB} depends on the composition of the electrolyte and the properties of the semiconductor which control E_f . The degree of band bending qV_b that occurs in a semiconductor is therefore equal to the difference between the flat band energy level E_{FB} and $E_{f,redox}$, Fig. 1.2.

1.3.1 The Semiconductor Electrode under Illumination.

Absorption of light by a semiconductor electrode generates electron-hole pairs, if the energy of the incident radiation exceeds the energy gap. If the semiconductor is illuminated from the electrolyte side, these carriers will be generated in the depletion region where

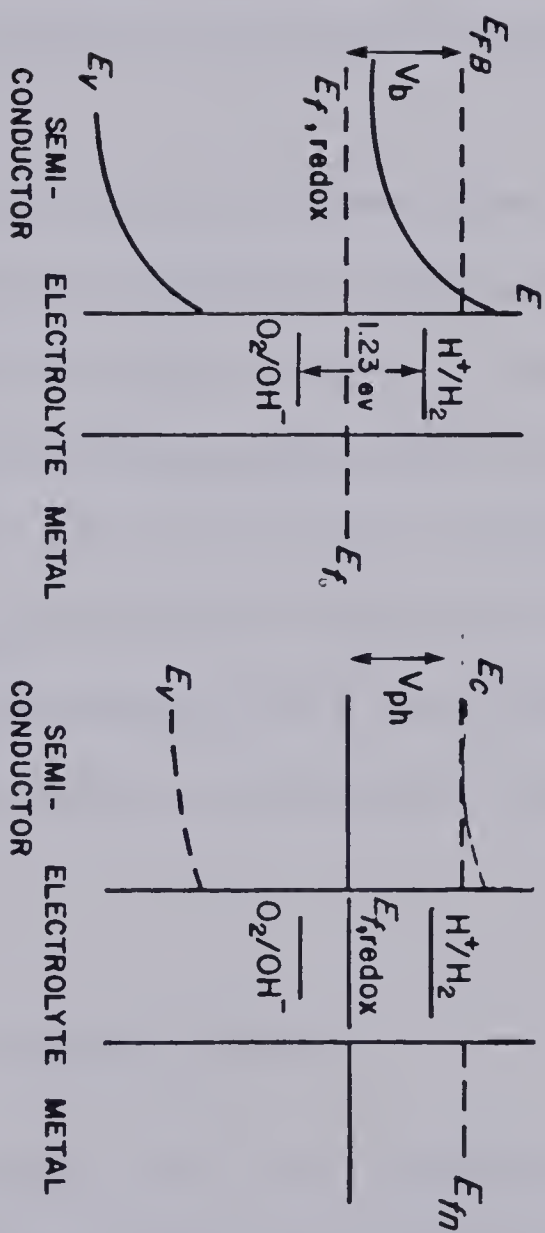


Fig. 1.2 Energy Band Diagram at a Semiconductor/
Electrolyte Interface.

they will be acted upon by the electric field present there. As a result, the majority carriers will move towards the bulk of the semiconductor while the minority carriers will be driven to the interface. If the minority carriers can leave the surface, because they react with electron donors in the electrolyte, a negative charge will be accumulated in the semiconductor, thus a photovoltage V_{ph} of a sign opposite to the initially present voltage is created, and the band bending is diminished [1.16].

Since the band bending in the dark has been shown to be dependent upon the redox electrolyte and the properties of the semiconductors, the photovoltage will also depend on the same variables. However, since photoelectrolysis cells differ from the conventional solar cells (as will be shown) in that they operate under short circuit conditions, the variability in the photovoltage and the fact that it can even be zero has no significance for the photoelectrolysis process because the photovoltage is not the potential available for driving the chemical reaction in the cell [1.17, 1.18].

1.4 DRIVING FORCE FOR WATER PHOTOELECTROLYSIS

In a water photoelectrolysis cell the illuminated semiconductor electrode is connected to a counter electrode to complete the circuit. Under short circuit conditions the Fermi level of the counter electrode is equal to that of the semiconductor. For water electrolysis to proceed two conditions must be fulfilled. First, two redox levels must be present in the electrolyte; the water oxidation level and the water reduction level. The energy difference between these two levels is

~ 1.23 eV. Second, two different redox reactions have to take place in opposite directions at the two electrodes of the cell. A schematic representation of a photoelectrolysis cell using an n -type semiconductor anode and a metal cathode is given in Fig. 1.3, in which η_a and η_c are anodic and cathodic overpotentials respectively.

Absorption of light by the semiconductor will be converted into energy of photogenerated carriers. Electronic equilibrium will therefore be disturbed in the illuminated zone (the depletion region in this case). As a consequence, the free energies of electrons and holes will deviate from each other and also from their equilibrium values. The amount of deviation from equilibrium depends on the light intensity, the absorption coefficient of the semiconductor, recombination kinetics, transport phenomena and the charge distribution in the illuminated zone [1.10, 1.19]. Under steady state illumination, the semiconductor electrolyte/interface can be treated in terms of separate quasi Fermi levels E_{fn} for electrons and E_{fp} for holes. The quasi Fermi levels are defined by

$$E_{fn} = E_f + kT \ln \frac{\delta n}{n_0}$$

$$E_{fp} = E_f - kT \ln \frac{\delta P}{P_0}$$

where δn and δP are the excess density of electrons and holes respectively, n_0 and P_0 are their respective thermal equilibrium concentrations, and E_f is the Fermi level in the bulk of the semiconductor. n_0 and P_0 are related to the band gap energy by

$$n_0 P_0 = n_i^2 = N_c N_v e^{-E_g/kT}.$$

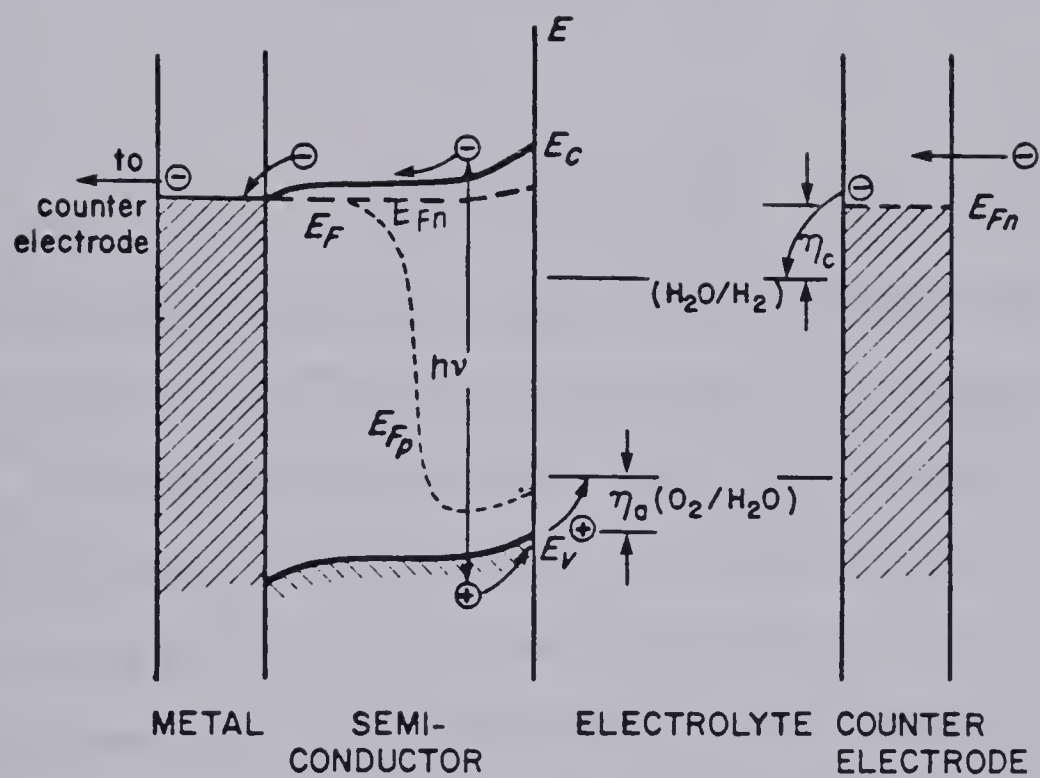


Fig. 1.3 Schematics of a Photoelectrolysis Cell Utilizing an n -type Semiconductor.

In the dark the quasi Fermi energies coincide with the equilibrium Fermi level E_f . Under illumination the amount of deviation from the equilibrium Fermi level (which is also the change in the free energy) is given by

$$\Delta E_{fn} = kT \ln \left(1 + \frac{\delta n}{n_0} \right) \quad (\text{for electrons})$$

and

$$\Delta E_{fp} = kT \ln \left(1 + \frac{\delta p}{p_0} \right) \quad (\text{for holes}) .$$

These equations clearly indicate that the quasi Fermi energy for majority carriers is approximately the same as the conventional Fermi level E_f in the bulk semiconductor. They also indicate that large deviations in the free energy occur only for minority carriers. In addition these deviations are more significant in large band gap semiconductors where the equilibrium concentrations are small. '

According to this theory, it is then possible for reactions such as oxidation or reduction, which were forbidden in the dark, to take place via the photogenerated minority carriers. The driving force for these reactions is the difference in the quasi Fermi levels for the majority carriers outside the space charge region and the minority carriers at the semiconductor/electrolyte interface. The illuminated depletion region acts as the generator of this force.

Since water photoelectrolysis cells operate under short circuit conditions and also because the maximum Fermi level permissible is the flat band energy level, hydrogen evolution will only be possible if the flat band level lies above the water reduction level, Fig. (1.4). If, however, the flat band potential lies below the water reduction level (for an n -type

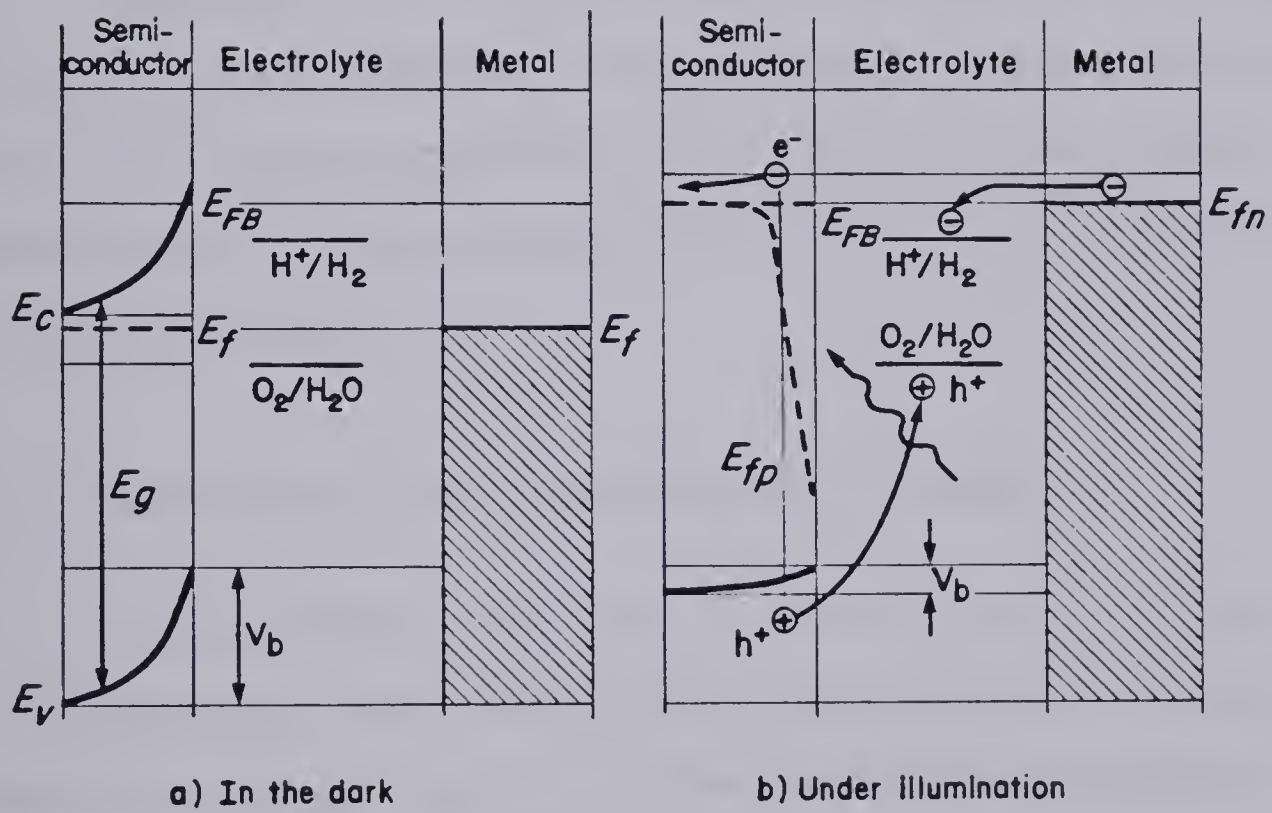


Fig. 1.4 Energy Band Diagram for an Electrochemical Cell Operating in a Water Photoelectrolysis Mode.

semiconductor) water will be oxidized to oxygen at the anode and the oxygen will be reduced to water at the cathode. Thus there will be no net chemical change in the cell and the cell will operate in a regenerative mode with no hydrogen evolution, Fig. 1.5. In order to raise the Fermi level above the water reduction level and also to increase the band bending of the semiconductor, an external anodic bias will be required.

According to this scenario, the flat band potential is probably the most important parameter in determining the combined energy band diagram of a photoelectrochemical cell. The flat band potential determines the conditions required for the semiconductor to promote a particular reaction.

1.5 PHOTODECOMPOSITION OF SEMICONDUCTOR ELECTRODES

All semiconducting materials in contact with electrolyte solutions can be decomposed under certain conditions by either an oxidation or a reduction reaction. This is a fundamental materials problem and represents a major obstacle to the realization of a practical photoelectrolysis cell. In brief, the photodecomposition of semiconductor electrodes can be explained as follows [1.19, 1.20].

A photogenerated electron-hole pair means that one of the electrons in a bonding orbital has been removed; the bond strength is thereby weakened and a chemical attack can be initiated. Since the decomposition reaction occurs exclusively at the surface and is controlled by the free energies of electrons and holes there, electronic energy states in the surface play a key role in such a reaction. Decomposition of the

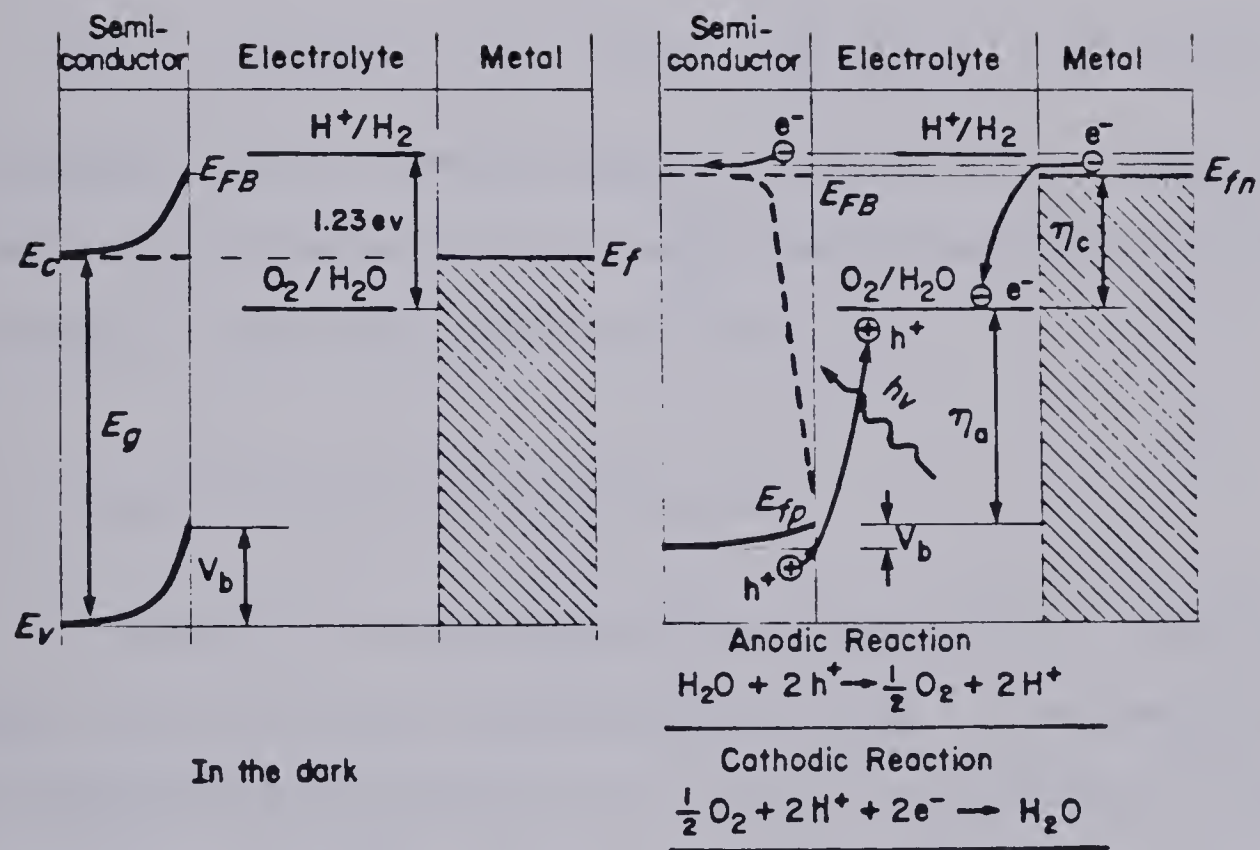


Fig. 1.5 Electron Energy Correlations for an Electrochemical Cell Operating in a Regenerative Mode.

semiconductor will occur only if the free energy of a charge carrier exceeds a certain critical value (decomposition energy level) E_{decomp} . Therefore, if both decomposition Fermi levels $E_{n,decomp}$ for electrons and $E_{p,decomp}$ for holes are known, one can predict whether a semiconductor in a particular redox electrolyte is thermodynamically stable at a given redox level E_{redox} according to the following criteria:

$$E_{p,decomp} < E_{redox} < E_{n,decomp} \quad (\text{for stability})$$

$$E_{redox} < E_{p,decomp} \quad \text{or} \quad E_{redox} > E_{n,decomp} \quad (\text{for instability}).$$

Consequently, four different stability criteria for the semiconductor electrodes, with regard to their photodecomposition behavior, may be envisaged. These are represented in Fig. 1.6.

1.6 CELLS FOR WATER PHOTOELECTROLYSIS

In the first report on water photoelectrolysis by Fujishima and Honda [1.5], an *n*-type TiO_2 electrode was used. It was demonstrated that the photovoltage generated in this cell was not sufficient for photoelectrolysis. Later [1.6, 1.21, 1.22], it was found that an additional voltage of the order of 0.25 - 0.5 V is needed in order to reach simultaneous oxygen evolution at the TiO_2 electrode and hydrogen evolution at the Pt counter electrode.

There are, however, some problems encountered with using *n*-type semiconducting TiO_2 electrodes for water electrolysis. One is the large band gap of TiO_2 (3.0 eV). This means it can absorb only a very small portion of the solar spectrum in the UV. Another is the unfavorable

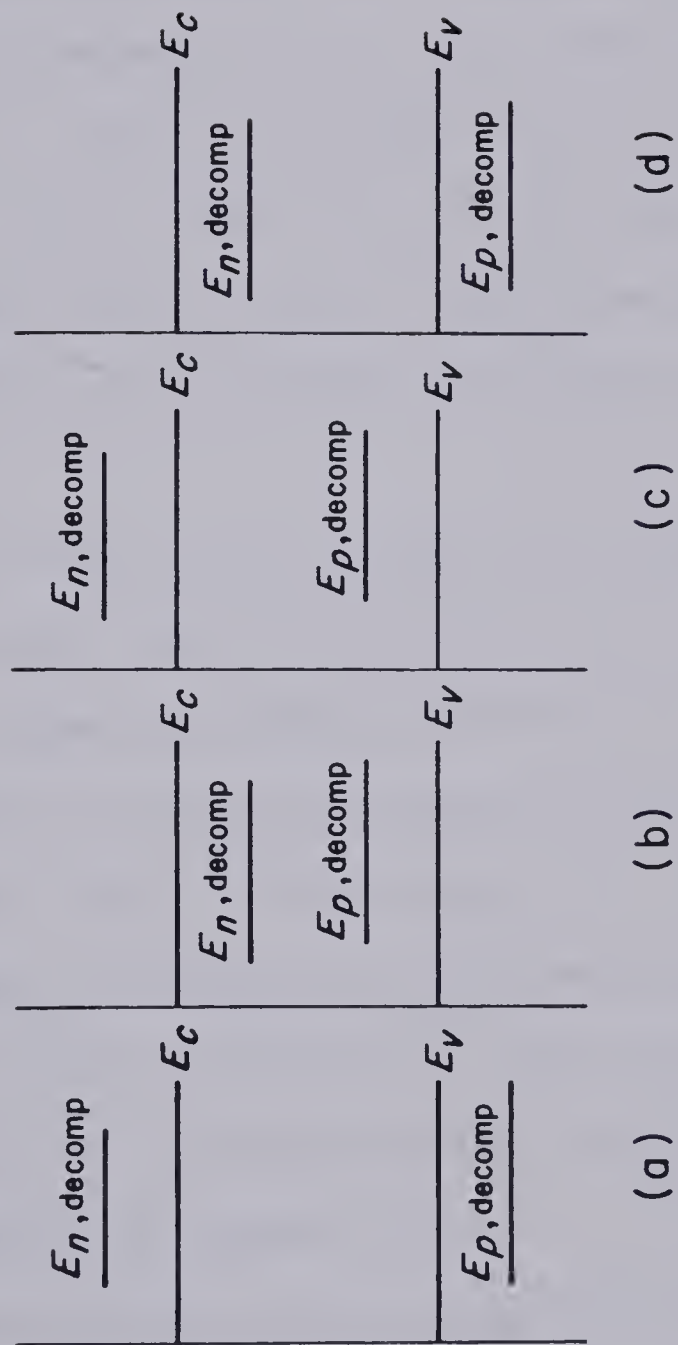


Fig. 1.6 Thermodynamics of Photodecomposition of Semiconductors.
 (a) stable, (b) anodically and cathodically unstable,
 (c) cathodically stable, (d) anodically stable.

position of the band edges. The conduction band edge is just slightly above the Fermi level for water reduction and the valence band edge is far below the Fermi level for water oxidation.

Semiconductors more suitable for water photoelectrolysis should have a somewhat higher position of the conduction band edge than TiO_2 and a position of the valence band edge much closer to the Fermi level for water oxidation. The first condition can be fulfilled with some other oxides like SrTiO_3 [1.23, 1.24], BaTiO_3 [1.25], KTaO_3 [1.26], ZrO_2 [1.27], Nb_2O_5 [1.27] or SnO_2 [1.28]. However, these oxides have even a wider energy gap than TiO_2 and are therefore less appropriate for solar light absorption.

A systematic study of the suitability of various *n*-type oxide semiconductors has been carried out by Kung et al. [1.29]. This study has included many oxides with band gaps similar to or smaller than TiO_2 . These materials have also been investigated by others (e.g., WO_3 [1.30, 1.31], Bi_2O_3 [1.32], YFeO_3 [1.33] and Fe_2O_3 [1.32, 1.34, 1.35]). This was done in the hope of increasing the efficiency through absorption of more of the solar spectrum. However, the flat band potential of all these oxides is below the hydrogen evolution level and consequently their use would require an external bias.

Other alternatives have been proposed which could help in solving the above problems. These include the *p-n* photoelectrolysis cell [1.36], the photochemical diode [1.37] and a combination of two junctions in series [1.38]. However the stability problem remains unsolved and much research has been devoted to overcome this problem.

The above survey shows that, despite its wide energy gap and unfavorable locations of its band edges, TiO_2 still remains the most popular material due to its resistance to chemical degradation.

1.7 THIN FILM APPROACH

According to the theory of the semiconductor/electrolyte interface explained before, the main features which must be considered in developing a technologically feasible and economically attractive water photo-electrolysis cell may be identified as follows.

i) For high quantum efficiency the incident light must be absorbed in the depletion region. This means that the depletion region width w should be equal to or greater than the penetration depth of light ($\delta = 1/\alpha$). For an n -type semiconductor one can write

$$\frac{1}{\alpha} \leq \left(\frac{2\epsilon V}{qN_D} \right)^{\frac{1}{2}}$$

where ϵ is the dielectric constant, N_D is the donor concentration, α is the absorption coefficient and V is the voltage drop across the depletion region. A much higher donor concentration N_D results in the decrease of the depletion region width and most of the light is lost by recombination in the bulk. A lower donor concentration will increase the resistance of the semiconductor and accordingly, the ohmic loss in the cell.

ii) The surface band bending V_b should be maximized in order to minimize electron-hole pair recombination in the space charge region. Since the band bending is determined by the flat band potential and the redox Fermi level, the semiconductor and the electrolyte must be chosen

such that the band bending is less than the energy band gap of the semiconductor to avoid the decomposition of the semiconductor itself.

iii) The energy gap of the semiconductor should be in the range 1.5 - 2.2 eV and the redox electrolyte must not absorb much light in the range of photosensitivity of the semiconductor.

iv) The semiconductor electrode must be stable against photo-decomposition.

Since carriers are generated near the semiconductor/electrolyte interface, carrier lifetime and mobility are of lesser importance and single crystals are not required. Thus, the significant material requirements are a semiconductor width of a few times the penetration depth of light, and a reasonable carrier concentration. Therefore, polycrystalline films can be used and structures using evaporated, sputtered or other thin film techniques are feasible. Of course it is not expected that thin films will have as high efficiency as single crystals, but they may be more amenable to low cost production.

It is in this last context that we are trying to make a contribution in the area of solar energy conversion in general, and the hydrogen production area in particular, using a triode sputtering technique. Our principal objective of research and development in this area at this time is to develop TiO_2 thin film electrodes for water photoelectrolysis on the one hand and to investigate the possibility of improving the efficiency on the other.

1.8 PRESENT WORK

In Chapter 2 of this thesis, a detailed description of the triode sputtering module is given. Also the sputtering target fabrication procedure is briefly explained.

In Chapter 3 the results of our primary investigations of TiO_2 film deposition using dc sputtering, rf sputtering and plasma anodization techniques are presented. In addition, a detailed description of a semiconducting TiO_2 thin film electrode fabrication process is presented and the results of our investigations on the behavior of these electrodes in photoelectrochemical cells are given.

In Part I of Chapter 4, fabrication of polycrystalline titanium suboxide thin films, by reactive sputtering from a Ti metal target, is explained. The effect of oxygen partial pressure on film deposition rate, crystal structure and optical properties are presented. In Part II a detailed description of the fabrication technique of a layered structure (n^+/n) stable semiconducting TiO_2 electrode is presented. The results of the investigations of the response of these electrodes in photoelectrochemical cells are presented.

In Chapter 5 a model for the photoexcited semiconductor electrode in photoelectrochemical cells is developed. The model lays particular emphasis on the effect of a drift field caused by an impurity gradient and takes into account the effect of surface reaction parameters at a semiconductor/electrolyte interface. Computer simulations of the developed model for the semiconducting TiO_2 electrodes were carried out and the results are presented.

In Chapter 6 the possibility of extending the spectral response of TiO_2 thin films utilizing an impurity doping approach is investigated using different doping techniques. The rationale behind the approach is first explained and results of the effect of doping on the absorption of TiO_2 films are graphically illustrated.

CHAPTER 2

THE SPUTTERING TECHNIQUE AND THE FABRICATION SYSTEM

2.1 INTRODUCTION

Sputtering is a process in which a solid target is bombarded with heavy ions of sufficient energy to eject material from its surface layer. Collection of the ejected target material on a substrate results in the formation of a thin film. The ejection of material from the target occurs through momentum transfer from the bombarding ions and consequently the target does not need to be heated.

The sputtered species are ejected from the target with energies typically in the range of 2-10 eV. This energy is very important as it produces a film that adheres strongly to the substrate [2.1].

Sputtering is now established as a very versatile and useful vacuum deposition technique that has proved to be an excellent production process for the deposition of insulating, resistive, semiconducting, and metallic thin films on integrated circuits [2.2]. This versatility arises because of the many possible permutations and combinations of process conditions.

At the present time sputtering is neither as fast nor as easy as evaporation. However, because the target does not have to be heated, it is possible to sputter materials that cannot be evaporated. In addition, the versatility of the sputtering process often allows one to tailor film properties in ways not always available with other methods of film deposition.

2.2 BASIC CONSIDERATIONS

Until recently, most thin film deposition by sputtering utilized a two electrode geometry (diode sputtering or glow discharge). The basic elements of such a system are a cathode, which consists of the source of material to be deposited as a film, and an anode onto which a substrate is placed. Upon application of a high voltage (3-5 kV) between the two electrodes, at a relatively high pressure (30-100 micron), a glow discharge will occur. While not going into the details of a glow discharge, it is important to note that most of the voltage drop in the glow discharge, and also the ionization necessary to sustain the glow, occur respectively across and at the edge of the dark space immediately surrounding the cathode [2.3, 2.4]. Ions and electrons created at the breakdown voltage are accelerated across this region. These energetic electrons produce more ions by collisions with the gas atoms in the negative glow, and the energetic positive ions strike the cathode to produce sputtering and emission of secondary electrons, which are essential for sustaining the glow. Due to the relatively high pressures involved in a diode sputtering system, there will be many collisions between sputtered atoms and gas molecules en route. These collisions cause the sputtered atoms to lose much of their initial energy and will result in back diffusion of atoms to the cathode. However, if the pressure is made sufficiently low, the dark space region will be increased until the plane of the anode is reached and the discharge is extinguished. For these reasons the deposition parameters in a diode sputtering system cannot be varied independently, and pressures generally greater than 30 microns are necessary for maintaining a stable glow discharge.

2.3 LOW PRESSURE SPUTTERING

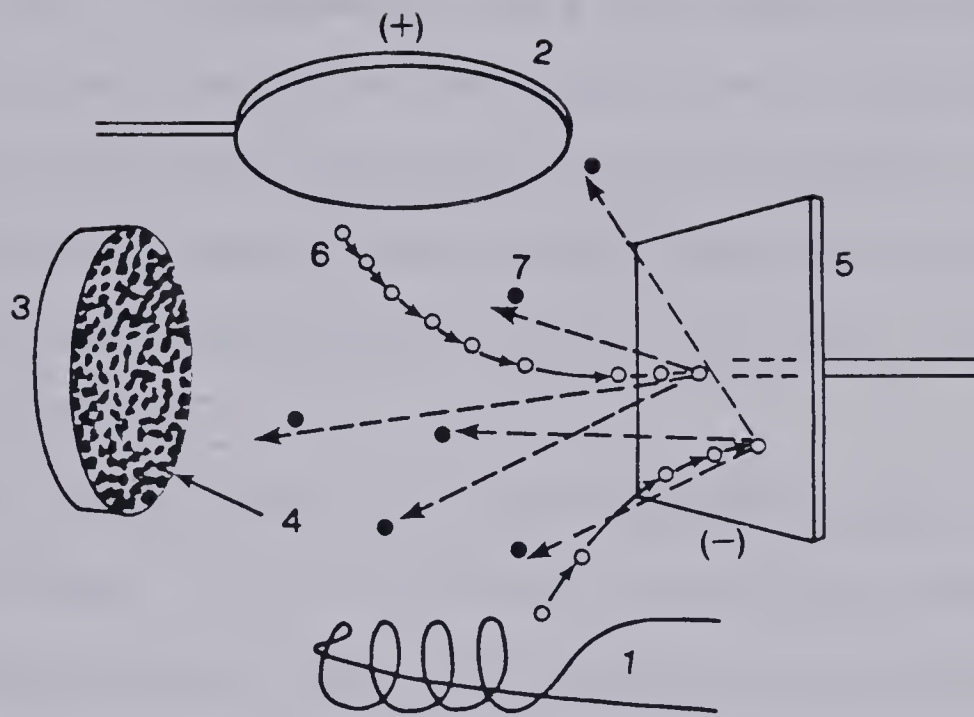
By operating at gas pressures where the mean free path of ions and sputtered atoms become comparable with or larger than the ion accelerating region or the chamber dimensions, one reduces or eliminates many of the complications inherent in the glow discharge.

In the "diode sputtering" system briefly explained before, operation at relatively low pressures is impossible, simply because the discharge becomes extinguished due to the inadequate ionization by the secondary electrons emitted at the cathode. In order to sustain the discharge, a supplemental means for either producing a discharge or increasing the trajectory of electrons must be provided [2.5]. This can be achieved as follows. Auxiliary electrons may be supplied thermionically from a filament. Both the total ionization and ionization efficiency are increased by accelerating electrons by means of a third electrode and then injecting them into the plasma. This assisted sputtering process, or "triode sputtering", is further enhanced by the presence of a magnetic field perpendicular to the lines of forces between the cathode and the anode.

2.3.1 The Sputtering Process in a Triode Sputtering System.

The basic components and their relative orientations in a triode sputtering system are shown in Fig. 2.1 [2.6]. The significant features of such a sputtering system that differentiate it from a conventional glow discharge system are:

- i) The use of a hot filament electron source which permits ionization of the gas at a pressure as low as 5×10^{-4} Torr.



1 - hot cathode, 2 - anode,
 3 - substrate, 4 - deposited thin film,
 5 - target, 6 - argon ions,
 7 - sputtered atoms or molecules.

Fig. 2.1 Basic Components of a Triode Sputtering System.

ii) The target or source material is introduced as a third element or Langmuir probe and is independent of the plasma formation.

An adequate description of the processes which take place at a target in contact with a low pressure plasma is supplied by Langmuir's probe theory [2.7]. The plasma has such a high conductivity that when a negative voltage, with respect to the plasma (or w.r.t. the anode), is applied to the target, the plasma electrons in the electron vicinity are repelled. A positive sheath is thus formed through which the ions stream from the plasma toward the electrode and over which most of the voltage drop will be localized.

In brief, the operation of a triode sputtering system may be explained as follows. A flow of electrons is established between the thermionic cathode and the anode. The voltage used to accelerate these electrons to the anode is usually of the order from 50 to 100 volts. The plasma is confined by the use of a magnetic field provided by an external coil. When a highly negative potential is applied to the target, positive ions impinge on the target with sufficient kinetic energy to sputter the target atoms. The sputtered atoms deposit on the substrate in the same fashion as before.

The main advantages of low pressure sputtering (or a Triode sputtering system) can be inferred in the following [2.8].

i) Control. In a thermionic cathode system the target is independent of the plasma producing system. This makes possible a much better control of the conditions in which the thin film is formed. The plasma density may be controlled by varying the emission of the cathode and the pressure of the working gas in the chamber and also by applying

a magnetic field and then changing its intensity. In addition, low energy sputtering is particularly suitable for achieving control over film composition. Many alloys and compounds may be sputtered directly with little change in the composition of the sputtered film. Alloys may also be deposited with compositional control by simultaneous sputtering of two or more source materials. The sputtering rate at each target may be independently controlled and monitored. Also, because of the low pressures involved, the distance between the substrate and the target can be less than the mean free path. Thus, the properties of the film produced by low pressure sputtering approach those of bulk materials more closely than those produced by glow discharge sputtering.

ii) Adherence. Adherence of films deposited by low pressure sputtering is quite strong. This is partly due to the high arrival energy of sputtered atoms. This high energy results in increased bonding to the substrate. In addition, the substrate may be cleaned by the plasma prior to deposition of a film. This is extremely difficult in diode sputtering as sputtering of the cathode occurs when the discharge is initiated.

The main limitation of this technique is that it is difficult to scale up to very large sizes because of the difficulties involved in producing a large volume uniform thermionically sustained discharge [2.9]. Therefore, due primarily to its greater experimental flexibility, a system having a triode configuration was first constructed for fabrication of ZnO thin film acousto optical transducers and has been modified for the fabrication of the thin film semiconductor electrodes described in the thesis.

2.4 THE DEPOSITION SYSTEM DEVELOPED

The semiconductor electrode fabrication system is shown schematically in Fig. 2.2.

The nucleus of the triode sputtering system was a six inch diameter six arm glass cross which was mounted on a 1000 litre/sec Carl Herman Associates high vacuum pumping station. Although the module was not bakeable, base pressures of about 2×10^{-7} Torr were easily obtained. A coaxial water cooled three element target changer assembly was fitted on one of the side arms of the cross such that sputtering was accomplished in the horizontal plane onto an adjustable substrate table, which was similarly mounted on the other opposite side arm. The substrate table temperature could be raised to 450°C. The other two opposing side arms of the glass cross were used to establish and magnetically confine the plasma beam used in the triode sputtering process. In this manner up to three different materials could be sequentially sputtered at will without breaking the system's vacuum. A cold cathode ionization gauge was installed on the top arm of the cross to permit continuous monitoring of the sputtering chamber pressure. A precision M.K.S. capacitance monometer pressure gauge was used so that the reactive sputtering gas mix could be more accurately monitored and controlled.

2.4.1 Gas Introduction System.

A steady state working argon pressure was achieved by the regulation of the gas admittance rate at a preset pumping speed. In reactive sputtering the reactive gas was first introduced into the chamber through

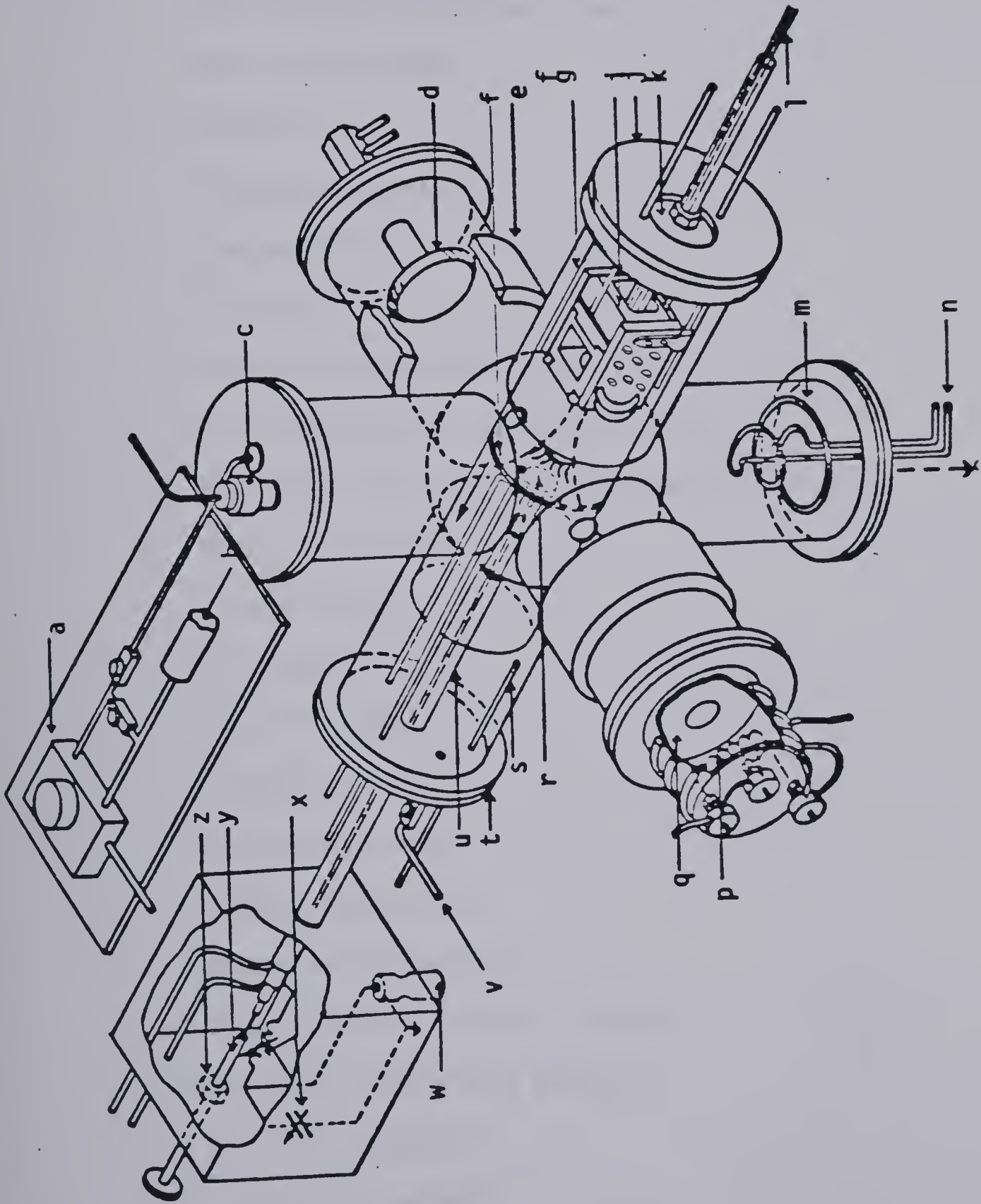


Fig. 2.2 Schematics of the Triode Sputtering System Developed.

Legend to Fig. 2.2

- a - Capacitance manometer pressure head
- b - To reference high vacuum
- c - Cold cathode ionization gauge
- d - Water cooled anode
- e - Magnet coil
- f - Pyrex target shield
- g - Chamber shield
- i - Substrate table
- j - Substrate arm vacuum plate
- k - Insulating Vespel feedthrough plate
- l - Electrical connections (thermocouple, heater)
- m - Meissner cold trap
- n - Liquid nitrogen
- o - To diffusion pump
- p - Dual filaments
- q - Filament shield
- r - Sputtering target
- s - Target changing arm
- t - Probe arm vacuum plate
- u - Coaxial probe (cooled, rf or dc)
- v - Gas inlet from mixing manifold
- w - rf or dc connector
- x - rf matching network
- y - Insulated target drawbolt
- z - Drawbolt nut

a Granville Phillips Company variable leak valve (100 to $10^{-10} \text{ cm}^3 \text{ sec}^{-1}$). Then argon was introduced through another leak valve. The two gases were thoroughly mixed before being admitted into the chamber. Initially a pyrex mixing manifold was used. Later, a coiled copper tube 6.5 mm internal diameter filled with glass beads (3 mm diameter) was used instead. This provided more flexibility and was easy to handle.

2.4.2 Pressure Measurement.

The accurate control of the partial pressures of the gases used in the chamber during reactive sputtering was difficult. This is because most of the gauges used for pressure measurement showed an intolerable dependence upon the gas species present. The M.K.S. capacitance monometer vacuum gauge, however, is species independent and proved to be adequate. This gauge measures the change in capacitance resulting from the deflection of a membrane which separates a constant pressure (high vacuum) reference chamber and the unknown pressure chamber. The pressure is directly measured from the number of molecular collisions per unit area per unit time and is not dependent upon a property peculiar to the gas, such as thermal conductivity or ionization potential.

It should be noted, however, that in reactive sputtering experiments, the true partial pressures, which are the significant parameters, can only be determined if the pumping speed of the individual gases as well as their respective throughput are known. As implied, all gases are generally not pumped equally by the pumping system. This may not be due only to the pump itself but also due to the selective getter

pumping by the vacuum chamber walls, filaments or the deposited thin film. In this case an accurate determination of the individual pumping speed is difficult. An ideal measurement system should consist of a species independent gauge used in conjunction with a microflow meter on each of the gas input lines. Because of these limitations in pressure measurement, the partial pressure measurements given in Chapter 4 of this thesis should not be considered as absolute.

2.4.3 Anode.

The anode was simply a profiled aluminum disc which was mounted on water cooled, insulated feedthroughs.

2.4.4 Filaments.

Different filament sizes of coiled tungsten wire were tried throughout the course of this study. The filament lifetime was significantly increased (two orders of magnitude) when the filament was wound (12 loops, 6 mm diameter) from a 0.5 mm diameter tungsten wire supplied by the Ventron Corporation. When run at 50 amps in a pure argon atmosphere a lifetime of approximately 400 hours was obtained. However, during reactive sputtering the lifetime was reduced to approximately 200 hours. The filaments were mounted on insulating water cooled feedthroughs. Two filaments were incorporated into the system but only one was used at a time; the other being used only in case of a filament failure during a sputtering run. The filament chamber was provided with a tantalum shield having a center aperture 5 cm in diameter. In this way, the

the system contamination from the filaments was reduced and, at the same time, the electron source was effectively centralized.

2.4.5 Electromagnets.

In order to confine, centralize the discharge, and further increase the trajectory of electrons, two cylindrical electromagnets were mounted as shown in Fig. 2.2. Plasma confinement allows stable discharges to be operated at low pressures. In this system sputtering was possible at pressures at 5×10^{-4} Torr with an anode potential of approximately 60 volts, and a magnetic flux density of 70 to 120 gauss. The magnetic field was produced by running a current of 2 amps through approximately 2000 turns of number 20 magnet wire.

2.4.6 Substrate Table.

During the course of our preliminary investigations on the possibility of fabricating thin film semiconducting photoelectrodes it became clear that a wide range of materials with many different types of films as well as different geometrical patterns would be required.

This being the case, a simple and unique substrate table was built, Fig. 2.3. The substrate table was heated using a 0.5 mm diameter, coiled tungsten wire. To avoid any short circuit between the heater and the substrate table and also to minimize the heat radiation, the coil was shielded using a 6 mm (ID) quartz tube. The temperature was monitored and controlled using a platinum temperature sensor probe. The substrate table could be electrically biased with respect to the anode because the heating element was electrically floated by connecting it to an isolation

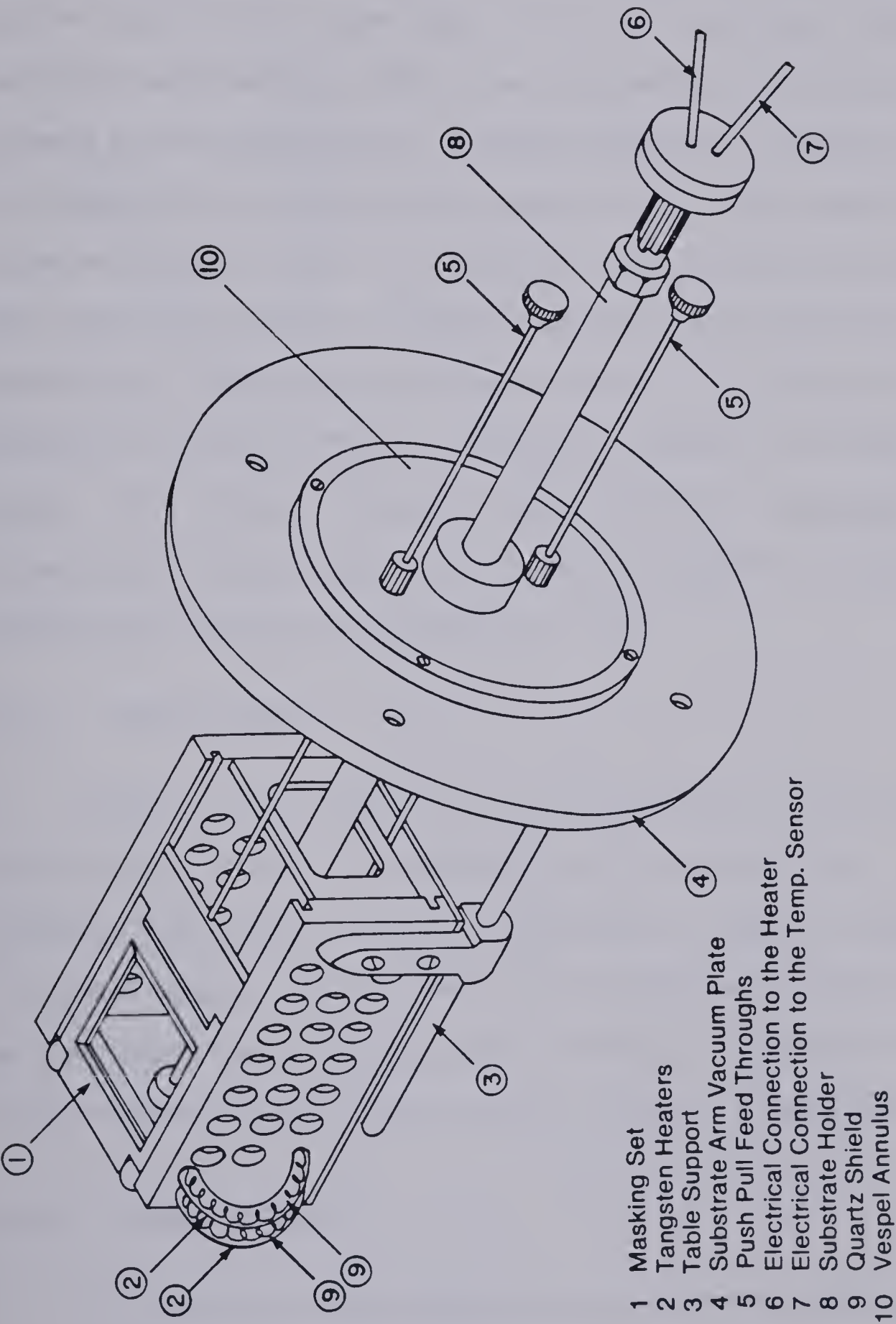


Fig. 2.3 Schematics of the Substrate Table Constructed.

transformer. In addition the vacuum linear feedthrough for the table was mounted in an insulating Vespel annulus, which in turn was supported by the substrate arm vacuum plate. The most significant feature of this substrate table design is that it was equipped with a masking set that allowed for the production of different geometrical patterns. This was achieved simply by masking during deposition to permit deposition only on selected substrate areas. In addition, this masking set provided a shutter that permitted presputtering of each target before deposition. The linear feedthrough (substrate holder) was necessary for varying the target-substrate distance as well as allowing for changing the target under vacuum. This feature, along with two other linear feedthroughs capable of push-pull rotation, enabled the mask to be sequentially changed without breaking the vacuum in the chamber, Fig (2.4).

2.4.7 Target Shield.

Mounted on the target arm vacuum plate was a linear feedthrough for the target shield. This target shield was made of pyrex. During sputtering the target shield was translated to a position adjacent to the unused targets. In this manner, back scattered, sputtered material was prevented from contaminating the surface of the targets not in use. It also provided a guard ring necessary during film deposition.

2.4.8 Chamber Shields.

To facilitate rapid cleaning of the sputtering module the four horizontal arms and the lower vertical arm were lined with fitted, removable glass liners. The main chamber liner was simply a pyrex

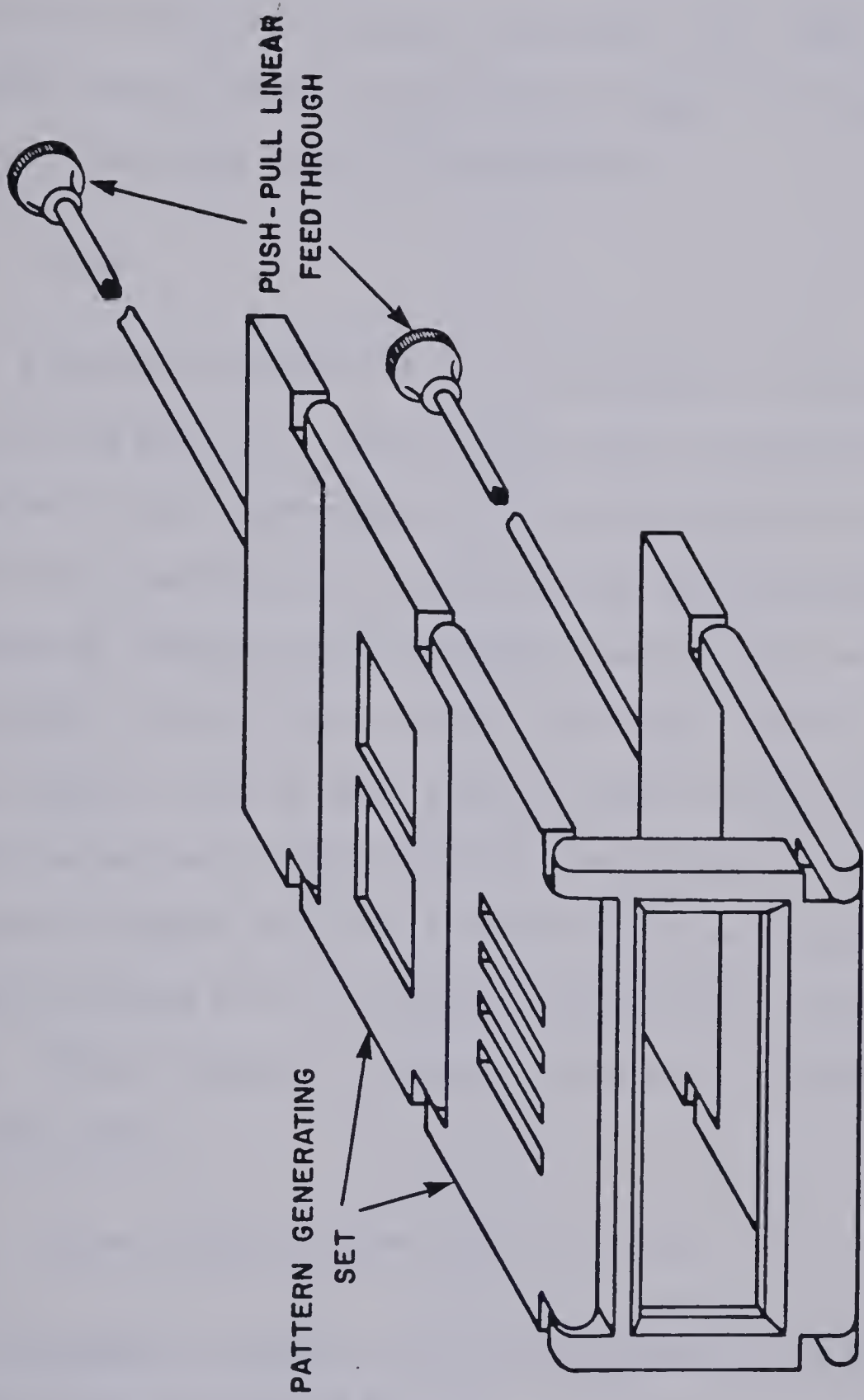


Fig. 2.4 Pattern Generation Masking Set.

cylinder with two, 1 inch diameter holes collinear with the plasma path. These apertures served to further confine the plasma and reduce the contamination from the discharge electrodes. This liner could not be separated into two smaller ones since it supports the target shield, previously mentioned, during its translation.

2.4.9 Probe.

A detailed structure of the rf/dc probe is illustrated in Fig. 2.5. Basically the device is a water cooled coaxial transmission line terminated in the target material. This design made it useful for rf as well as dc sputtering. It has a tapered termination which was found necessary for guiding the target probe as well as for the formation of an acceptable thermal contact between the target and the probe. The target drawbolt could be moved linearly along the probe axis. The drawbolt vacuum seal is located at the matching network end. This vacuum seal, between the inner and outer probe conductors, is of a swedge-lock nature and is located approximately two inches from the target. Finally the outer conductor vacuum seal is located on the probe arm vacuum plate.

2.4.10 Target Changing Assembly and Procedure.

A schematic diagram of the target mounted in the changing arm assembly is shown in Fig. 2.6.

The target itself was epoxied with "Cerac Hot Pressing Inc., Silver Epoxy" onto a copper backing plate in the back center of which was a hard soldered tapped brass insert. Above this insert a tapered seat was

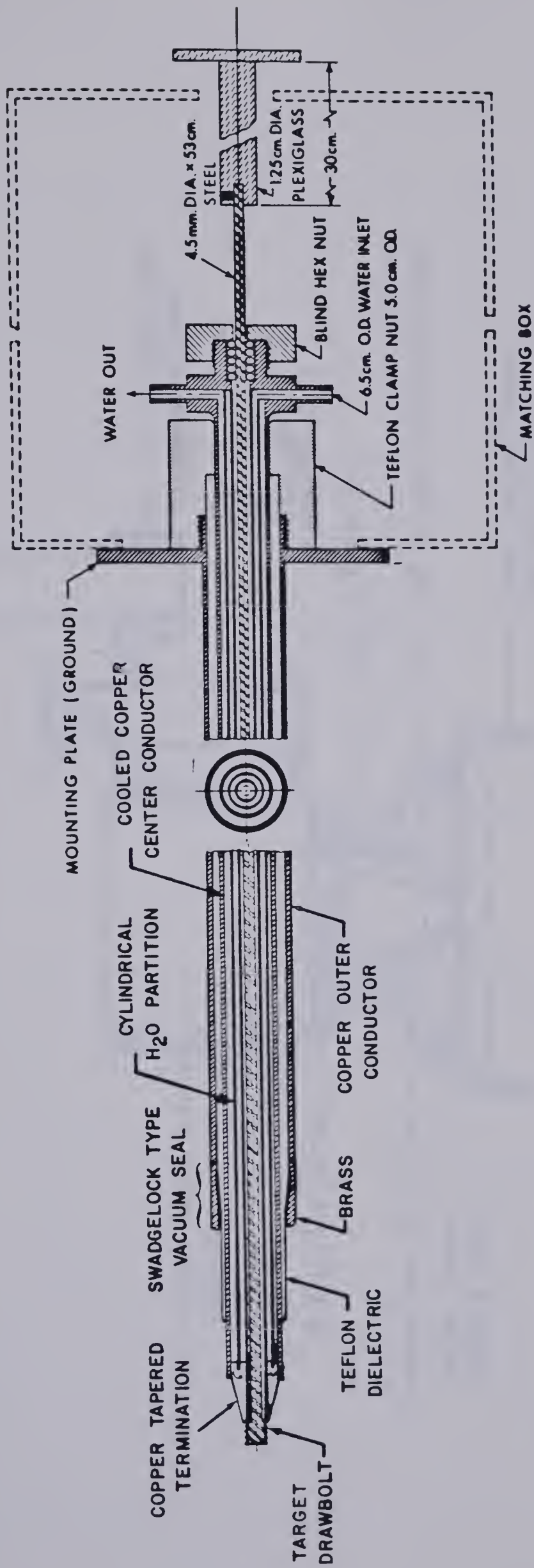


Fig. 2.5 A Detailed Structure of the rf/dc Probe.

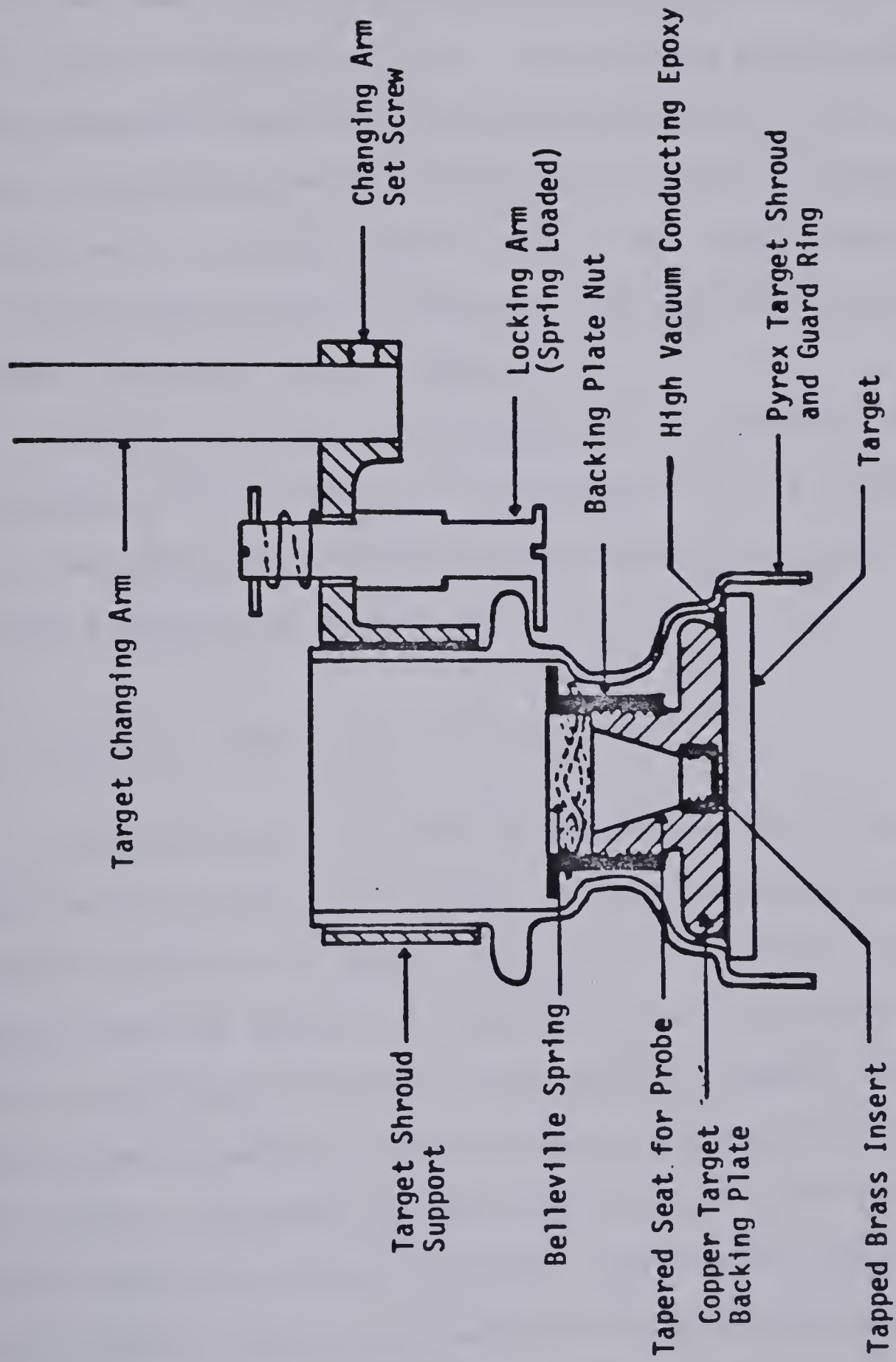


Fig. 2.6 Cross Section of the Target Changing Arm Assembly.

machined in the copper backing plate to identically match the probe termination taper. The backing material was spring loaded into the glass shroud using the backing plate nut. The insulating shroud guarded against sputtering from the target edge and the backing plate. It also served as the means by which the target was connected to the target changing arm. The target shroud was held in the target shroud support by a spring loaded, slotted, locking arm. By simply rotating this arm 180° a new target could be inserted.

Securing the targets to the probe was accomplished by centering the targets on the probe through the manipulation of the target changing arms, then changing the drawbolt in the threaded insert, and finally by again tightening the drawbolt nut.

2.5 SPUTTERING TARGET PRESS

A target press that allowed for the fabrication of sputtering targets with precise and easy control of their compositions and from virtually any powder (or powders) was specially designed. Initially, a graphite mould was built in an effort to produce "hot pressed" target pellets utilizing an induction heating approach. However, because of many problems encountered with the strength of the graphite mould along with problems associated with the extraction of the sintered pellets, these attempts were not very successful. Nevertheless, these problems were overcome by using a steel mould and utilizing a cold pressing approach instead, followed by a separate baking cycle. A schematic representation of the sputtering target press is given in Fig. 2.7.

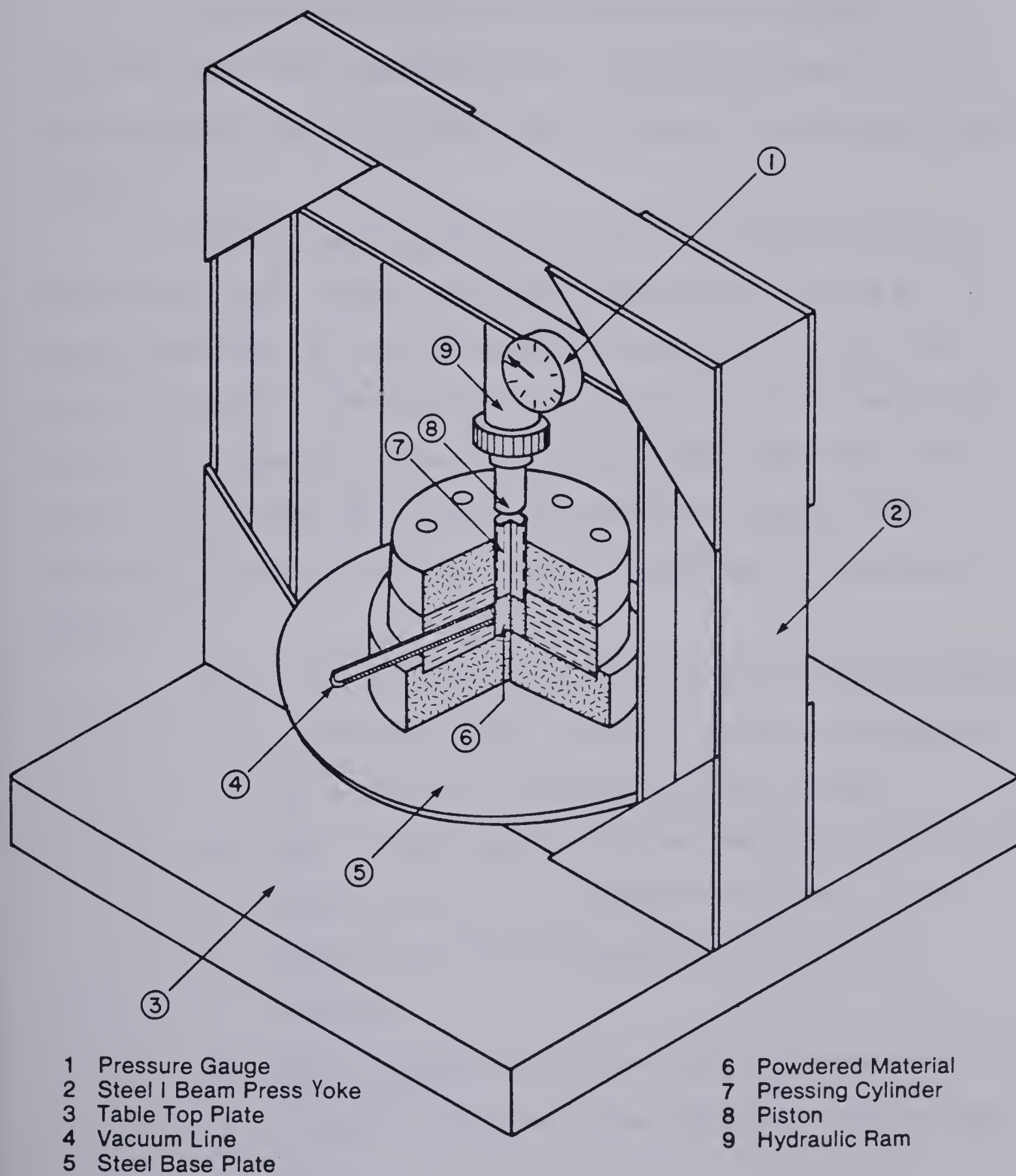


Fig. 2.7 Schematic Illustration of the Sputtering Target Press Designed.

The cold pressed pellets were solidified according to the following scheme.

i) Oxide powder pellets were fired in an air atmosphere in a type 51441 oven from Lindberg Division of Sola Basic Industries. The heating element used was nichrome wire, and the wall shielding was made of ceramic.

ii) Metallic powder pellets were heated in a Vacuum Industries Series 2100, vacuum furnace. The furnace was mounted on a C.H.A. Inc. pumping station and a steady state working pressure of 1×10^{-6} Torr was easily reached. The heating elements were tungsten rods which were individually connected to water cooled solid copper electrodes. Heat losses were minimized using dimpled molybdenum and stainless steel shielding surrounding the working volume. The furnace was operated as follows.

- (a) In the beginning the temperature was increased gradually to avoid the sudden increase in the pressure caused by the outgasing of the surfaces of the furnace.
- (b) When a steady state was reached, where the outgasing became negligible, the temperature was set at the desired value and the operation was switched to automatic.
- (c) When the heating process was over, the furnace was allowed to cool down to room temperature, before being vented.

It is worth emphasizing here that metal targets fabricated by the above procedure were generally characterized by exceptionally high quality.

CHAPTER 3

FABRICATION OF SEMICONDUCTING TiO_2 ELECTRODES BY dc SPUTTERING FROM A TiO_2 TARGET

3.1 PRIMARY INVESTIGATIONS

3.1.1 Deposition Parameters.

In order to determine the optimal operating conditions for the sputtering system and because of the many parameters involved in the sputtering technique, metallic films were first grown over a wide range of parameters such as gas pressure, flow rates, plasma beam current, target bias voltage, target to substrate distance, and substrate bias voltage, etc. It was found that,

i) A minimum working pressure for argon of about 5×10^{-4} Torr is necessary to maintain a stable gas discharge.

ii) A magnetic field of 50 Gauss is adequate for proper device operation. This magnetic field is utilized to collimate the plasma beam to ~ 2.5 cm diameter.

iii) A target to substrate distance of about 5 cm provides the highest deposition rate. Decreasing this distance causes the disappearance of the plasma beam since in this case the substrate table will be located between the thermionic cathode and the anode. However, because of the relatively low operating pressure, the mean free path of the sputtered atoms is relatively long and it was easy to maintain uniformity in film thickness.

3.1.2 dc Sputtering from a TiO_2 Target.

The sputtering target used throughout the course of these investigations was a 5 cm diameter by 6 mm thick, sintered TiO_2 pellet (99.97% pure) obtained from the Cerac Corporation. Sputtering was carried out in an argon plasma atmosphere (99.9% pure) and films were deposited on unheated glass substrates (standard microscope slides 75×25 mm). In situ thickness measurement was monitored by including in the system a Sloan Digital Thickness Monitor, Model DTM-2000. The density of the deposited film and the target were assumed to be the same for these measurements.

Films deposited from a TiO_2 target were highly insulating and the deposition rates achieved were relatively low. After sputtering, the target surface turned grey. This was apparently due to the reduction of the target surface and could be eliminated by presputtering the target for ~ 30 minutes in an argon plasma containing a relatively high partial pressure of oxygen.

The very low deposition rates achieved while dc sputtering from a TiO_2 target was probably due to the insulating properties of the target material. When the target is insulating, the dc accelerating potential is not applied directly to the target surface, which then prevents neutralizing of the positive charge that might accumulate on the target surface during ion bombardment.

3.1.3 rf Sputtering of TiO_2 .

The problem of very low deposition rates may be partly overcome by application of a radio frequency potential to the target backing

electrode. In this way, power can be fed into the plasma via the displacement current through the target material itself. Sputtering can now take place because the insulator will be alternately electron and ion bombarded. The positive charge which accumulates on the target surface during the negative (or sputter) portion of each cycle will be neutralized by electrons during the positive part of the cycle. Since electrons are more mobile than positive ions, more electrons are attracted to the front surface of the target during the positive half cycle than positive ions in the negative half cycle. The resultant electron current causes the target surface to acquire an increasing negative bias voltage during successive cycles until a stage is reached when the surface is positive for a short period of time. During this period enough electrons are attracted to the target surface to neutralize the positive ion charge accumulated during the rest of the cycle.

In these investigations the rf drive power was supplied by a tunable McDowell rf generator. This energy was transformed from the generator's 50 Ω output cable to a high impedance probe by a tunable π matching network contained in a shielded air cooled box at the probe head. Tuning of the matching network was accomplished through manipulation of a variable high power inductor and capacitor while monitoring the incident and reflected powers on a Philco Bidirectional power monitor.

3.1.4 Plasma Anodization of a Predeposited Titanium Layer.

The technique of plasma anodization was described in 1963 by Miles and Smith [3.1] . The principle underlying this method consists

of the oxidization of a metal or a semiconductor element in an oxygen plasma atmosphere. That is, if a metal or a semiconductor is biased positively w.r.t. the anode, it may be anodized with bombarding oxygen ions in the glow discharge.

We adopted this idea of plasma anodization in an attempt to overcome the problems encountered with films deposited by both dc and rf sputtering techniques. Since our main objective was to investigate the feasibility of fabricating inexpensive TiO_2 electrodes for use in photo-electrolysis cells, we restricted our efforts to plasma anodization of titanium thin films. The oxide films were fabricated as follows.

First, a titanium layer was deposited on a glass substrate by sputtering from a titanium metal target in an argon plasma atmosphere. Sputtering from the titanium metal target not only provided the titanium layer to be oxidized, but also provided a conducting path between the nonconducting glass substrate and the metallic substrate table. This connection was necessary for biasing the deposited film.

The substrate table was then positively biased w.r.t. the anode in an oxygen plasma atmosphere at a pressure of $\sim 5 \times 10^{-4}$, for different periods of time.

By utilizing this plasma anodization approach our results indicated that although the dc sputtering rate from a Ti metal target was approximately five times faster than that obtained from an oxide target, the plasma oxidization process was sufficiently slow that the overall deposition rate did not improve. In addition, another difficulty encountered with the metal film oxidation technique was the inconsistency in the final product. Here it was observed that many of the TiO_2 samples

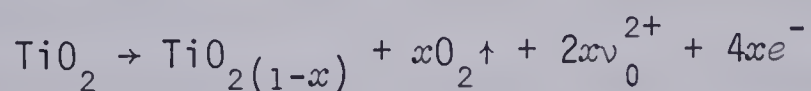
produced, developed a highly insulating layer at the surface, which again rendered them unsatisfactory for the application under investigation.

However, since the growth of the oxide film takes place due to the ionic and vacancy diffusion of either the metal or oxygen, or both, and depends upon the relative mobilities of ions in the oxide, it might have been possible to fabricate uniform oxide films by externally heating the substrate prior to, during, and after the oxidation process. This aspect was not investigated further, due to limitations imposed by the sputtering system at that time.

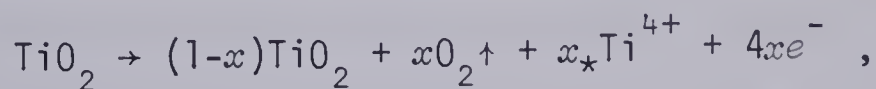
3.2 ELECTRODE FABRICATION BY SPUTTERING FROM A REDUCED TiO_2 TARGET

3.2.1 Introduction.

TiO_2 is an insulator. However, by heating a TiO_2 specimen (solid or powder) in a reducing atmosphere (vacuum, hydrogen, or CO) TiO_2 changes from an insulator to an *n*-type semiconductor [3.2]. The origin of the donor centers is still in dispute and two reducing reactions have been thought possible. These are:



or



where ν_0 indicates an oxygen vacancy and $_*\text{Ti}$ indicates an interstitial titanium atom. Both can trap one or more electrons.

A large number of papers have been published concerning the question; which of these reactions is most likely to occur? Initially it was concluded that the oxygen vacancy is the dominant point defect [3.3, 3.4]. Hurlen [3.5] was probably the first to mention the possibility of occurrence of isolated Ti^{3+} interstitials in the lattice. Kosfstad [3.6] presented a model in which oxygen vacancies predominate at low reduction temperatures while the interstitial titanium ions are prevalent at higher reduction temperatures. Recently Iguchi et al. [3.7] have shown that besides the interstitial titanium ions oxygen vacancies are also introduced at reduction temperatures $T_r > 600^\circ\text{C}$.

3.2.2 Experimental.

Initially the target used in these investigations was an insulating TiO_2 target supplied from the Cerac Corporation. To make it semiconducting, the target was heated in a hydrogen atmosphere at a pressure of $\sim 1 \times 10^{-5}$ Torr and a temperature of 600°C for ~ 6 hours. In this way, the target turned into a blue greyish color which is apparently due to oxygen deficiency.

Subsequently, we have produced equally acceptable reduced TiO_2 targets by cold pressing a 200 mesh TiO_2 powder at 8000 psi for 4 hours. These pellets were then reduced in one of the following procedures:

i) The cold pressed pellet was heated in air at 1000°C . As a result, the initially soft and delicate cold pressed pellet was transformed into a strong ceramic like material. These pellets were then heated in a hydrogen atmosphere as before.

ii) The cold pressed pellet was heated in vacuum for ~ 6 hours at a temperature of 1000°C and a pressure of $\sim 1 \times 10^{-6}$ Torr. This vacuum heating provided the simultaneous solidification and reduction of the pellet.

Sputtering was carried out in a pure argon plasma atmosphere at a pressure of 5×10^{-4} Torr. Initially, the ohmic contact required for the back surface of the deposited semiconducting films was provided by depositing a thin layer of gold on the glass substrate prior to TiO_2 deposition; later, as outlined in the Results, a titanium backing layer was used instead. The semiconducting oxide film was then grown on this metallic layer by sputtering from a reduced TiO_2 target through an aperture of 1 cm^2 . The size and position of this aperture were chosen such that a uniform film thickness could be obtained. In order to obtain the highest possible purity in electrode fabrication, all targets were presputtered for 30 minutes before any of the films were actually deposited on the substrate.

Under the above conditions, the deposition rate achieved was about 1000 \AA/hr . Although this deposition rate was about three times higher than the deposition rate obtained by sputtering from an insulating TiO_2 target, the deposition rates of our sputtering system were still relatively low. However, this was not of major concern at this stage of the investigation, and consequently no specific attempts were made at improvement. Our primary interests in this study were concerned with the physical and electrical properties of the semiconducting films produced by a particular sputtering approach.

3.2.3 Measurements.

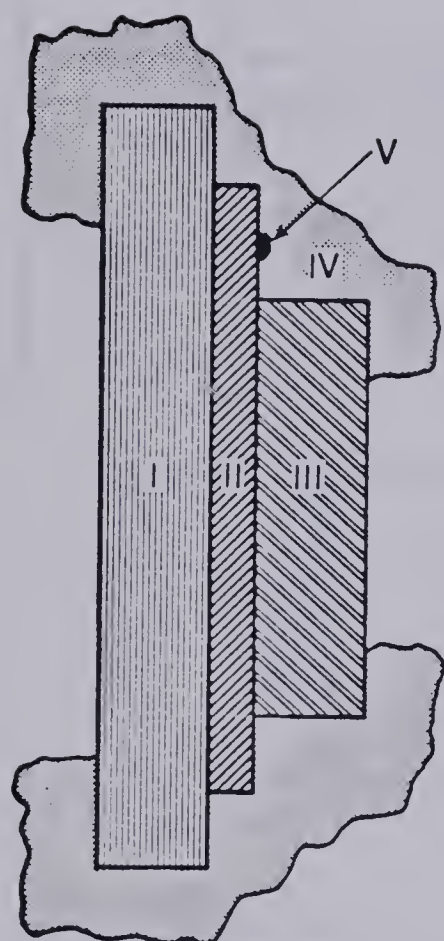
For the study of electrode performance for photoelectrolysis, a copper wire was attached to the metallic backing layer using a conducting silver paint. The metallic backing layer, copper wire and a portion of the semiconducting electrode were then masked using epoxy, leaving an active area for contact with the electrolyte, Fig. 3.1. The electrolyte used was 1 M NaOH and the counter electrode was simply platinum foil (10 cm²).

The spectral response of these electrodes (short circuit current versus wavelength) was determined using the experimental setup shown in Fig. 3.2. A 400-1000 Watt Osram Xenon lamp and a Spec "Minimate" grating monochromator were used for this purpose. The infrared radiation was eliminated using a distilled water filter installed at the output of the light source. The light intensity was measured at the exit slit of the monochromator using a Pyroelectric Radiometer Model PR 200.

The short circuit current was determined by measuring the voltage drop across a resistance of known value. Film crystal structure was examined utilizing a modified Debye Scherre X-ray diffraction technique.

3.3 RESULTS

Thin film semiconducting electrodes prepared by dc sputtering from a reduced TiO₂ target onto gold backing films were generally characterized by poor mechanical properties. That is, these films peeled off either during the deposition process itself or mechanical failure took place in the electrolyte (without illumination). On the



- I Glass Substrate
- II Gold or Titanium Backing Layer
- III Semi-Conducting Film
- IV Epoxy
- V Copper Wire

Fig. 3.1 Electrode Configuration.

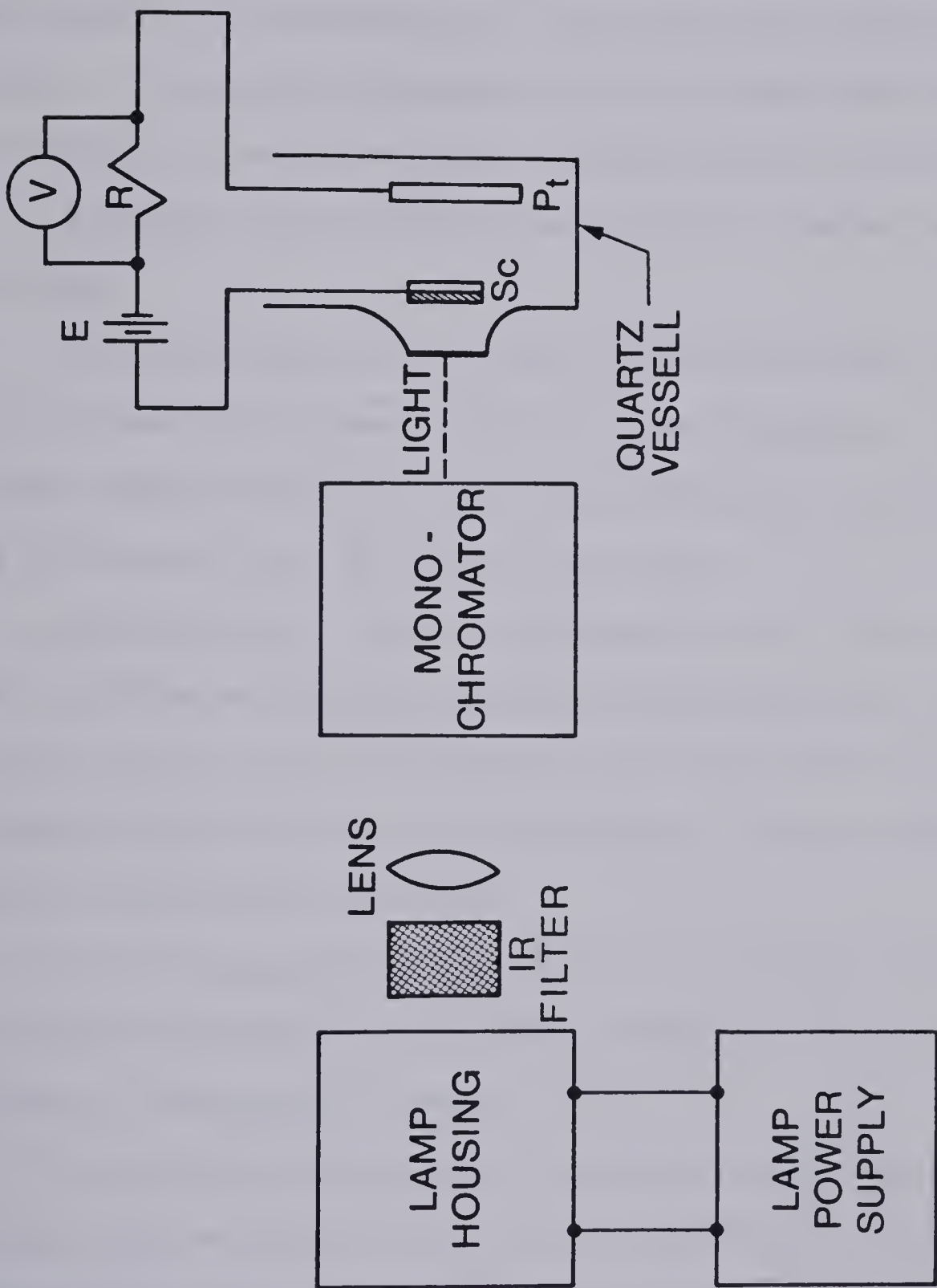


Fig. 3.2 Experimental Setup for Photoresponse Measurements.

other hand, films deposited on titanium backings (deposited on glass substrates) were mechanically better. X-ray diffraction studies for these films did not, however, show any crystal structure. Consequently, when tested for photoelectrolysis, these electrodes showed very low response. In addition, prolonged immersion of these electrodes in the electrolyte (in the dark) eventually caused peeling of the films.

A somewhat speculative explanation of the observed results is as follows.

i) Since bonding of many metal films to glass substrates occurs via an intermediate layer of oxide at the metal/substrate interface [3.8] the weak adherence of gold films to glass substrates may be attributed to a low chemical activity of gold with oxygen.

ii) The internal stresses that develop in the film during its growth could be sufficient to overcome the gold/substrate interfacial adhesion and thus result in peeling of the film, especially if adherence is only due to physical adsorption. This was probably the case for the gold/glass interface.

iii) The mechanical failure of films deposited on titanium backings and unheated substrates may have been a stress relief phenomenon occurring by means of fracturing or flaking.

iv) The poor photoresponse of electrodes deposited on titanium backings could be possibly due to either the amorphous structure of the semiconductor and/or insufficient film thickness.

The above results implied that the key to understanding the performance of sputtered thin film electrodes in photoelectrolysis

cells is to be able to reproduce polycrystalline thin films that adhere strongly to the glass substrate.

This being the case, an extensive study on the influence of deposition parameters and reactions which take place at the target surface, in the gas discharge or at the substrate was undertaken. This study revealed that the substrate temperature plays a dominant role in determining the stability and structure of the deposited films. It was therefore felt that a good way to overcome the above problems may be by externally heating the substrate during film deposition.

The effect of the substrate temperature on the film properties can be inferred as follows [3.9].

i) An increase in the substrate temperature may promote film adherence to the substrate.

ii) Increasing the substrate temperature may decrease the sticking probability of the inert gas and accordingly may decrease its entrapment in the growing film. The entrapment of the inert gas may be one of the possible reasons for the poor mechanical properties of the films deposited on unheated substrates.

iii) An increase in the substrate temperature will increase the surface diffusion in the growing films. This will probably decrease the stresses induced in the films during their growth.

iv) The increase in the substrate temperature may improve the film crystalline structure of the deposited films by:

- a) aiding the desorption of the adsorbed surface contaminants;
- b) providing sufficient kinetic energy for the already deposited material for annealing, thus structure

- reordering of amorphous films may be possible;
- c) enhancing recrystallization due to the coalescence of islands by increasing surface and volume diffusion;
 - d) post deposition annealing may increase the crystallite size.

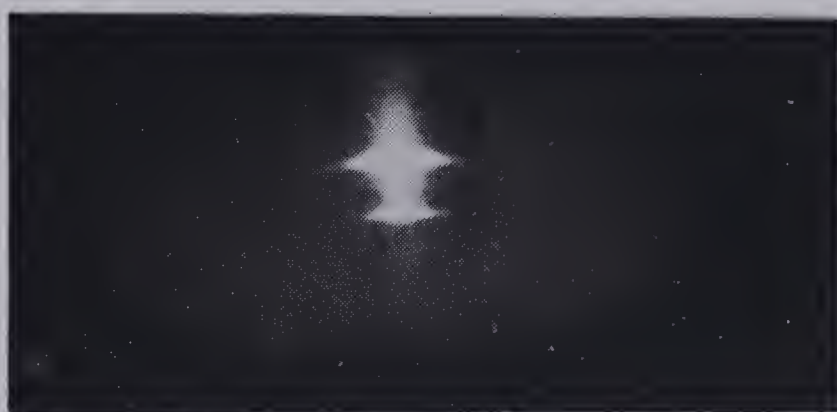
By externally heating the substrate to 250°C during film deposition it became possible to fabricate electrodes of any desired thickness on titanium backing films without experiencing any mechanical failure. These films were normally hard, dark and very adherent to the glass substrates. Adhesion was greatly promoted when films were deposited on a layer by layer basis and post annealed at ~ 350°C after deposition of each layer. X-ray diffraction studies indicated a change in film structure from an amorphous to a polycrystalline state by heating the substrate during and post film deposition, Fig. 3.3.

3.3.1 Cell Photoresponse.

Electrodes prepared by depositing on externally heated substrates, when tested for photoelectrolysis, were chemically stable and no mechanical failure has taken place thus far. These electrodes showed a considerably higher photoresponse compared to that exhibited by films deposited on unheated substrates. That is, when the semiconductor was illuminated under short circuit conditions (the Pt and the TiO_2 electrodes connected together), currents were detected although there was no hydrogen evolution. In addition, application of a positive bias to the TiO_2 electrode (~ 0.35 V) resulted in a higher photocurrent and gasses were evolved at both electrodes.



unheated substrate



$T_S = 250^\circ\text{C}, \theta = 16^\circ$



$T_S = 250^\circ\text{C}, \theta = 15^\circ$

Fig. (3.3)

X-ray diffraction photographs of d c sputtered reduced TiO₂ electrodes.

The spectral response of these electrodes was investigated and a main absorption edge of ~ 400 nm was obtained, Fig. 3.4. This corresponds to an energy gap of ~ 3.1 eV. It is worth emphasizing that these results were reproducible and that the main absorption edge is essentially the same as that reported elsewhere for bulk TiO_2 materials [3.10]

The improved photoresponse of films deposited on heated substrates, may be attributed to a number of factors. Firstly, the crystallization effect, where it is expected that charge carrier mobility, lifetime and hence diffusion length will be greatly increased as the film goes from the amorphous to the crystalline state [3.11]. Secondly, the thickness effect, since the stresses developed during film fabrication on unheated substrates hindered the possibility of fabricating reasonably thick electrodes. It is possible that films deposited on heated substrates were thick enough to provide a space charge region essential for charge carrier separation. Thirdly, it is possible, by heating the substrate during and post film deposition, that the titanium backing layer extracted oxygen from the oxide film (or partly diffused into it) resulting in a highly reduced oxide layer at the metal/oxide interface. In this manner a back surface field, which opposes the motion of minority carriers towards the back surface, was automatically built in [3.12]. As a result, recombination at the back surface was reduced and the short circuit current was increased.

3.3.2 Effect of Light Intensity.

The excess carrier concentration of minority carriers in the surface region of a semiconductor electrode depends in a complicated way on the light intensity, the absorption coefficient, the quantum yield for

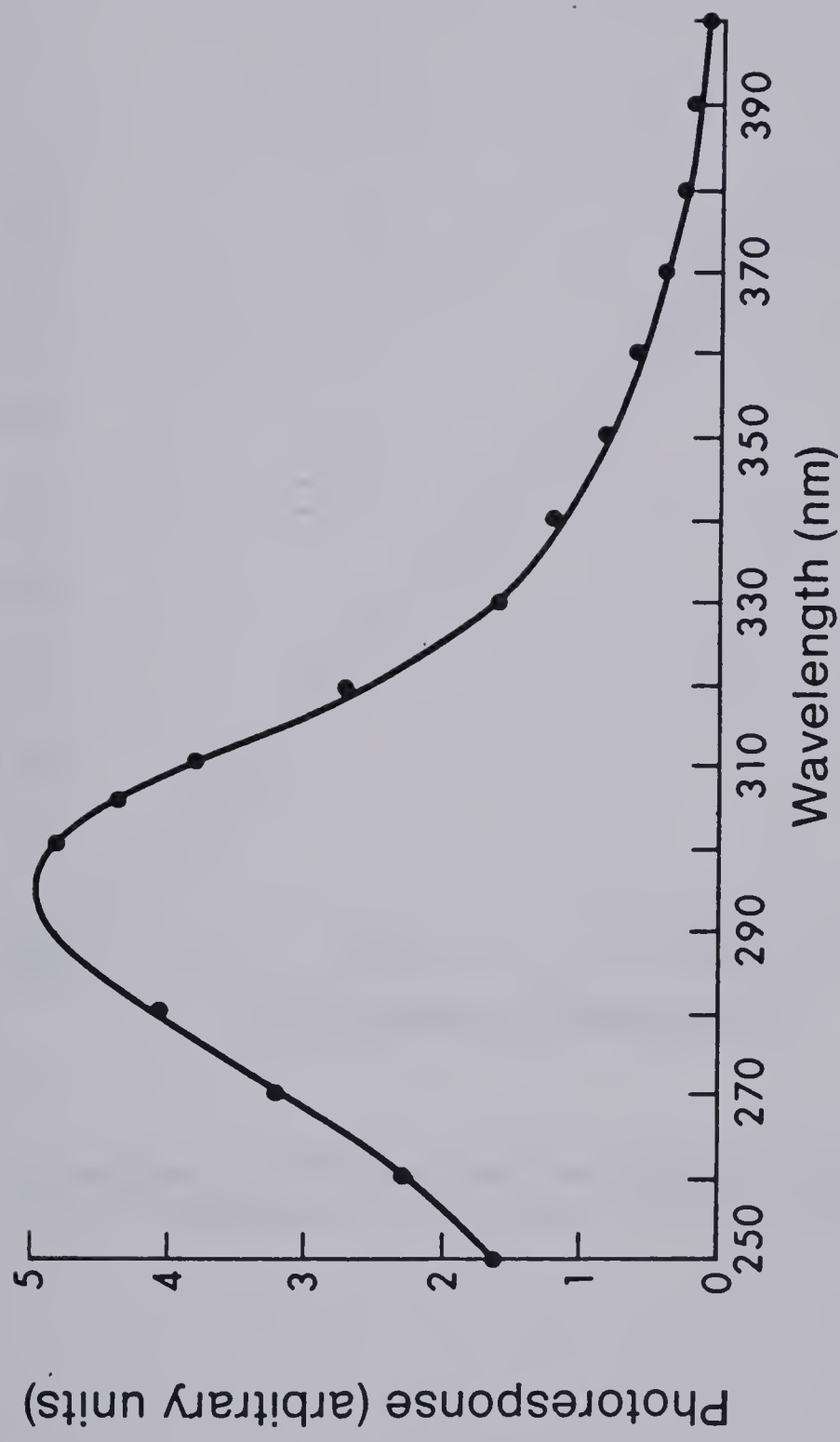


Fig. 3.4 Spectral Response of a Sputtered TiO_2 Electrode in a Water Photoelectrolysis Cell.

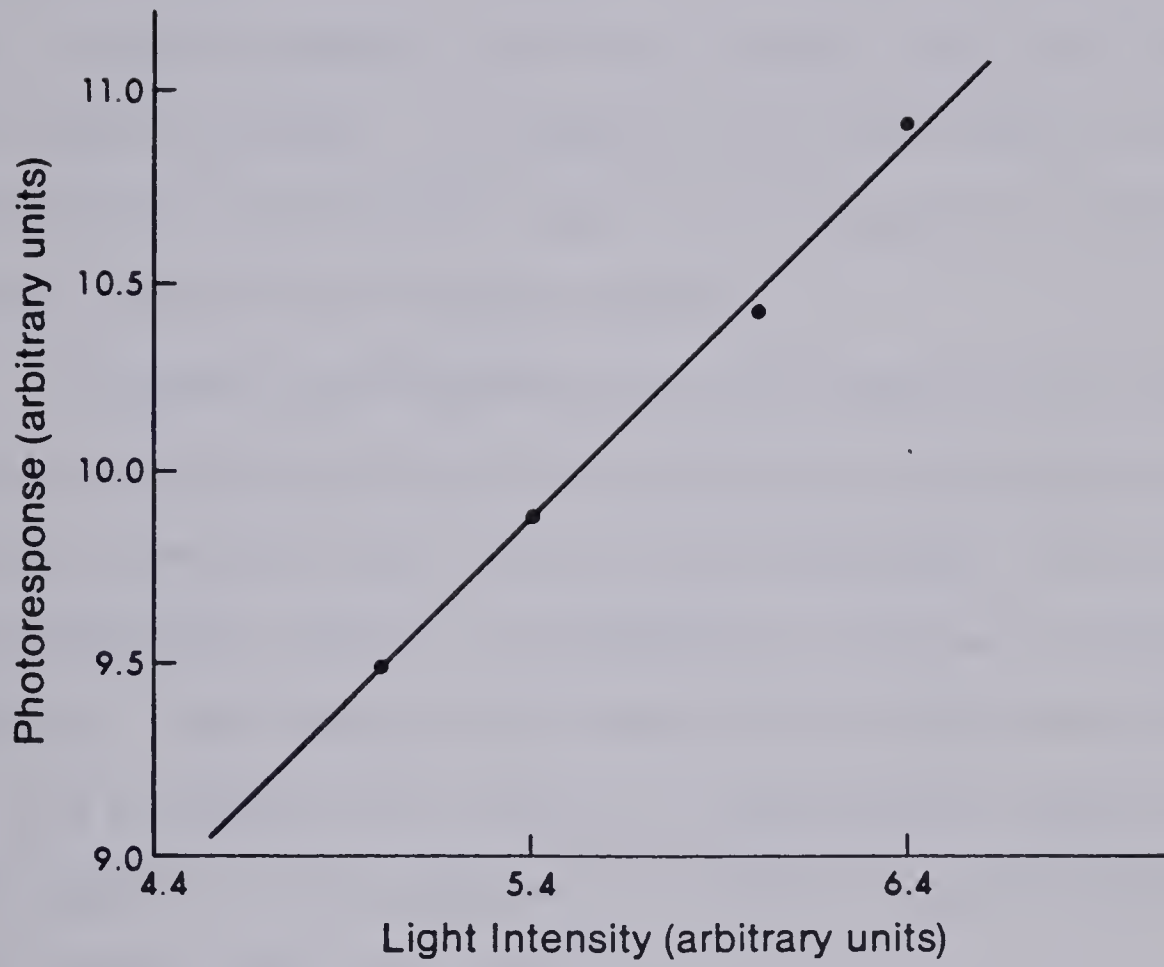


Fig. 3.5 Dependence of Photocurrent on Light Intensity for Sputtered TiO_2 Electrodes at Low Levels of Illumination.

electron-hole pair generation, recombination rates in the space charge region and on transport phenomena. For low enough light intensities, all kinetics can be approximated by linear equations and the result is that the surface concentration of minority carriers (and accordingly, the photocurrent) varies linearly with light intensities. At higher light intensities however, nonlinear processes take control and finally one reaches saturation. At saturation the band bending in the space charge layer is drastically reduced and the potential distribution is close to that of the flat band situation.

In order to check whether the rate limiting step in cell operation was the generation of electron-hole pairs, the dependence of the short circuit current on light intensity was investigated. The cell was illuminated by monochromatic radiation corresponding to the peak of its spectral response. These investigations showed that for low levels of illumination (up to 3 m Watt/cm²), the relation is approximately linear, Fig. 3.5. This behavior is to be expected if electron-hole pair generation is the rate limiting step [3.13, 3.14].

3.3.3 Flat Band Potential.

As was mentioned in Chapter 1, the flat band potential V_{FB} of the semiconductor electrode is probably the most important parameter in determining the combined energy band diagram of a photoelectrochemical cell. The flat band potential determines the conditions required for the semiconductor to promote a particular semiconductor reaction.

The best technique to determine the flat band potential is from capacitance measurement and the graphical extrapolation of the linear

part of the Schottky-Mott relation $1/C_{sc}^2 = \frac{2}{q\epsilon N_D}(V - V_{FB} - \frac{kT}{q})$ to the intersection point with the potential axis V . However, this method is not always applicable. The validity and limitation of this technique can be explained with the help of Fig. 3.6 as follows [3.15, 3.16], where C_M is the capacitance of the metal electrode interface, C_H is the Helmholtz double layer capacitance at the semiconductor/electrolyte interface, and C_{ss} is the capacitance due to surface states.

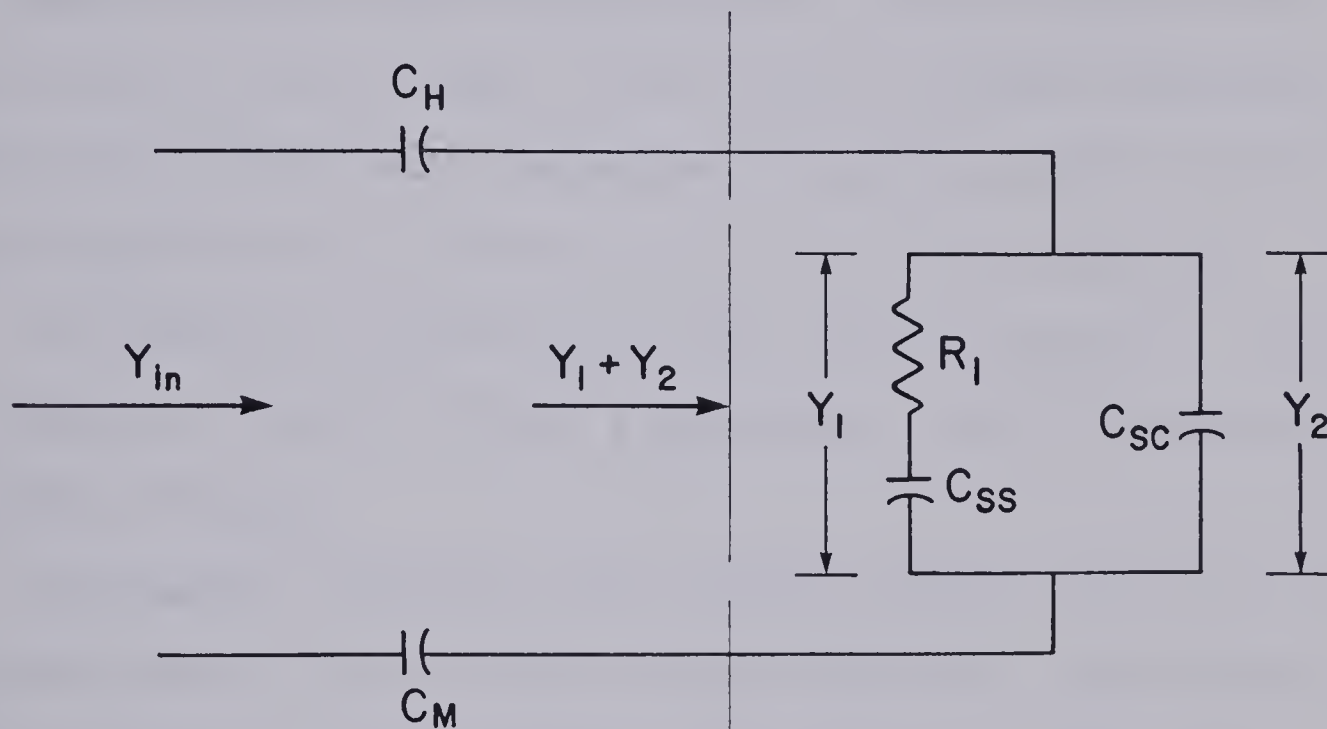


Fig. 3.6 Equivalent Circuit of the Semiconductor Electrode in a Photoelectrochemical Cell.

The complex admittance of the semiconductor electrode Y_{in} is given for high values of C_H and C_M by,

$$Y_{sc} = Y_1 + Y_2 .$$

That is,

$$Y_{sc} = j\omega C_{sc} + \frac{j\omega C_{ss}}{1 + R_1(j\omega C_{ss})}$$

which takes the form

$$Y_{sc} = j\omega C_{sc} + \frac{j\omega C_{ss}}{R_1^2 \omega^2 C_{ss}^2 + 1} + \frac{R_1 \omega^2 C_{ss}^2}{1 + R_1^2 \omega^2 C_{ss}^2} . \quad (3.1)$$

According to Eqn. 3.1 the imaginary part of the complex admittance of the interface can be represented by a single capacitor only at high frequencies where the second term on the R.H.S. is negligible. Therefore, the measurement of the flat band potential from capacitance measurement is valid only at high frequencies. At high frequencies the semiconductor electrode can be represented as a frequency independent capacitor connected in series with a resistor. How high this frequency must be will depend on the particular semiconductor, surface preparation and availability of surface states. That is why the frequency dependence of the cell impedance must be determined in order to specify the frequency range in which the interface can act as a single capacitor.

This aspect was investigated in the frequency range of 1 - 20 kHz and, indeed, our results did show a dependence of the cell impedance on measurement frequency.

Consequently, because of this and test equipment limitations, the flat band potential has not been precisely determined. Nevertheless, a flat band potential of approximately -0.85 volts (w.r.t. SCE) was obtained when measured using a dc biased HP 4260 universal bridge at 1 kHz. This value is somewhat higher than that reported for bulk TiO_2 [3.17].

3.4 CONCLUSION

dc sputtered thin film TiO_2 electrodes showed satisfactory performance in water electrolysis cells. Thin film electrodes prepared by sputtering from a reduced TiO_2 target, which was fabricated utilizing a simple cold pressing technique, showed photoresponse characteristics similar to those of single crystal TiO_2 and other polycrystalline TiO_2

electrodes. Films deposited on heated glass substrates and titanium metal film backings were chemically stable and did not exhibit any photodecomposition.

The mechanical and chemical stability of the sputtered electrodes, along with the simplicity of the sputtering target fabrication technique, suggest that sputtering could be a potentially viable method for producing thin film electrodes for photoelectrochemical applications in general and for water electrolysis in particular. This sputtering technique allows for the possibility of fabricating crystalline films from virtually any amorphous solid or powdered material and on amorphous glass substrates.

Further investigations on the effect of target reduction conditions (temperature, atmosphere and period), along with the influence of the sputtering conditions (in particular the substrate temperature) on the properties of the sputter deposited electrodes, are required.

CHAPTER 4

REACTIVE SPUTTERING AND ITS APPLICATION FOR FABRICATING THIN FILM SEMICONDUCTING TiO_2 ELECTRODES

4.1 INTRODUCTION

Our previous experience in the fabrication of thin semiconducting TiO_2 films by a dc sputtering technique (from a reduced TiO_2 target), coupled with further studies of plasma anodization (of a predeposited Ti film), ultimately prompted our investigations of another alternative fabrication process which conceivably might permit altering and controlling film properties during deposition. This is the reactive sputtering technique which is considered in this chapter.

Reactive sputtering is the intentional inclusion of a reactive gas (oxygen in this case) in the sputtering plasma atmosphere, in order to alter or control film properties. Thus, the synthesis of a target metal into an oxide is achieved by sputtering the target in a plasma containing a partial pressure of oxygen. The actual proportions of the oxygen to the inert gas in the plasma required to produce films of any particular property are dependent on the sputtering conditions and the particular sputtering system.

Because of the many possible permutations and combinations of the reactive sputtering conditions, and since our main objective in this area of reactive sputtering was to investigate the feasibility of fabricating thin film semiconducting TiO_2 electrodes for water electrolysis, an understanding of the kinetics of reactive sputtering and a basis for

predicting the reactive plasma conditions needed for fabricating such films is necessary.

This being the case, a brief review of the theory of reactive sputtering from a metallic target, together with the results of our investigations of the kinetics of film growth, is given in Part I of this chapter. In Part II, application of reactive sputtering for fabricating thin film semiconducting TiO_2 electrodes is considered in detail.

PART I

4.2 MECHANISM OF REACTIVE SPUTTERING

The exact mechanism by which oxides are formed during reactive sputtering from a metallic target is not clearly understood as the precise time of reaction has not been determined [4.1]. The oxidation reaction could occur at the target, in the gas phase, on collision with the substrate or by diffusion and reaction following film deposition on the substrate.

The possibility of reaction in the gas phase appears to be quite limited for the following reasons: i) because of the low pressures involved, the mean free path of the sputtered atoms is relatively long and the number of possible collisions between these atoms and the reactant molecule is negligible and; ii) since some means for the release of the reaction as well as the kinetic energy of atoms would be necessary to prevent spontaneous decomposition [4.2].

At low partial pressures of oxygen, and because of the long mean free path at the pressures involved, the reaction is most likely to occur at the substrate.

4.2.1 Target Oxidation and Deposition Rate.

At higher pressures of oxygen, a reaction at the metallic target is more likely. Several investigators [4.3, 4.4] have found that an abrupt decrease in the deposition rate takes place during the sputtering of a metallic target in an oxygen-argon plasma atmosphere. Such an abrupt decrease in the deposition rate (or sputtering rate) has been considered to be related to a chemical reaction between the target surface and the reactive gas.

Heller [4.5] presented a model in which the rapid decrease in the sputtering rate is explained on the basis of a relationship between the oxidation rate and the sputtering rate at the target surface, for various partial pressures of oxygen.

According to the model, the sputtering process is strongly influenced by the formation of an oxide layer on the target surface. For the oxide formation the ratio ($\xi = (\text{sputtering rate})/(\text{oxidation rate})$) as a function of the oxide film thickness is decisive. No oxidation of the target is possible if $\xi > 1$. If $\xi < 1$, a steady state is reached where an oxide layer with constant thickness exists on the target surface.

In the steady state of sputtering there is a critical pressure of oxygen $P_{O_2}^*$, below which the target surface is free of oxide and the sputtering rate is constant, and above which oxidation of the target proceeds in combination with a decrease of the sputtering rate. The critical oxygen pressure $P_{O_2}^*$ is a function of the sputtering parameters.

Abe and Yamashina [4.6] presented a model in which they offered an explanation for the deposition rate of films during reactive sputtering using computer simulation of the processes occurring at the target

surface. However, they stated that further work on the nature of the chemical compounds formed on the target surface is required.

4.3 EXPERIMENTAL

A steady state working pressure for the sputtering system was achieved by regulation of the gas admittance rate at a preset pumping speed. For the reactive sputtering gas mix, a precision M.K.S. Inst. Inc. baratron electronic pressure meter was used. The partial pressures of oxygen and argon were controlled by pressure regulators and variable leak valves. The two gasses were thoroughly mixed before being admitted into the chamber. The total pressure of argon and oxygen was kept at a constant value, 5×10^{-4} Torr. Cleaning of the target surface was carried out before each run by presputtering for 45 minutes in pure argon.

Film deposition experiments were conducted using quartz and standard microscope slides as substrates. Film thickness was measured by measuring the average height of material deposited through a 1 cm^2 mask onto 2.5×2.5 preweighted quartz substrates utilizing an interference method. The density of reactively sputter deposited films was determined from weight change and thickness measurement.

Base electrodes for film resistance measurement were provided by first depositing four equally spaced titanium metal strips on the glass substrate. The oxide film was then deposited on top of these strips by reactive sputtering from a Ti metal target.

Optical spectra in the UV and visible regions were determined using a PYE-UNICAM spectrophotometer, Model No. 1700.

4.4 RESULTS

The effect of oxygen concentration on the deposition rate of titanium suboxide films sputtered from a 2.5 cm (diameter) and 7 mm (thick) metal target onto glass substrates can be seen in Fig. 4.1.

A significant transition in the deposition rate is observed in an oxygen partial pressure range from $\sim 1.5 \times 10^{-5}$ to $\sim 2.5 \times 10^{-5}$ Torr. In this range of oxygen partial pressure, the deposition rate falls sharply from $\sim 70 \text{ Å}/\text{m}$ to $\sim 14 \text{ Å}/\text{m}$. The deposition rate is almost independent of the oxygen partial pressure for $P_{O_2} < P_{O_2}^l$ and $P_{O_2} > P_{O_2}^u$.

Optical measurements in the UV and visible regions of the spectrum for films deposited at oxygen partial pressures higher than $P_{O_2}^l$ showed no absorbance in the visible range. These measurements revealed a main absorption edge of $\sim 3.1 \text{ eV}$, Fig. 4.2. On the other hand, films deposited in the low partial pressure range of oxygen were metallic in appearance and no optical measurements were carried out for these films.

X-ray diffraction studies indicate polycrystalline structures for films deposited in low as well as high partial pressures of oxygen, Fig. 4.3. The type of crystal structure was not investigated since this is beyond the scope of this study.

4.5 DISCUSSION

The results quoted above indicate that in the reactive sputtering of titanium, there is an oxygen partial pressure range, $P_{O_2}^l < P_{O_2} < P_{O_2}^u$ in which the deposition rate falls sharply by a factor of about five. Since the sputtering rate depends strongly on the sputtered species and is usually

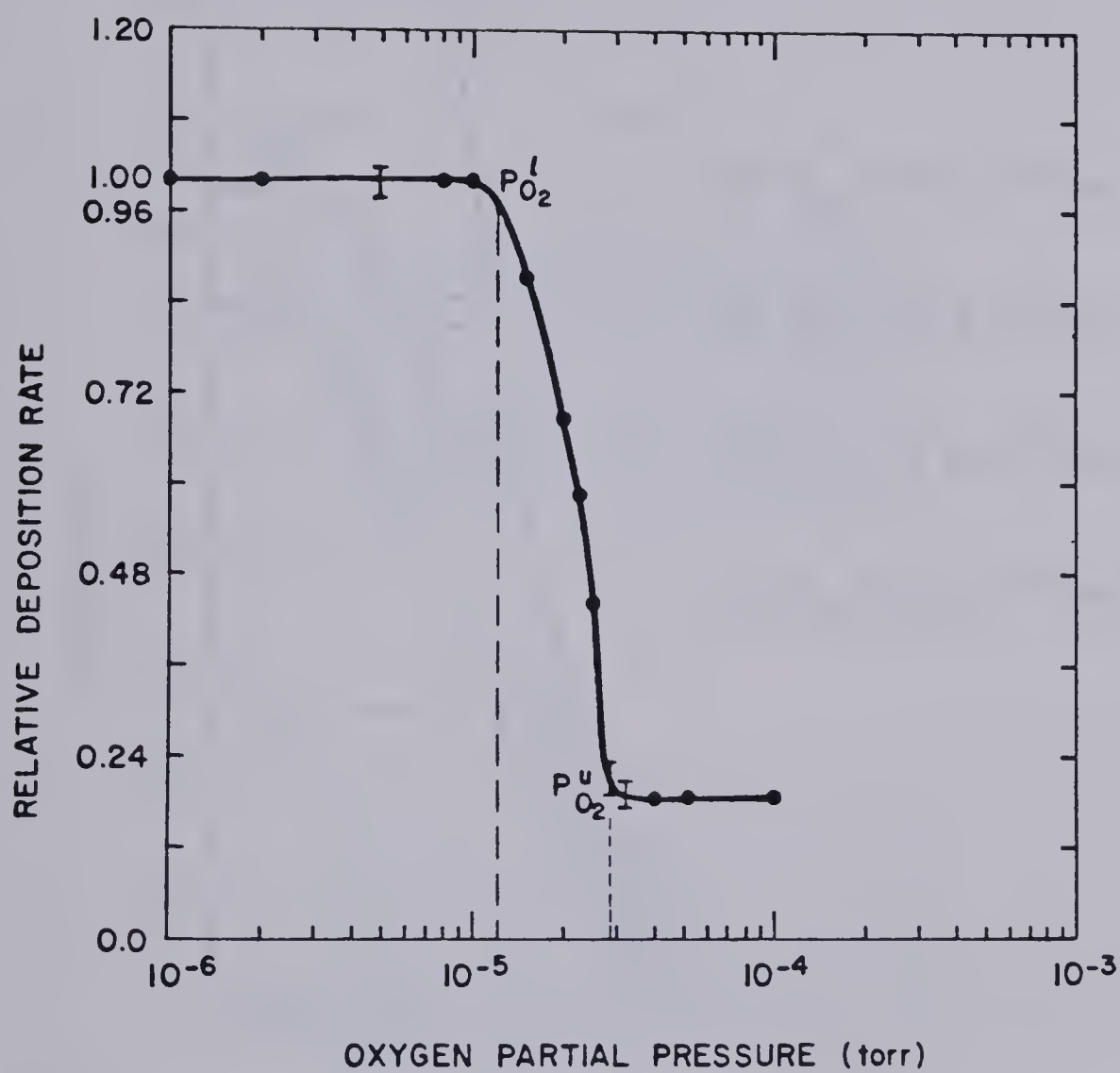
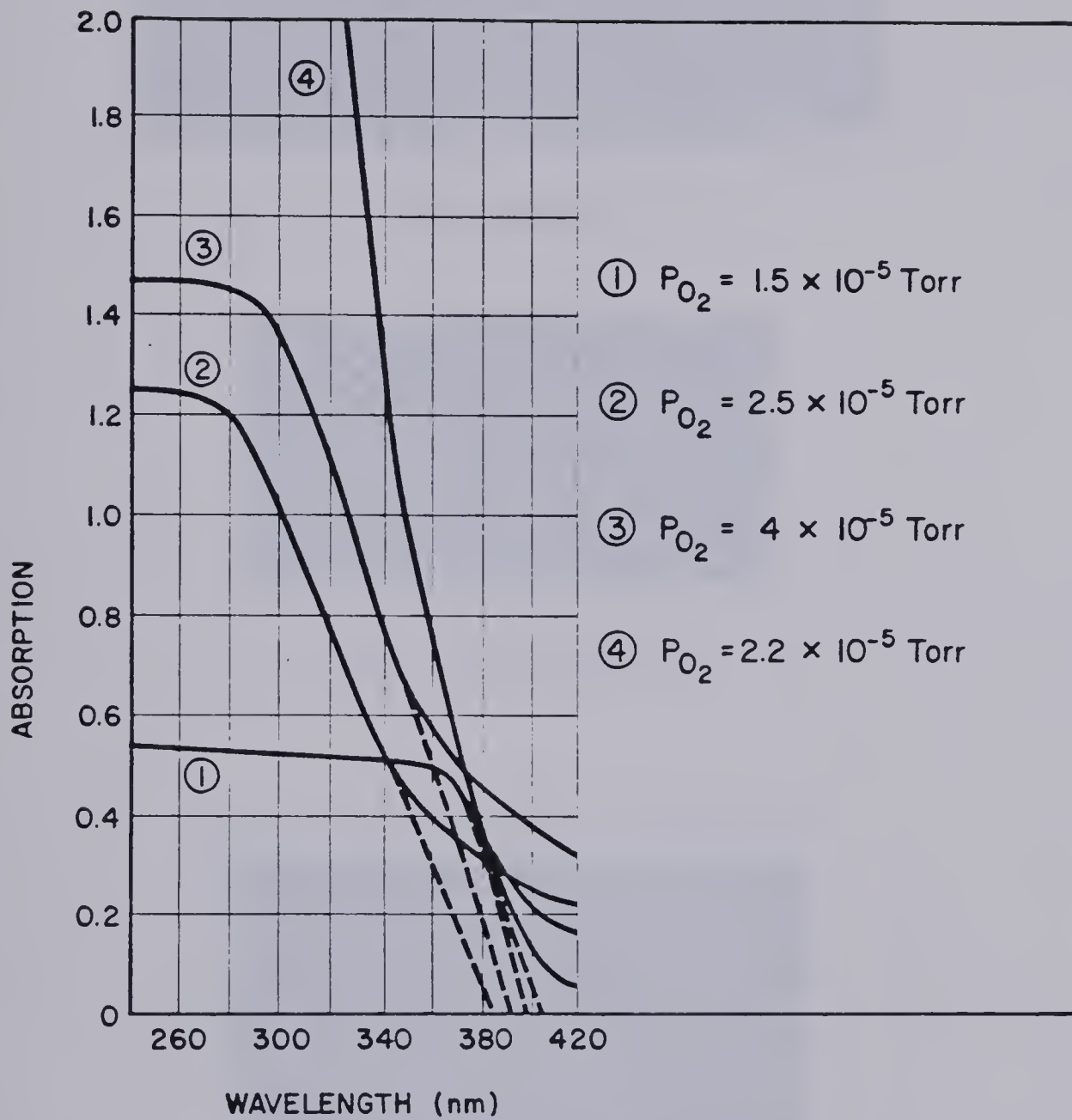
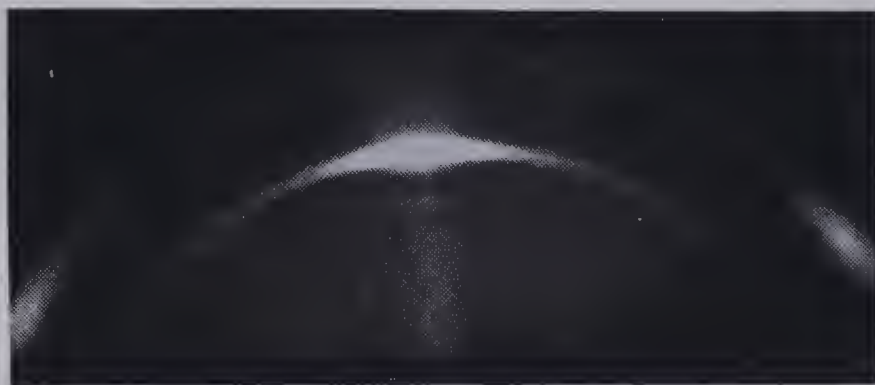


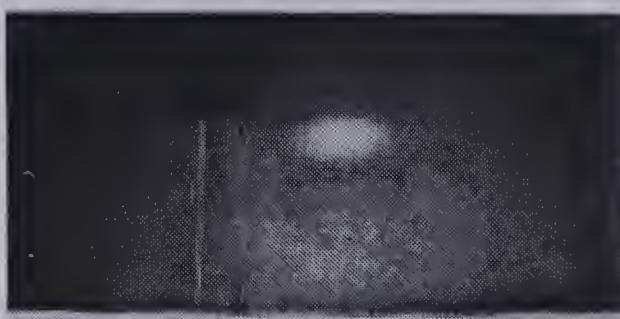
Fig. 4.1 Effect of Oxygen Partial Pressure on the Deposition Rate.



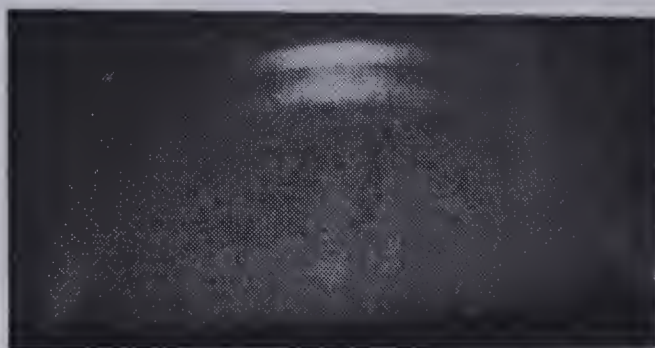
4.2 A UV Spectrograph for TiO_x Thin Films Deposited under Several Oxygen Plasma Conditions.



No oxygen



$P_{O_2} = 5 \times 10^{-6}$ Torr



$P_{O_2} = 7 \times 10^{-6}$ Torr

Fig. (4.3)



$$P_{O_2} = 1 \times 10^{-5} \text{ Torr}$$



$$P_{O_2} = 2 \times 10^{-5} \text{ Torr}$$



$$P_{O_2} = 1 \times 10^{-4} \text{ Torr}$$

Fig. (4.3)

X-ray diffraction Pattern of TiO_2 thin films deposited by reactive sputtering of Titanium under different oxygen plasma conditions ($T_S = 250^\circ\text{C}$)

lower for oxides than for pure metals, the magnitude of the deposition rate observed in the pressure range $0 < P_{O_2} < P_{O_2}^L$, indicates that the titanium target was free of oxides. In this range, the flux of titanium incident on the substrate surface will be equal to the sputtered flux of a metallic target, whereas, the flux of oxygen to the substrate surface is derived entirely from collision activated oxygen in the plasma. It is, therefore, most likely that the oxidation reaction takes place at the substrate.

If this explanation is valid, then the ratio σ between the rate of arrival of the titanium atoms and oxygen at the substrate (in the range $0 < P_{O_2} < P_{O_2}^L$ of oxygen partial pressure) should play a decisive role in altering or controlling film properties.

This aspect was investigated by studying the effect of variation of deposition parameters, such as the sputtering pressure and the target bias voltage (for a certain partial pressure of oxygen) on film properties.

Results indicate that the degree of film oxidation increased with an increase in the sputtering pressure and vice versa. On the other hand, the oxygen to titanium ratio in the deposited films decreased with increasing target bias voltage.

Since the mean free path of the sputtered titanium atoms decreases with increasing sputtering pressure, the titanium flux to the substrate will accordingly decrease. As a result, the metal content in the film will decrease. Similarly, since the sputtering yield increases with an increase in the target bias voltage (with all the other deposition parameters kept constant), increasing the target potential (more

negative) will increase the flux of the titanium atoms arriving at the substrate, where they react with oxygen. Therefore, an increase in the metal to oxygen ratio is expected.

These results reveal that it is neither the oxygen partial pressure nor its concentration in the sputtering plasma atmosphere, but rather the availability of titanium and oxygen at the substrate, which control the film properties. That is, in order to maintain a particular film property, the ratio between the rate of arrival of the titanium atoms and oxygen to the substrate must be kept constant. This confirms the earlier conclusion that in the range $0 < P_{O_2} < P_{O_2}^l$ of oxygen partial pressure the ratio σ plays a decisive role in controlling film properties.

The abrupt fall in the deposition rate at the critical pressure of oxygen $P_{O_2}^l$, suggests that at this pressure the condition of the target surface undergoes a significant change, and the decrease in the deposition rate is most probably due to the oxidation of the target surface. The presence of an insulating layer on the target surface results in the buildup of a positive charge which exerts a retarding influence on the bombarding ions, thus reducing the sputtering yield. The result is that the titanium flux is reduced due to both the lower sputter yield and the lower percentage of titanium in the target oxide, while the oxygen flux is derived from activated plasma oxygen and from the sputtered target oxide. The constant deposition rate for oxygen partial pressures $P_{O_2} \geq P_{O_2}^u$ suggests that in this range the sputtering yield from a metal target is the same as the sputtering yield from a TiO_2 target.

PART II

4.6 REACTIVELY SPUTTERED LAYERED STRUCTURE n^+/n SEMICONDUCTING TiO_2 FILMS FOR WATER PHOTOELECTROLYSIS

4.6.1 Cell Fabrication.

Two different sputtering metal targets were used in these investigations; namely i) a high purity titanium (99.97% pure) 5 cm diameter by 7 mm thick hot pressed pellet supplied from the Cerac Corporation and, ii) a cold pressed, high purity, vacuum heated 325 mesh titanium powder pellet. Since the sputtering yield depends to some extent on the target preparation conditions, it was found that the sputtering rate from the pressed metal powder is slightly higher than that from the hot pressed titanium pellet. This problem was easily overcome by controlling the sputtering conditions, and similar films were obtained from both targets.

Films were deposited on glass substrates (standard microscope slides 75×25 mm). The ohmic contact was provided by first depositing a layer of titanium by the dc sputtering of the titanium target, in a pure argon plasma atmosphere. A semiconducting titanium film was then deposited on this titanium layer through an aperture, simply by sputtering in an argon plasma containing a partial pressure of oxygen. Films were deposited at $\sim 3 \times 10^{-5}$ Torr partial pressure of oxygen and a total pressure of 5×10^{-4} Torr. The optimum value of the oxygen partial pressure was determined from our previous investigations on the effect of oxygen partial pressure on film properties. The target bias voltage

was kept at -2.5 kV and the plasma current was 1.2 A. The substrate table was kept at 240°C during film deposition.

For studying electrode performance for photoelectrolysis, a copper wire was attached to the titanium metal backing using a conducting silver paint; the whole cell was masked using epoxy and an area of $\sim 0.3 \text{ cm}^2$ of the semiconducting electrode was left for contact with the electrolyte. The experimental setup is similar to that reported in Chapter 3. The electrolyte used was 1 M NaOH. The primary cell configuration is shown in Fig. 4.4.

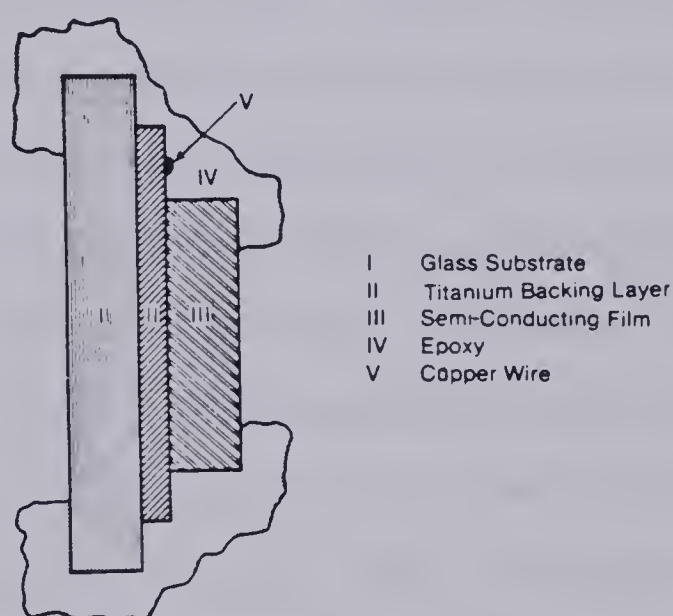


Fig. 4.4 Primary Cell Configuration.

4.7 RESULTS AND DISCUSSION

Thin film semiconducting electrodes fabricated as described above, did not show any mechanical failure during the sputtering process or when immersed in the electrolyte. Films had a dark blue-greyish color and were identical to those obtained by sputtering from a reduced

target. Films were hard and strongly adherent to the glass substrates. In addition, films were easily reproduced utilizing the same sputtering conditions. However, when tested for photoelectrolysis these films were chemically stable and the photoresponse was low.

The low response of these films may be attributed to either i) a film thickness that is not sufficient to provide a space charge region essential for separation of opposite photogenerated charge carriers, or ii) high resistance of the cell caused by oxidation of the titanium backing layer during reactive sputtering.

The problem of insufficient thickness can be easily overcome by depositing for a longer period of time. However, the formation of an oxide layer on the top of the metallic backing layer is a much more difficult situation to ameliorate. Nevertheless, it may still be overcome if it is possible to find a material that has a low chemical activity with oxygen, makes an ohmic contact with TiO_2 , and adheres strongly to glass substrates. In general these are contradicting requirements.

In the discussion of Chapter 3, it was mentioned that when gold was chosen as a backing metallic layer, films were characterized by poor mechanical properties and that mechanical failure of these films took place, either during the deposition process itself, or in the electrolyte. However, continued investigations indicated that strong adherence of gold films to glass substrates could be obtained by providing a diffusion type of interface, or an intermediate layer of an oxygen-active metal which has solid solubility with gold.

In these investigations titanium was chosen as the oxygen active material. The cells were fabricated using the same procedure as before,

but in different configurations, where the different metallic layers II, III and IV, (Fig. 4.5) were deposited to serve the following purposes.

i) The titanium layer (II) provides the diffusion type interface between the gold layer and the glass substrate.

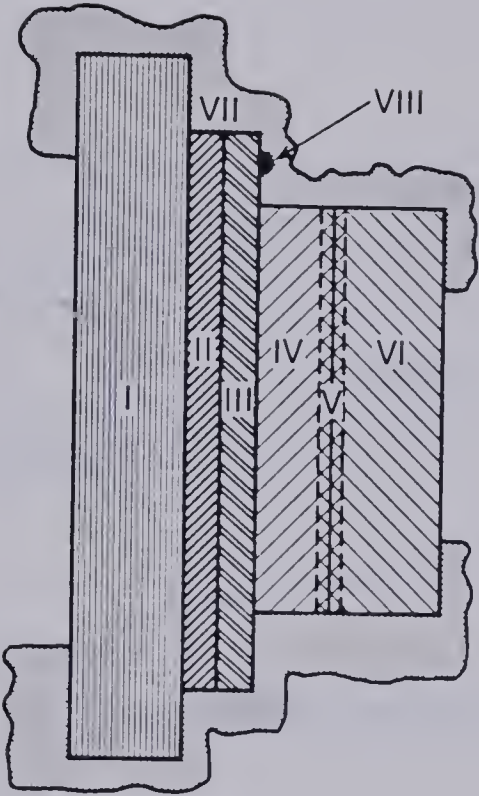
ii) The gold layer (III) provides electrical contact to the external circuit (but not the ohmic contact).

iii) The functions of the titanium layer (IV) are briefly explained as follows:

a) as an ohmic contact to the semiconducting TiO_2 film;

b) by sputtering on a heated substrate and further annealing of the cell, there is a possibility that the titanium layer will extract oxygen from the semiconductor (or partly diffuse into it) resulting in a highly reduced (more doped) semiconducting layer, n^+ (layer V, Fig. 4.5).

In this way a layered structure of a lightly doped film deposited on a heavily doped layer of the same material, n^+/n is formed. One advantage of this arrangement can be explained with the help of the energy band diagram of Fig. 4.6 as follows. An n -type semiconducting layer can be deposited at a partial pressure of oxygen that makes it doped (reduced) to a level that provides a reasonable space charge region width (essential for separation of opposite charge carriers at the semiconductor/electrolyte interface) without paying the penalty of high resistive loss in the bulk of the semiconductor. Also, since the Fermi level of the n^+ -layer is slightly higher than that of the n -layer, a back surface field (BSF) is created at the n^+/n junction, Fig. 4.6. This BSF opposes the diffusion of holes from the n -layer to the n^+ -layer,



- I Glass Substrate
- II Titanium Film
- III Gold Layer
- IV Titanium Layer
- V Diffused Region (n⁺)
- VI n-Type Semi-Conductor
- VII Epoxy
- VIII Copper Wire

4.5 Configuration of a Layered Structure TiO_2 Electrode Fabricated by Reactive Sputtering.

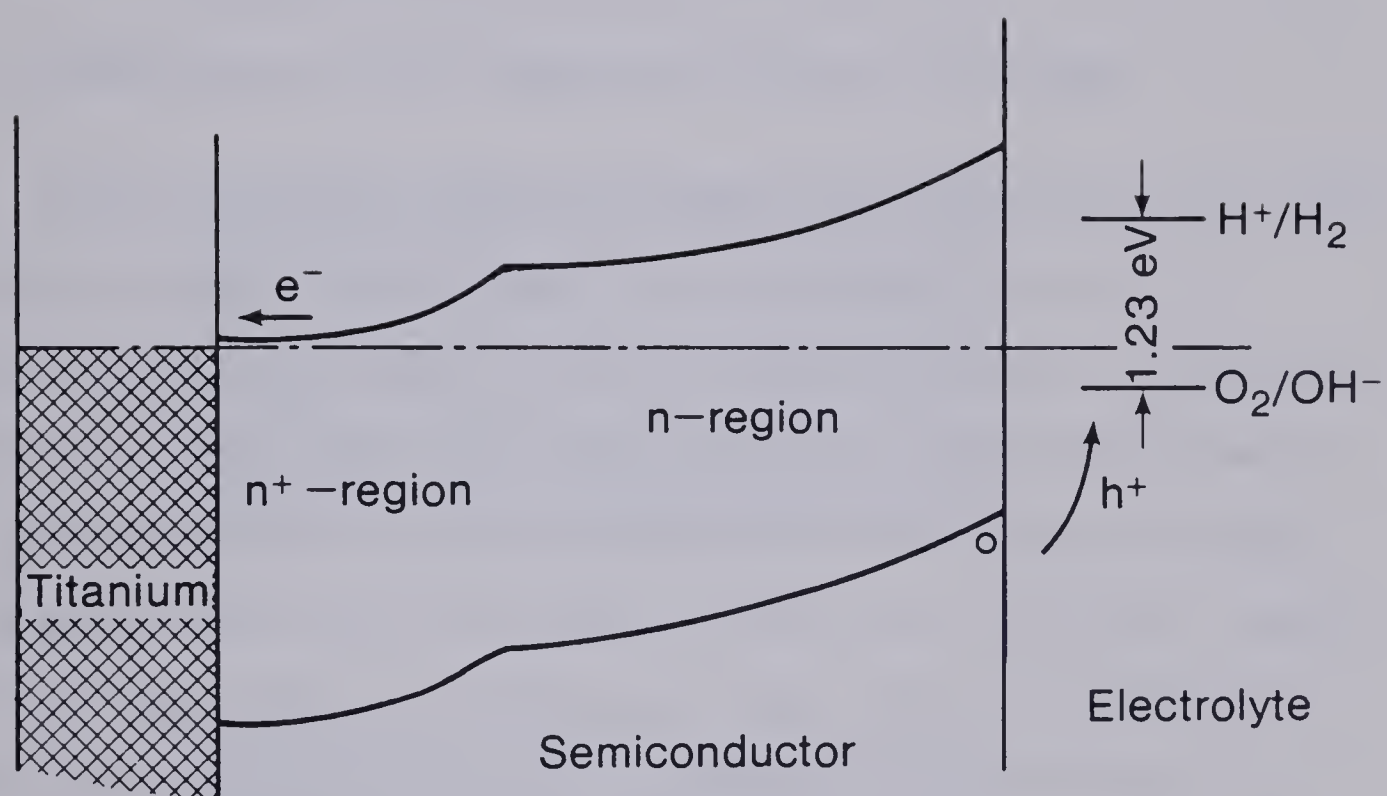


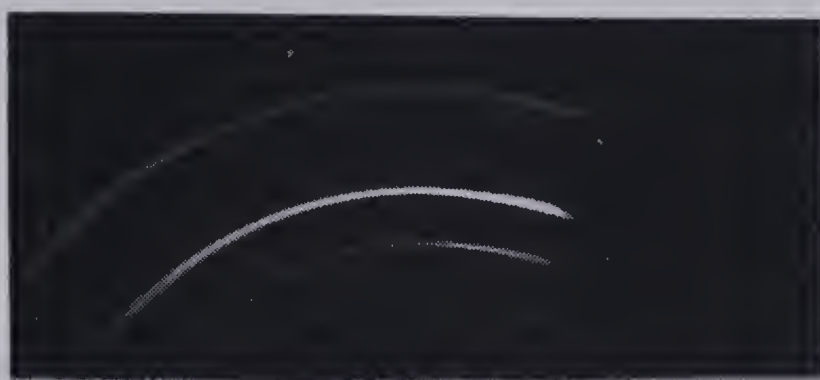
Fig. 4.6 Energy Band Diagram for an n -type Semiconductor/Electrolyte Interface with an n^+ Region.

while favoring the transport of electrons. Thus the BSF enhances charge carrier separation and tends to confine the holes towards the n -region from the ohmic contact (where the surface recombination velocity is infinite). Therefore, an increase in the conversion efficiency is expected [4.7, 4.8].

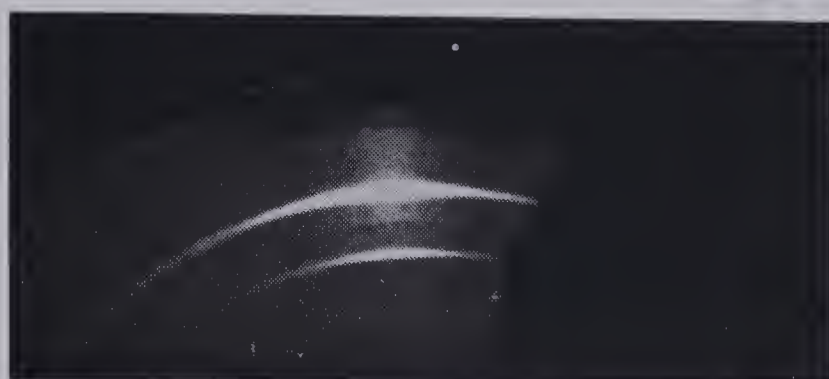
4.7.1 Photoresponse of BSF Reactively Sputtered Electrodes.

X-ray diffraction studies indicated that semiconductor electrodes fabricated in the preceding manner were polycrystalline, Fig. 4.7. In order to investigate the behavior of these electrodes in water photoelectrolysis cells, they were first employed in a photoelectrochemical cell consisting of a 1 M NaOH electrolyte and a platinum foil cathode. In the dark, short circuit and anodic currents were both zero. However, when these electrodes were illuminated (under zero bias conditions) a significantly higher photoresponse (compared to those fabricated as in Fig. 4.4) was obtained. In this case the cell was most probably operating in a regenerative mode with no hydrogen evolution at the platinum cathode. In addition, when these electrodes were immersed in the anolyte of a heterogeneous photoelectrochemical cell (consisting of 1 M NaOH as the anolyte, H_2SO_4 as the catolyte and platinum foil as the cathode) gas evolution at a high rate was observed at both electrodes.

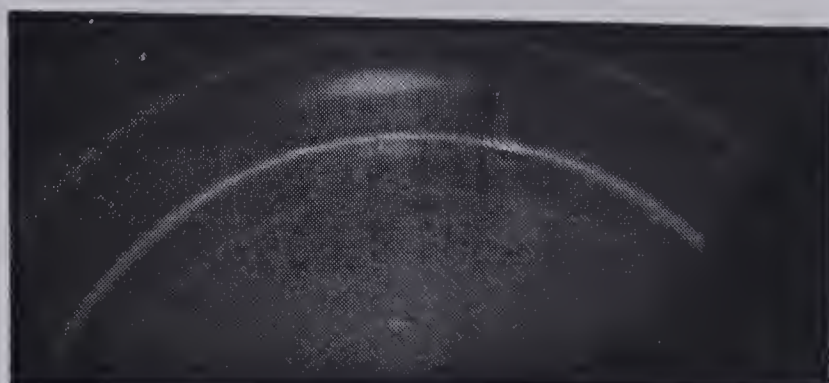
The short circuit current versus wavelength was also investigated. The spectral response for three different samples deposited under the same sputtering conditions, but for slightly different periods of time, are shown in Fig. 4.8. An average thickness of the semiconducting film was estimated to be $\sim 2 \mu\text{m}$. As can be seen from Fig. 4.8, the peak



$T_S = 200^\circ\text{C}$ and $\theta = 18^\circ$



$T_S = 250^\circ\text{C}$, $\theta = 19^\circ$



$T_S = 250^\circ\text{C}$, $\theta = 15^\circ$

Fig. (4.7)

X-ray diffraction for three samples prepared by reactive sputtering from a Titanium metal target for different periods of time.

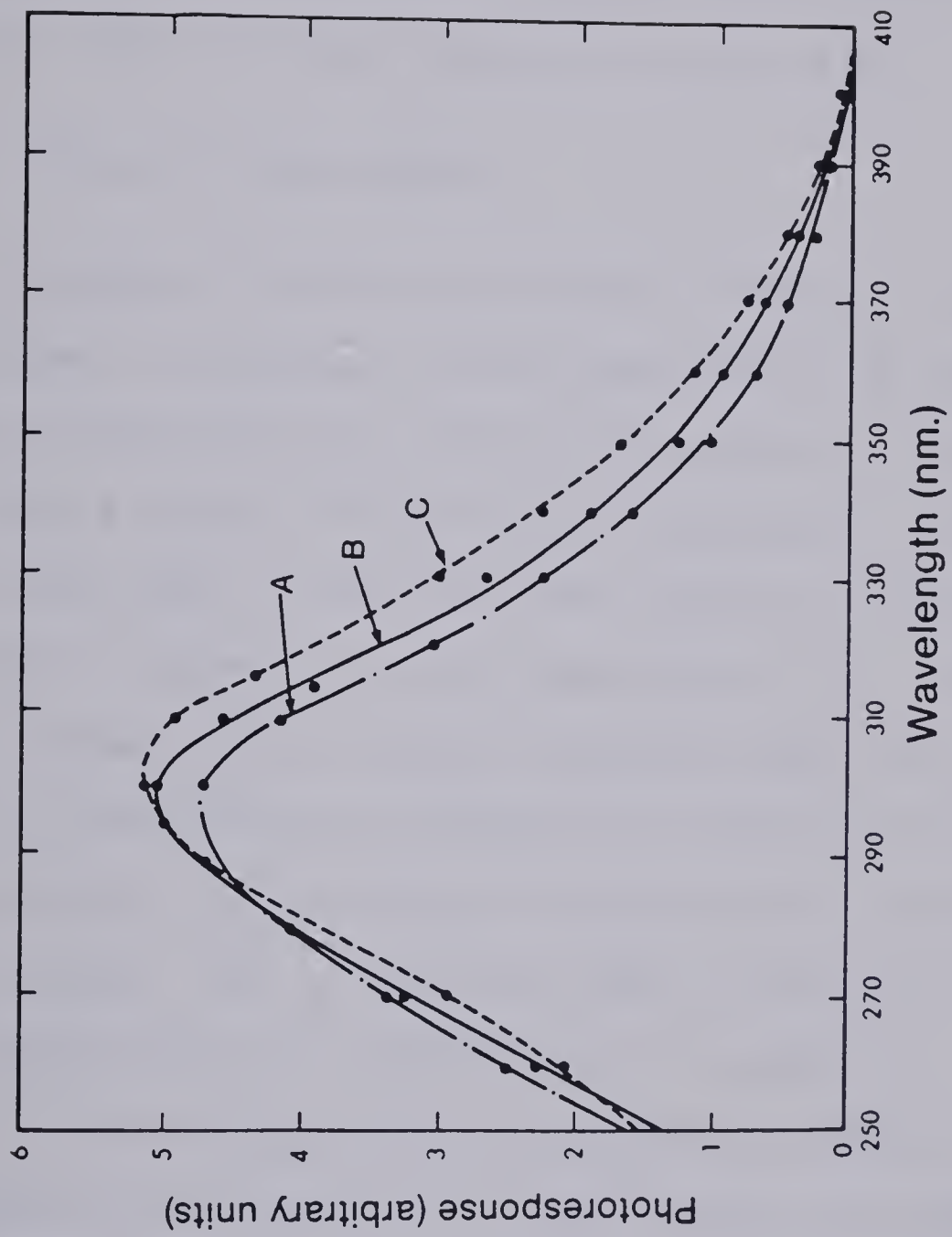


Fig. 4.8 Spectral Response of BSF Reactively Sputtered TiO_2 Electrodes in a Water Photoelectrolysis Cell.

response of the different samples occurs at the same wavelength, and that a main absorption edge at ~ 410 nm was obtained for each cell. This value of 410 nm main absorption edge corresponds to a band gap of about 3 eV and is almost the same as obtained for electrodes prepared by sputtering from a reduced TiO_2 target [4.9] and is also consistent with that reported for bulk TiO_2 material [4.10, 4.11].

4.7.2 Effect of Light Intensity.

Generation of minority carriers by illumination will cause a photocurrent if the minority carriers can react at the interface with species of the electrolyte, otherwise the separation of charge carriers will create a counter voltage which will compensate for the voltage drop in this region. Under this latter condition, electron-hole pair generation is compensated for by recombination [4.12]. Therefore, if it is assumed that all photons with energy higher than the energy gap of the semiconductor are absorbed, the electron-hole pair generation and accordingly, the short circuit photocurrent will be proportional to light intensity. This is valid only under low levels of illumination where electron-hole pair recombination can be neglected.

In order to check whether the rate limiting step in cell operation was indeed the photogeneration of charge carriers, the dependence of the short circuit current on light intensity was investigated. The semiconductor was irradiated with monochromatic light, the wavelength of which corresponds to the peak of the spectral response for each individual cell. As shown in Fig. 4.9, the dependence is, as expected, rather linear for illumination levels up to 3 mW/cm^2 .

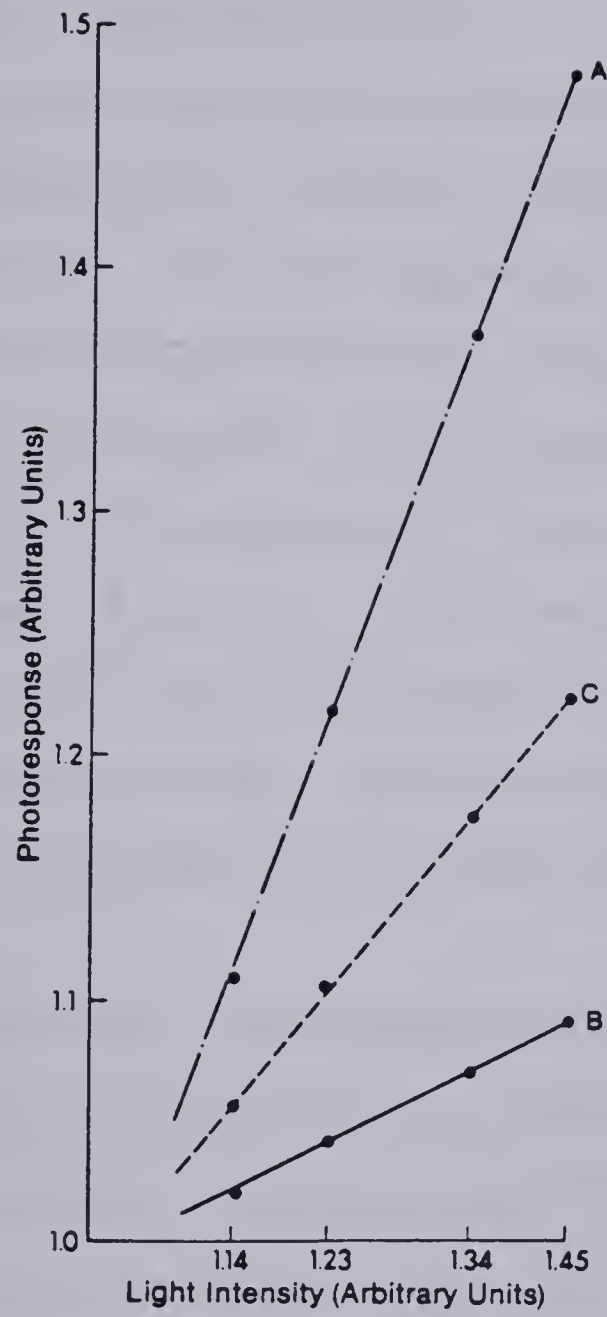


Fig. 4.9 Effect of Light Intensity on the Photocurrent of BSF Reactively Sputtered TiO_2 Electrodes at Low Levels of Illumination.

4.8 CONCLUSION

The study of dc reactive deposition rates of titanium suboxides showed that polycrystalline films were deposited at 240°C over the entire range of oxygen partial pressures studied. A wide variety of films, ranging from metallic through semiconducting to dielectric specimens were deposited in a reproducible manner.

This study shows that the site of oxidation in reactive sputtering is principally determined by the partial pressure of oxygen in the sputtering atmosphere. From 0% of oxygen up to a critical pressure $P_{O_2}^l$, determined by the relative arrival rates of oxygen and titanium, oxidation occurs mainly at the substrate. In this region it is highly probable that the oxygen content in the sputtered thin films depends on the partial pressure of oxygen. Above this critical partial pressure, oxidation occurs mainly at the target, and films are formed by sputtering of the oxide from the target surface. The actual value of this critical oxygen partial pressure will depend on the deposition parameters in the sputtering process.

On the other hand, stable semiconducting thin film electrodes were easily fabricated by sputtering from a titanium metal target in an oxygen-argon plasma atmosphere. Films were deposited on heated glass substrates and were fabricated in such a way that a layered structure n^+/n of a lightly doped semiconductor deposited on a heavily doped layer of the same material was easily formed at the back surface by diffusion. In this manner, an abrupt doping level change in a very thin region was formed and a back surface field was created.

Lastly, these results reveal that reactive sputtering from a metallic target is an attractive technique not only for microcircuit application but also for fabricating thin film electrodes for water electrolysis. In addition the reproducibility of the results along with the case of creating a BSF are noteworthy and encouraging topics for further research.

CHAPTER 5

MODELLING OF THE PHOTOEXCITED SEMICONDUCTOR ELECTRODE

5.1 INTRODUCTION

In most of the studies of the photoassisted electrolysis of water using a semiconductor electrode, little attention has been paid to the carrier generation and the transport properties of the photoexcited electrode. Experimental investigations, however, have shown that the physical characteristics of the particular semiconductor is one of the major factors determining the efficiency of these photoelectrolysis cells. Consequently, the physical properties of the semiconductor electrode and the degree to which they can be modified to optimize cell performance are important and topical areas of research. This being the case, it is in this chapter of the thesis where an approximate theoretical model for the photoexcited semiconductor electrode is developed. Theoretical expressions showing how the cell response of an illuminated electrode can be expected to behave as a function of the wavelength of the incident radiation (absorption constant or penetration depth), carrier diffusion length (carrier lifetime), carrier concentration, surface reaction rates, depletion region width and the voltage drop across the space charge region, are presented.

In the model developed here particular emphasis is laid upon the effect of built-in drift fields caused by impurity gradients. Such fields have been suggested for the enhancement of the photoresponse of photovoltaic solar cells [5.1, 5.2].

5.2 THE SEMICONDUCTOR ELECTRODE MODEL

Only an n -type semiconductor is analyzed here, however, the treatment is also valid for a p -type material. An energy band diagram for the semiconductor/electrolyte interface is shown in Fig. 5.1. For the electrolysis of water into oxygen and hydrogen to proceed, two redox levels corresponding to the donor (oxidation) state, and acceptor (reduction) state with an energy difference of 1.23 eV, must be present in the electrolyte. The model developed here is derived on the basis of the depletion approximation, where it is assumed that the semiconductor is divided into two distinct regions; a region that is entirely depleted of free charge carriers ($0 < z < w$), and an interior region of perfect charge neutrality ($z > w$).

Derivations are performed for the general case of nonuniform distribution of impurities, from which the simplified special case of uniform doping is easily obtained. The analysis provides a compact form for the current equation that removes the separation between the drift and diffusion components of minority carriers generated outside the space charge region, showing that the current is proportional to the gradient of the relative excess density of minority carriers.

In addition, the analysis takes into consideration the effect of surface reaction rates at the semiconductor/electrolyte interface. A formulation for the width of the space charge region for the case of a nonuniform doping profile is also presented.

In the analysis presented in this chapter it is assumed that the semiconductor is illuminated from the electrolyte side and only low levels of injections are considered.

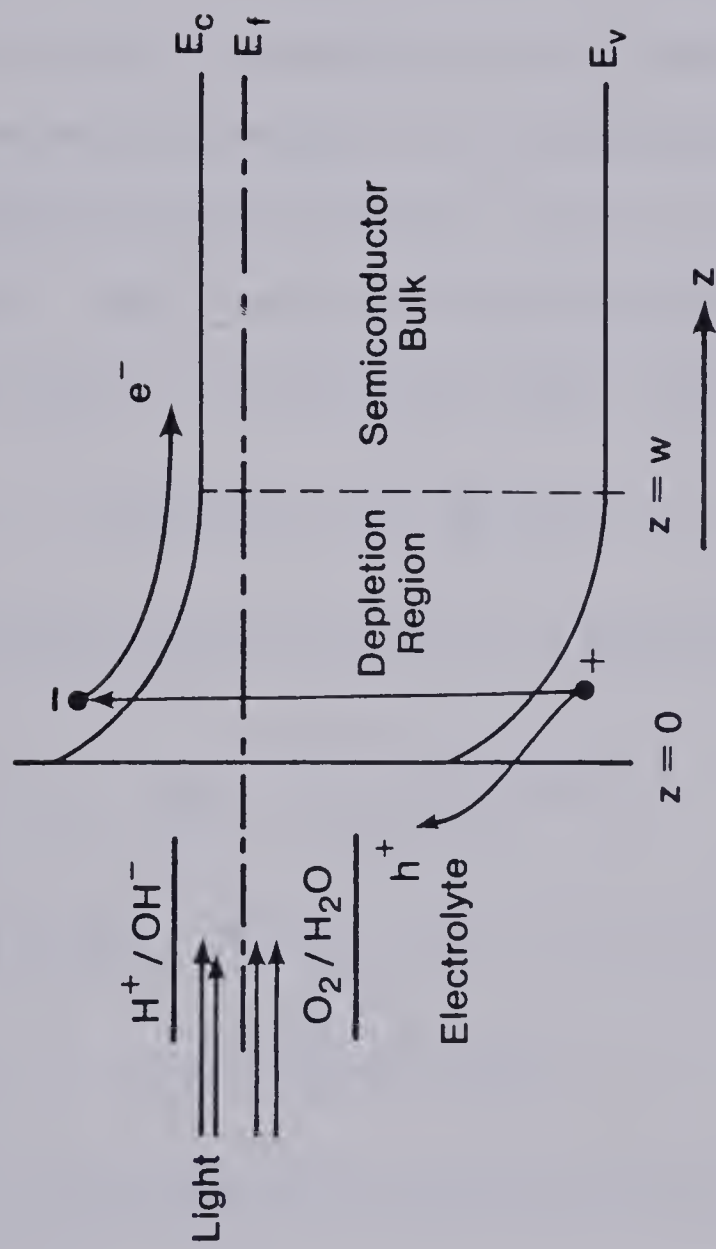


Fig. 5.1 An Energy Band Diagram of an *n*-type Semiconductor Electrode in a Photoelectrochemical Cell.

5.3 MATHEMATICAL ANALYSIS

If all the donor atoms $N(z)$ are assumed to be ionized, then, according to the neutrality equation, the majority carrier concentration $n(z)$ is given by

$$N(z) \simeq n(z) .$$

Because the donor concentration is a function of z , the gradient of the electron density produces a diffusion current unless an electric field and an opposing equal current is set up to restrain the motion of these electrons. Hence, under equilibrium conditions, the majority carrier current (drift + diffusion) is zero. That is,

$$qN(z)\mu_n E_d + qD_n \frac{d}{dz} N(z) = 0 ,$$

from which the built-in drift field E_d is given by

$$E_d = - \frac{D_n}{\mu_n} \frac{1}{N(z)} \frac{d}{dz} N(z) . \quad (5.1)$$

According to Einstein's relation, this can be written as

$$E_d = - \frac{kT}{q} \frac{1}{N(z)} \frac{d}{dz} N(z) , \quad (5.1')$$

where D_n and μ_n are the diffusion coefficient and mobility of electrons respectively.

The hole current density (at a specific wavelength) J may be represented in the form of two components; the current associated with carriers generated inside the space charge region itself, J_d , and the current associated with the minority carriers generated outside the space charge region J_p . That is,

$$J = J_d + J_p .$$

The current density component J_d associated with the minority carriers generated in the space charge region is given by

$$J_d = -q \int_0^w \alpha(\lambda) Q'_0(\lambda) e^{-\alpha(\lambda)z} dz = -q Q'_0(\lambda) \{1 - e^{-\alpha(\lambda)w}\} , \quad (5.2)$$

in which $\alpha(\lambda)$ is the absorption coefficient corresponding to a certain wavelength λ , $Q'_0(\lambda)$ is the photon flux of the solar spectrum, and w the depletion region width of the semiconductor.

The contribution of the minority carriers photogenerated outside the space charge region to the total current is given by the relation

$$J_p = -q D_p \frac{d}{dz} \{P_0(z) + \delta P(z)\} + q \{P_0(z) + \delta P(z)\} \mu_p E_d , \quad (5.3)$$

where $P_0(z)$, $\delta P(z)$, D_p and μ_p are the hole thermal equilibrium concentration, hole excess carrier concentration, hole diffusion coefficient and hole mobility respectively.

It should be noted that inclusion of the hole thermal equilibrium concentration in Eqn. 5.3 is necessary since it is also a function of z . However, consideration of the dark equilibrium condition ($J_p = 0$ and $\delta P(z) = 0$) shows that the terms in $P_0(z)$ cancel identically in Eqn. 5.3. Equation 5.3 can therefore be written as

$$J_p = q D_p \frac{d}{dz} \delta P(z) + q \delta P(z) \mu_p E_d . \quad (5.4)$$

If the built-in drift field E_d given by Eqn. 5.1 is substituted in Eqn. 5.4, one gets

$$J_p = q D_p \frac{d}{dz} \delta P(z) + q \delta P(z) \mu_p \left\{ - \frac{D_n}{\mu_n} \frac{1}{N(z)} \frac{d}{dz} N(z) \right\} .$$

Using Einstein's relation, $D_p = \frac{\mu_p}{\mu_n} D_n$, this becomes

$$J_p = -qD_p \left\{ \frac{d}{dz} \delta P(z) + \frac{\delta P(z)}{N(z)} \frac{d}{dz} N(z) \right\},$$

which simply can be written as

$$J_p = -q \frac{D_p}{N(z)} \frac{d}{dz} \{ \delta P(z) N(z) \}. \quad (5.5)$$

The expression for J_p as given by Eqn. 5.5 can be further simplified if expressed in terms of the relative excess density $b'(z)$ instead of $\delta P(z)$, where

$$b'(z) = \frac{\delta P(z)}{P_0(z)} = \frac{\delta P(z) N(z)}{P_0(z) N(z)} = \frac{\delta P(z) N(z)}{n_i^2},$$

and accordingly

$$J_p = -qD_p \frac{n_i^2}{N(z)} \frac{d}{dz} b'(z). \quad (5.6)$$

Equation 5.6 provides a compact form for the current equation that removes the separation between the drift and diffusion components for carriers photogenerated outside the space charge region. This then shows that the current is proportional to the gradient of the relative excess density.

The starting point for the derivation of the current density component J_p is the solution for the steady state continuity equation for holes as minority carriers. That is,

$$\frac{1}{q} \nabla \cdot J_p = \alpha(\lambda) Q'_0(\lambda) e^{-\alpha(\lambda)z} - \frac{\delta P(z)}{\tau_p}, \quad (5.7)$$

where τ_p is the hole lifetime, and where a constant illumination level of monochromatic radiation is assumed so that $Q'_0(\lambda)$ and $\alpha(\lambda)$ are

constants for a certain wavelength. In addition the density of photo-generated minority carriers is assumed to be smaller than their thermal equilibrium value.

Combining Eqns. 5.6 and 5.7 and replacing $\alpha(\lambda)$ by α and $Q'_0(\lambda)$ by Q'_0 gives

$$\begin{aligned} \frac{d^2 b'(z)}{dz^2} - \frac{1}{N(z)} \frac{db'(z)}{dz} \frac{dN(z)}{dz} + \frac{db'(z)}{dz} \frac{1}{D_p} \frac{d}{dz} D_p \\ - \frac{b'(z)}{L_p^2} + \frac{\alpha N(z)}{D_p n_i^2} Q'_0 e^{-\alpha z} = 0, \end{aligned} \quad (5.8)$$

where $L_p^2 = D_p \tau_p$.

Equation 5.8 is a general diffusion equation which may be solved numerically. However, since the objective here is to develop an approximate analytical model, the approach adopted is to assume constant parameters, τ_p , D_p and μ_p . In this case an analytical solution for Eqn. 5.8 can be readily obtained only if the quantity $\frac{1}{N(z)} \frac{dN(z)}{dz}$ is constant w.r.t. the independent variable z . This case corresponds to an exponential distribution of impurities, which fortunately, represents a fair approximation to the impurity distribution usually obtained [5.3]. Consequently, this will be the impurity profile under consideration in this analysis.

If the donor impurity profile is taken as an exponential

$$N(z) = N_0 e^{\beta z} \text{ (cm}^{-3}\text{)},$$

where N_0 is the surface concentration (cm^{-3}) and β is a constant (cm^{-1}), then, according to Eqn. 5.1, since the donor concentration increases from the surface, its rate of change is positive and therefore the electric

field is negative. That is, the field direction points from the interior of the semiconductor towards the surface, thereby helping the minority carriers (holes injected by light) to travel towards the semiconductor/electrolyte interface.

For an exponential impurity distribution, Eqn. 5.8 can be written as

$$\frac{d^2 b'(z)}{dz^2} - \beta \frac{db'(z)}{dz} - \frac{b'(z)}{L_p^2} = -Y_1 e^{-\gamma z}, \quad (5.9)$$

where $\gamma = (\alpha - \beta) \text{ (cm}^{-1}\text{)}$ and $Y_1 = \frac{\alpha Q'_0 N_0}{n_i^2 D_p} \text{ (cm}^{-2}\text{)}$.

A general solution of Eqn. 5.9 is given by

$$b'(z) = Y_2 \{A_1 e^{M_1 z} + A_2 e^{M_2 z} - e^{-\gamma z}\}, \quad (5.9')$$

where $M_1 = \beta/2 - F_1 \text{ (cm}^{-1}\text{)}$, $M_2 = \beta/2 + F_1 \text{ (cm}^{-1}\text{)}$, $F_1 = \{(\beta/2)^2 + (1/L_p^2)\}^{1/2} \text{ (cm}^{-1}\text{)}$, and $Y_2 = \frac{Y_1}{\gamma^2 + \gamma\beta - 1/L_p^2}$. A_1 and A_2 are constants to be obtained from following boundary conditions:

(i) $b'(z)$ is finite; this gives $A_2 = 0$.

(ii) At the depletion region edge $z = w$, the hole current density J_p is proportional to the hole concentration $\delta P(z) \Big|_{z=w}$, [5.4]. That is,

$$J_p(z) \Big|_{z=w} = -qS\delta P(z) \Big|_{z=w},$$

which, in terms of the relative excess density, can be written as

$$D_p \frac{d}{dz} b'(z) \Big|_{z=w} = S b'(z) \Big|_{z=w}. \quad (5.10)$$

In using condition (ii), it should be born in mind that the photo-current component J_p is, in general, a function of the excess hole density $\delta P(z)$. That is,

$$J_p = f\{\delta P(z)\} ,$$

where f is some unknown function of $\delta P(z)$. However, for low levels of injection $\delta P(z)$ is small, and $f\{\delta P(z)\}$ can be expanded into a series w.r.t. $\delta P(z)$. This gives

$$J_p = qf\{P_0(z)\} + q\delta P(z) \left. \frac{df}{dz} \right|_{P=P_0} .$$

Under equilibrium conditions the photocurrent is zero and accordingly, $f\{P_0(z)\}$ is zero. Therefore, J_p may take the form given by Eqn. 5.10.

The constant of proportionality S in Eqn. 5.10 has the dimensions of velocity, and is a boundary condition parameter determined by the depletion region properties and the mechanism of hole disappearance at the semiconductor/electrolyte interface [5.4, 5.5].

From Eqns. 5.9 and 5.10 we have

$$D_p Y_2 \{M_1 A_1 e^{M_1 w} + \gamma e^{-\gamma w}\} = Y_2 \{A_1 e^{M_1 w} - e^{-\gamma w}\} S$$

from which the constant A_1 is given by

$$A_1 = \frac{S/D_p + \gamma}{S/D_p - M_1} e^{-(\gamma + M_1)w} . \quad (5.11)$$

The relative excess density $b'(z)$ is therefore

$$b'(z) = \left\{ \frac{S/D_p + \gamma}{S/D_p - M_1} e^{M_1 z} \cdot e^{-(M_1 + \gamma)w} - e^{-\gamma z} \right\} Y_2 . \quad (5.12)$$

The contribution of the minority carriers photogenerated outside the space charge region to the total minority carrier current can therefore be written according to Eqns. 5.6, 5.10 and 5.12 as

$$J_p = -qS \frac{n_i^2}{N(z)} b'(z) \Big|_{z=w},$$

which, for an exponential impurity profile, gives

$$J_p = -qS \frac{n_i^2}{N_0} e^{-\beta w} \cdot Y_2 \left\{ \frac{S/D_p + \gamma}{S/D_p - M_1} - 1 \right\} e^{-\gamma w} \quad (5.13)$$

and the current density J will be accordingly given by the addition of Eqns. 5.2 and 5.13 after substituting for Y_1 and Y_2 , as

$$J = -qQ'_0 \left\{ (1 - e^{-\alpha w}) + S/D_p \left(\frac{\gamma + M_1}{S/D_p - M_1} \right) Y_3 e^{-\alpha w} \right\}, \quad (5.14)$$

where $Y_3 = \frac{\alpha}{\alpha^2 - \alpha\beta - 1/L_p^2}.$

The current density expression given by Eqn. 5.14 is for the general case, but the current density for the special case of a uniform distribution of impurities can be derived simply by setting $\beta = 0$ and substituting for Y_3 and γ . That is,

$$J \Big|_{\beta=0} = -qQ'_0 (1 - e^{-\alpha w}) - qQ'_0 \left\{ \frac{\alpha L_p}{\alpha L_p + 1} \right\} \left\{ \frac{L_p}{L_p + D_p/S} \right\} e^{-\alpha w}. \quad (5.15)$$

Equation 5.15 is identical to that obtained earlier by Wilson [5.6]

5.4 VOLTAGE DEPENDENCE OF PHOTOCURRENT

The derivation given above can be extended to show the dependence of the photocurrent on the voltage drop across the depletion region. Basically the connection is made by giving the relationship between the voltage drop across the depletion region V , and the parameters S and w . In what follows, such a dependence will be derived on the basis of the depletion region approximations.

5.4.1 Dependence of the Parameter S on the Voltage Drop across the Depletion Region V .

As was mentioned before, the parameter S is determined by the properties of the depletion region width and the loss mechanism for holes at the semiconductor/electrolyte interface. Two mechanisms are possible for hole disappearance at the interface; namely, electron-hole recombination via surface states, and hole transfer to donor levels in the electrolyte. According to [5.6, 5.7], the surface recombination current density J_r can be expressed in terms of a surface recombination velocity S_r as

$$J_r = -qS_r \delta P(z) \Big|_{z=0}.$$

According to Boltzman's statistics, this can be written as

$$J_r = \left\{ -qS_r \delta P(z) \Big|_{z=w} \right\} e^{qV/kT}. \quad (5.16)$$

Similarly, the hole transfer current density J_t may be expressed in terms of a surface transfer velocity S_t as

$$J_t = \left\{ -qS_t \delta P(z) \right\}_{z=w} e^{qV/kT}.$$

Substituting for $\delta P(z)$ from the relation $\delta P(z) = \frac{b'(z)n_i^2}{N(z)}$, and adding the two current components J_r and J_t , the total current density J may then take the form

$$J = -q(S_r + S_t) \left\{ \frac{b'(z)n_i^2}{N(z)} \right\}_{z=w} e^{qV/kT}. \quad (5.17)$$

Since, under steady state conditions, the rate of hole disappearance at the semiconductor/electrolyte interface is equal to the rate of hole arrival at the interface (by both drift and diffusion), the two current expressions given by Eqns. 5.14 and 5.17 above must be equal. That is,

$$\begin{aligned} \frac{Y_3}{D_p} \frac{(S_r + S_t)(\gamma + M_1)}{S/D_p - M_1} e^{-\alpha w} \cdot e^{qV/kT} \\ = (1 - e^{-\alpha w}) + Y_3 S/D_p \left\{ \frac{\gamma + M_1}{S/D_p - M_1} \right\} e^{-\alpha w}, \end{aligned}$$

from which the surface parameter S is given by

$$S = \frac{Y_3(S_r + S_t)(\gamma + M_1)e^{-\alpha w}}{1 + \{Y_3(\gamma + M_1) - 1\}e^{-\alpha w}} \cdot e^{qV/kT} + \frac{D_p M_1(1 - e^{-\alpha w})}{1 + \{Y_3(\gamma + M_1) - 1\}e^{-\alpha w}}. \quad (5.17')$$

5.4.2 Dependence of the Depletion Region Width w on V .

For uniformly doped semiconductors the depletion region width w and the potential drop across the depletion region V are related by

$$\frac{w^2}{0} = \frac{2\epsilon}{qN_0} V,$$

where N_0 is the donor concentration (cm^{-3}) and ϵ is the dielectric

constant. For impurity graded structures this relationship is no longer valid [5.8] and so a correction for the depletion region width must be made in the analysis.

The starting point for the determination of this correction is Poisson's equation written for the immobile charge carrier region $0 < z < w$. That is,

$$\frac{d^2V(z)}{dz^2} = -\frac{q}{\epsilon} N(z) ,$$

which by direct integration gives,

$$\frac{dV(z)}{dz} = \frac{dV(z)}{dz} \Big|_{z=0} - \frac{q}{\epsilon} \int_0^z N(z) dz , \quad (5.18)$$

and accordingly gives

$$\frac{dV(z)}{dz} \Big|_{z=w} = \frac{dV(z)}{dz} \Big|_{z=0} - \frac{q}{\epsilon} \int_0^w N(z) dz . \quad (5.18')$$

Integration of Eqn. 5.18 after substituting for $\frac{dV(z)}{dz} \Big|_{z=0}$ from Eqn. 5.18' gives

$$V(z) = V(z) \Big|_{z=0} + z \left\{ \frac{dV(z)}{dz} \Big|_{z=w} \right\} + \frac{zq}{\epsilon} \int_0^w N(z) dz - \frac{q}{\epsilon} \int_0^z \left\{ \int_0^v N(\eta) d\eta \right\} dv$$

from which,

$$V(w) = V(0) + w \left\{ \frac{dV(z)}{dz} \Big|_{z=w} \right\} + \frac{wq}{\epsilon} \int_0^w N(z) dz - \frac{q}{\epsilon} \int_0^w \left\{ \int_0^v N(\eta) d\eta \right\} dv .$$

The potential drop across the depletion region $V(w) - V(0) = V$ is accordingly given by

$$V = w \left\{ \frac{dV(z)}{dz} \Big|_{z=w} \right\} + \frac{wq}{\epsilon} \int_0^w N(z) dz - \frac{q}{\epsilon} \int_0^w \left\{ \int_0^v N(\eta) d\eta \right\} dv . \quad (5.19)$$

Since by definition, $-\frac{dV(z)}{dz}$ is the electric field, then according to Eqn. 5.1', one can write

$$\left. \frac{dV(z)}{dz} \right|_{z=w} = \frac{kT}{q} \frac{1}{N(w)} \left. \frac{dN(z)}{dz} \right|_{z=w} . \quad (5.20)$$

Combining Eqns. 5.18 and 5.20 gives

$$V = w \left\{ \frac{kT}{q} \frac{1}{N(w)} \left. \frac{dN(z)}{dz} \right|_{z=w} \right\} + \frac{wq}{\epsilon} \int_0^w N(z) dz - \frac{q}{\epsilon} \int_0^w \left\{ \int_0^v N(\eta) d\eta \right\} dv. \quad (5.21)$$

Equation 5.21 again is a general expression relating the depletion region width to the potential drop across the depletion region for any impurity profile. For the exponential impurity distribution under consideration here, the relation simplifies to

$$V = \frac{wkT}{q} \beta + \frac{qN_0}{\epsilon\beta^2} \{(\beta w - 1)e^{\beta w} + 1\} . \quad (5.22)$$

The special case of a uniform impurity distribution can also be obtained by taking the limit when $\beta \rightarrow 0$. Thus

$$V \Big|_{\beta=0} = \lim_{\beta \rightarrow 0} \frac{w_0 kT}{q} \beta + \lim_{\beta \rightarrow 0} \frac{qN_0}{2\epsilon\beta} \{\beta w_0^2 e^{\beta w_0}\} .$$

That is,

$$V = \frac{qN_0}{2\epsilon} w_0^2 . \quad (5.23)$$

5.5 THEORETICAL PRESENTATION

Equations 5.14, 5.15' and 5.22 contain several variables such as, β , V , w , N_0 , L_p , $(S_r + S_t)$, Q'_0 and α . Among these variables, the photon flux density Q'_0 and the absorption coefficient α depend strongly on the

wavelength λ of the incident radiation. A computer program was written to generate curves for current density versus wavelength and quantum efficiency versus wavelength for a typical TiO_2 electrode. A block diagram of the general calculation procedure is shown in Fig. 5.2.

The relative dielectric constant for TiO_2 was given the value $\epsilon_r = 173$ [5.9] and a hole mobility equal to unity (corresponding to a hole diffusion constant $D_p = 0.025 \text{ cm}^2/\text{sec}$ was assumed [5.10]). Values for the absorption coefficient α for TiO_2 were taken from the absorption-versus λ curve given in [5.11], Fig. 5.3. Values for the photon flux Q'_0 corresponding to a certain wavelength were calculated using the relation [5.12],

$$Q'(\lambda) = \frac{E(\lambda)\lambda}{19.8} \times 10^{16} \text{ photons/cm}^2\text{sec } \mu\text{m} ,$$

where λ is in microns and $E(\lambda)$ is in $\text{watt/m}^2\mu\text{m}$. Values for $E(\lambda)$ in the wavelength range of interest were taken from the tables given by Moon [5.13], for AMO. In this case the current density J assumes the dimensions of $\text{mA/cm}^2\mu\text{m}$.

Values of surface reaction parameters S_r and S_t are not known. Consequently, for simplicity of the analysis, the summation $S_r + S_t$ will be taken as a constant parameter throughout these investigations.

5.6 RESULTS AND DISCUSSION

5.6.1 Effect of Surface Reaction Parameters, S_r and S_t .

This was investigated utilizing two different approaches; first, by studying the effect of the voltage drop across the depletion region V

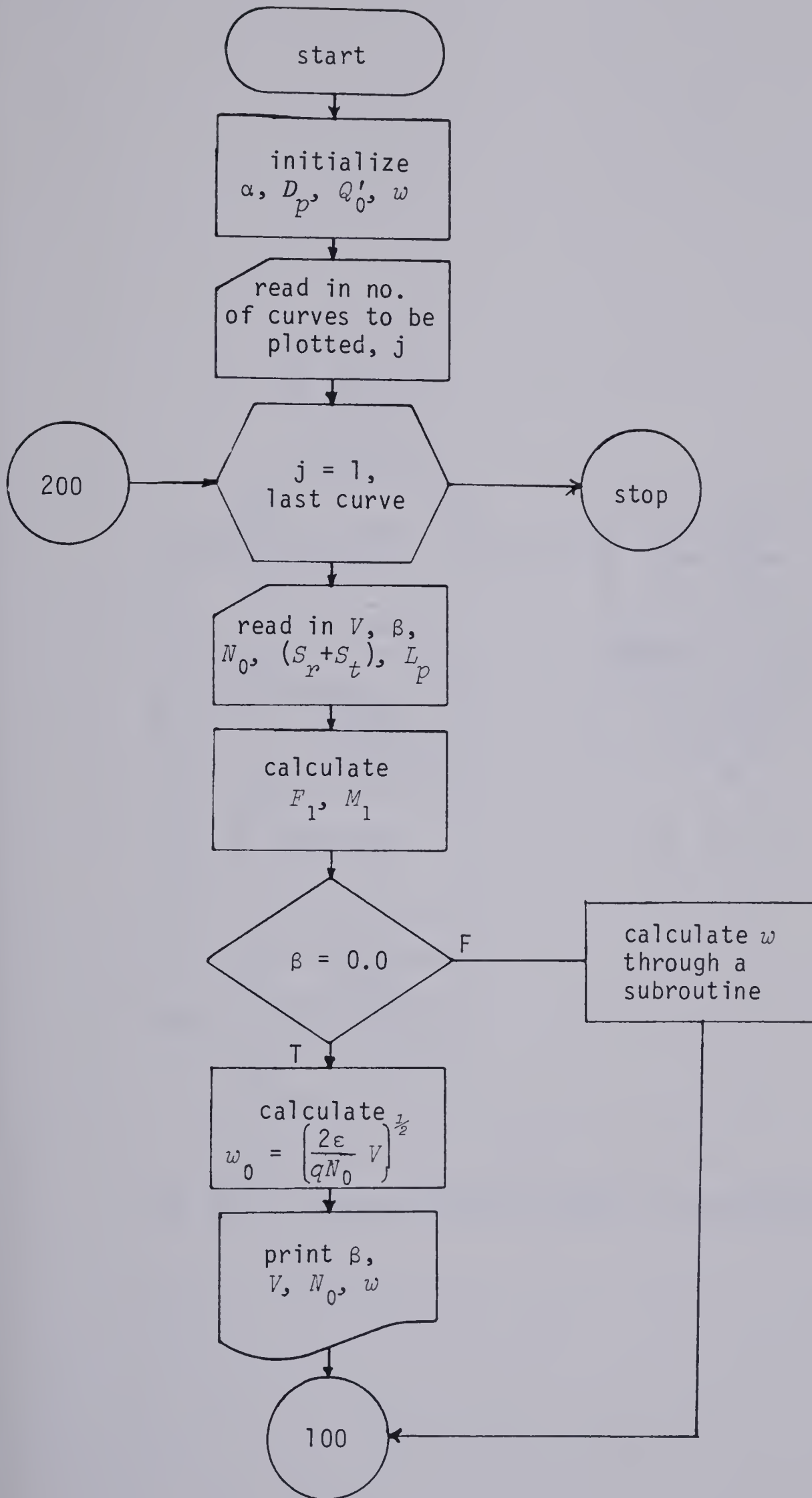


Fig. 5.2

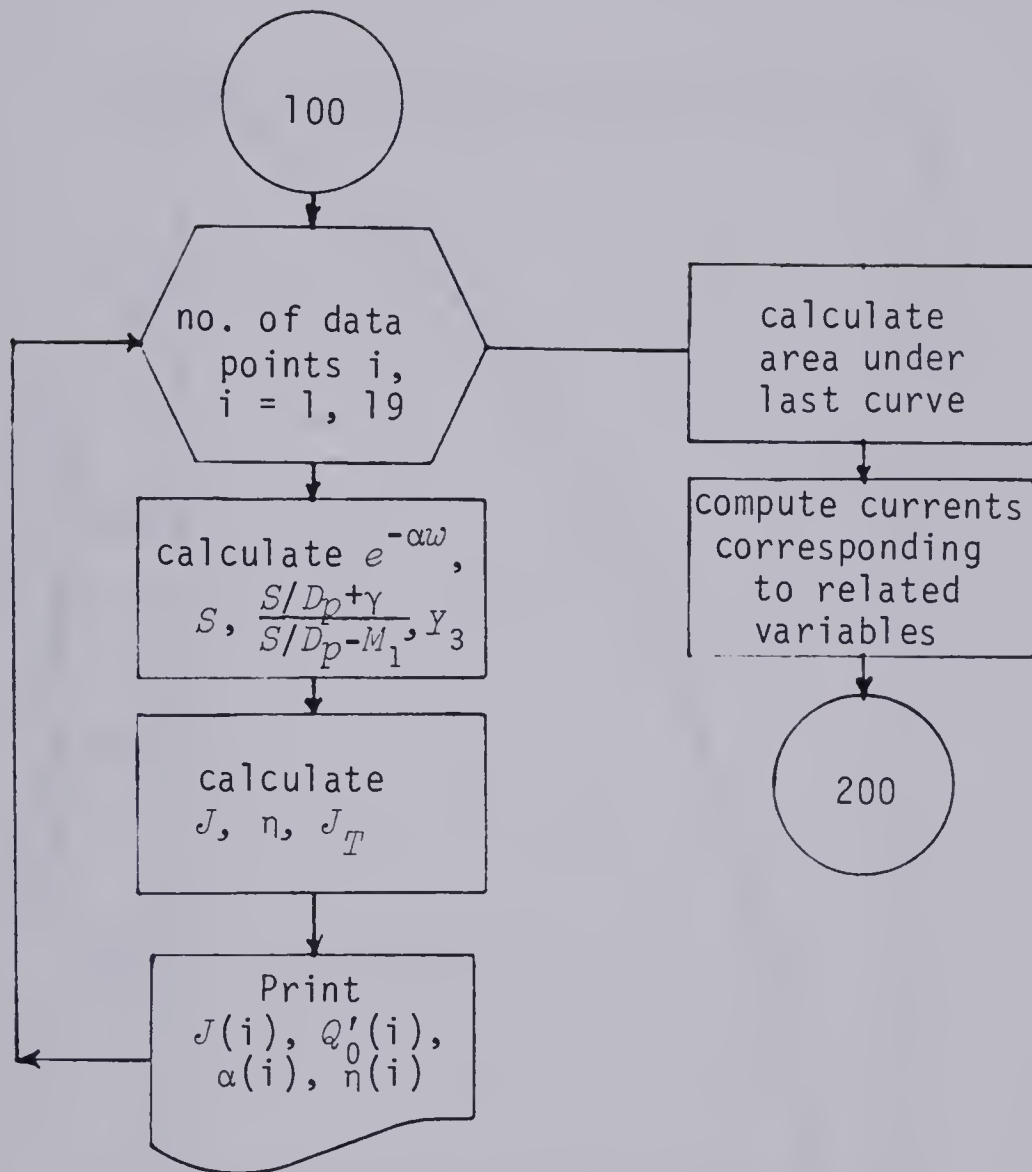


Fig. 5.2 Algorithm for the General Calculating Procedure.

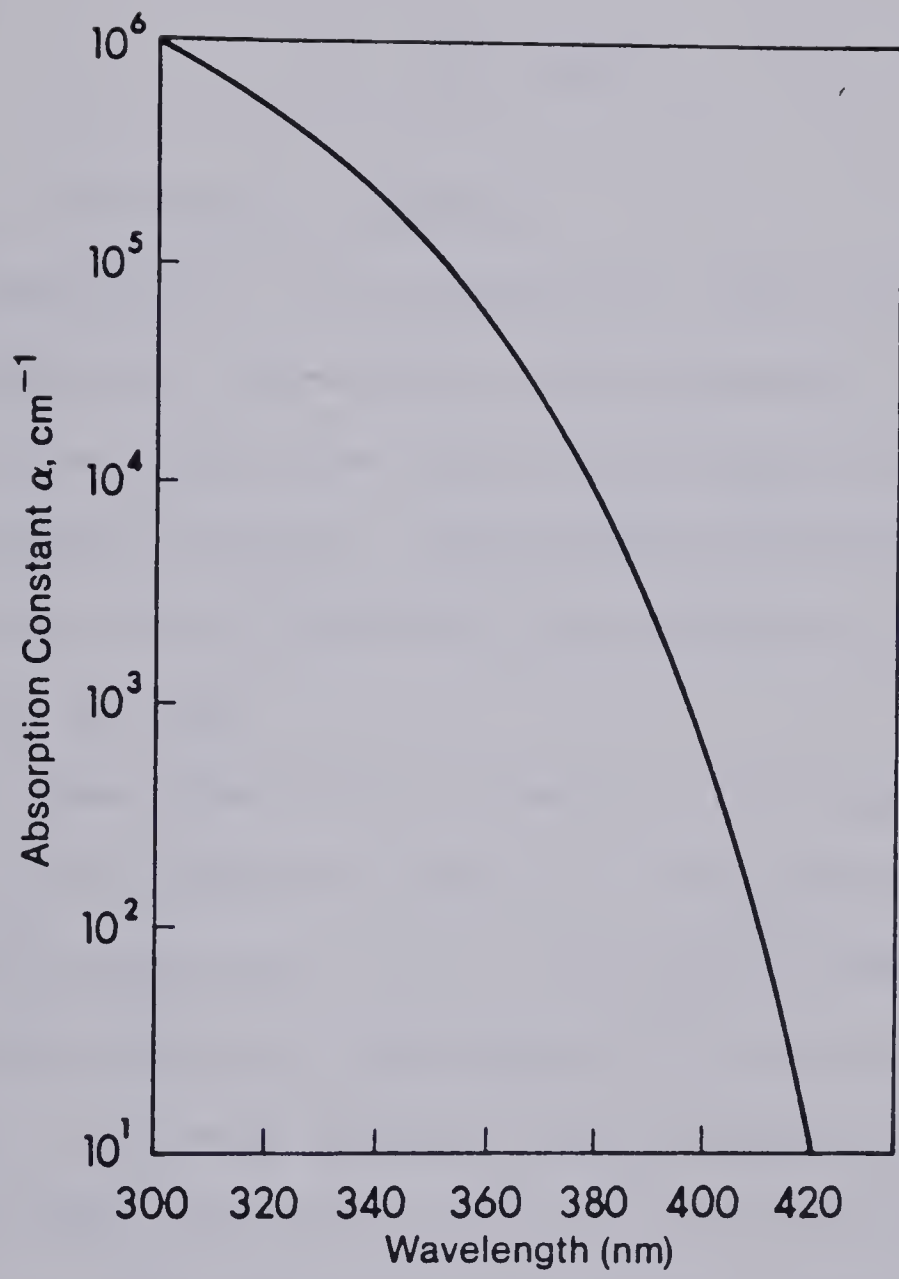


Fig. 5.3 Absorption Constant of TiO_2 .

on the total current density J_T with $S_r + S_t$ taken as a parameter, Fig. 5.4, and second, by studying the effect of $S_r + S_t$ on the total current density for different values of V . In both cases the total current density J_T was calculated by numerical integration of the relation

$$J_T = \int_{\lambda_1}^{\lambda_2} J(\lambda) d\lambda ,$$

where $\lambda_1 = 300$ nm and $\lambda_2 = 420$ nm.

Results (for $\beta = 0$) indicate that, unless the quantity $S_r + S_t$ is unreasonably small, the surface reaction parameters have almost no effect on the cell performance (as long as the voltage drop across the depletion region exceeds 0.15 volts). These results were further confirmed by studying the effect of variation of the parameter $S_r + S_t$ on the spectral response of the cell.

A somewhat speculative explanation of the above result is as follows. Since, according to Eqn. 5.17' the surface reaction parameter S increases sharply with V (for $V > 0$), and also because the surface recombination velocity S_r decreases with increasing V , it is possible that for $V > 0.15$ volts the hole transfer reaction is a dominant process.

If these speculations are correct, and since for uniformly doped structures a voltage drop across the depletion region is essential for the separation of charge carriers, it is highly improbable that surface recombination plays any important role in the cell operation. This is particularly valid for a TiO_2 electrode which must be operated at a small anodic bias.

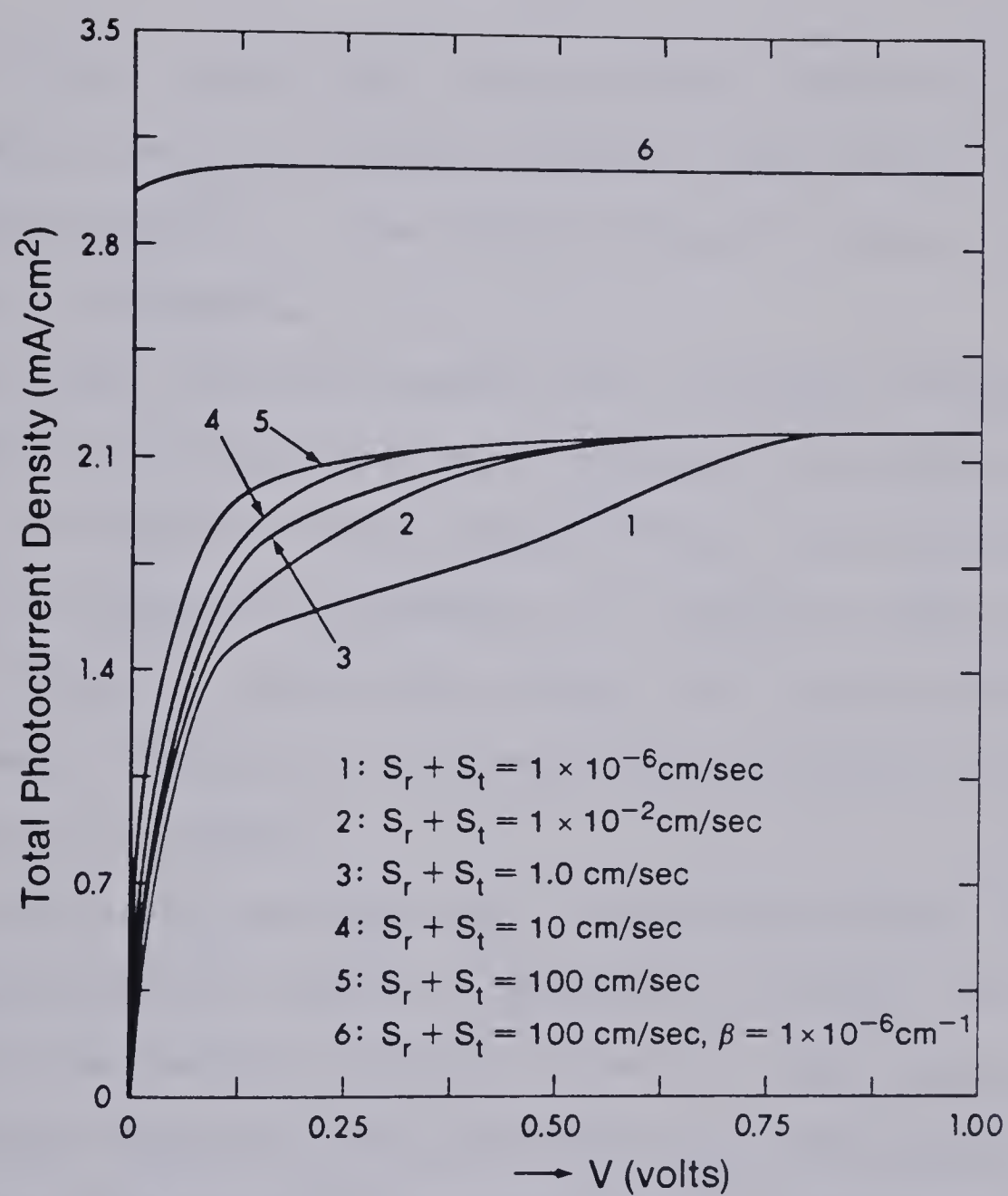


Fig. 5.4 Current Voltage Characteristics with $S_r + S_t$ as a Parameter.

As can be seen in Fig. 5.4, cell performance is almost independent of surface reaction parameters for $\beta = 1 \times 10^6 \text{ (cm}^{-1}\text{)}$, curve 6. This can be easily explained using Eqn. 5.14 for J . For $\beta \gg 1/L_p$, M_1 is zero and consequently the expression for J is independent of the parameter S .

5.6.2 Effect of Diffusion Length, L_p .

In Figs. 5.5a and 5.5b, current density J (mA/cm²μm) and quantum efficiency η , are plotted versus wavelength λ , for different values of the diffusion length L_p . The choice of values for the other parameters is given in the legend.

As shown, the results indicate that in the long wavelength range, the response is strongly affected by variations in the diffusion length. That is, the response increases with an increase in the diffusion length. In the short wavelength range however, the response is rather insensitive to such variations in the diffusion length, and a unity quantum efficiency is achieved. This behavior can be explained by using Eqns. 5.14 for J and 5.22 for η as follows.

In the short wavelength range of the spectrum, that is, for non-penetrating radiation, photons are absorbed in a very thin layer just beneath the semiconductor/electrolyte interface. Thus, electron-hole pairs will be generated in the space charge region where they will be acted upon by the electric field present there. Electrons will move towards the bulk of the semiconductor and then through the external circuit to the counter electrode, while holes will be driven to the interface where they react. The current in this wavelength range is therefore due to carriers generated in the space charge region only, where the diffusion length plays no role.

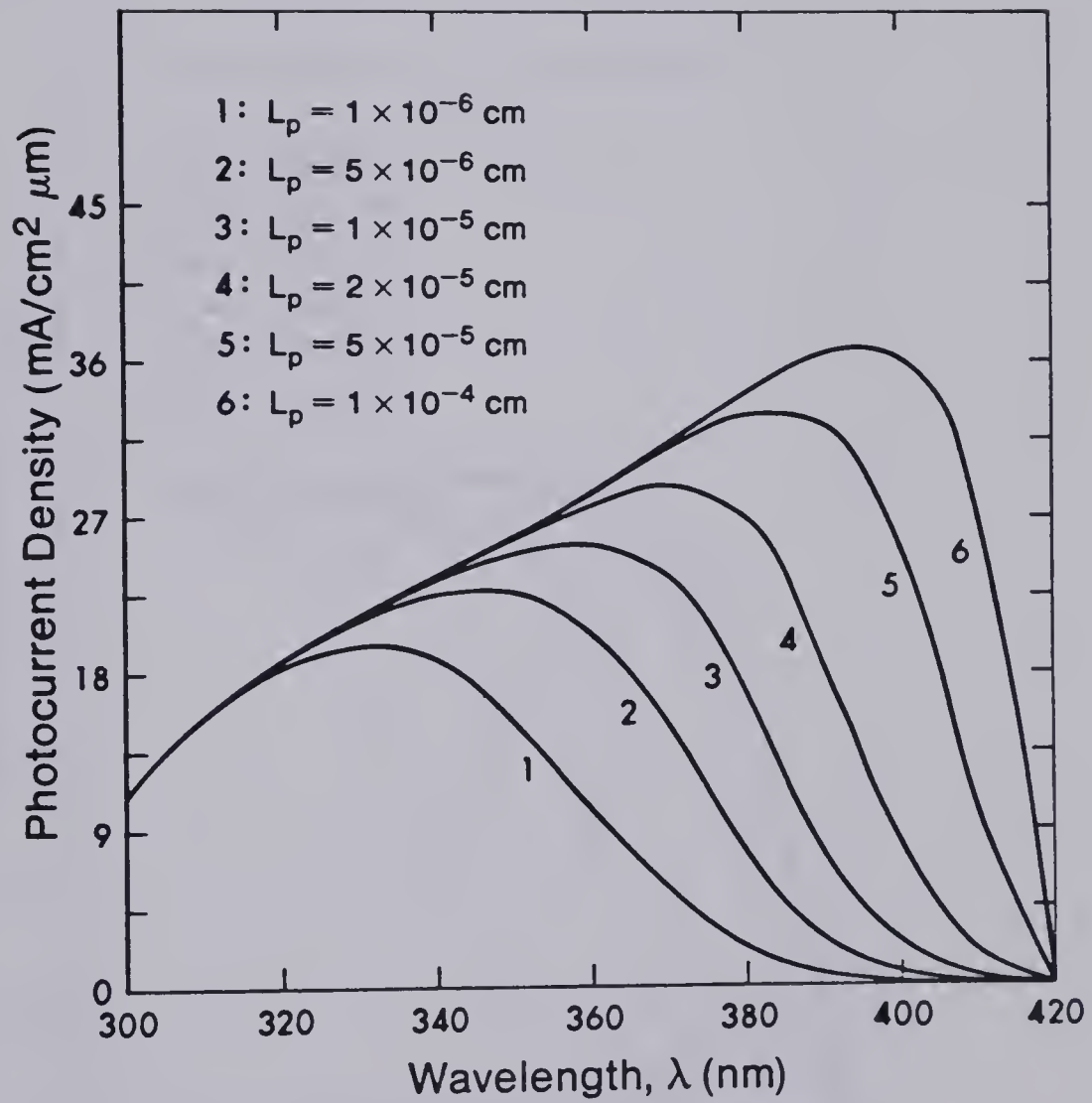


Fig. 5.5a Spectral Response of a TiO_2 Photoelectrolysis Cell, L_p as a Parameter.

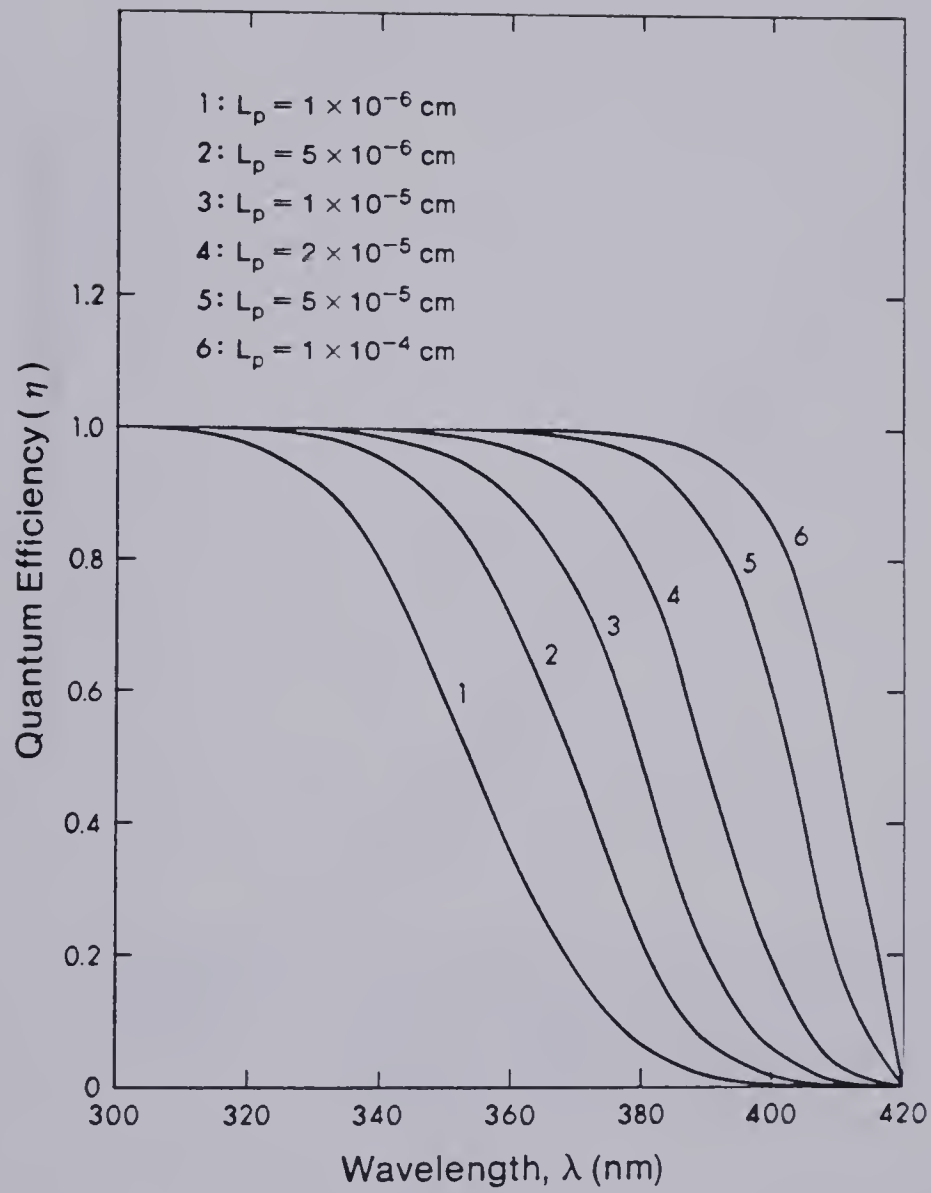


Fig. 5.5b Variation of Quantum Efficiency with λ , L_p as a Parameter

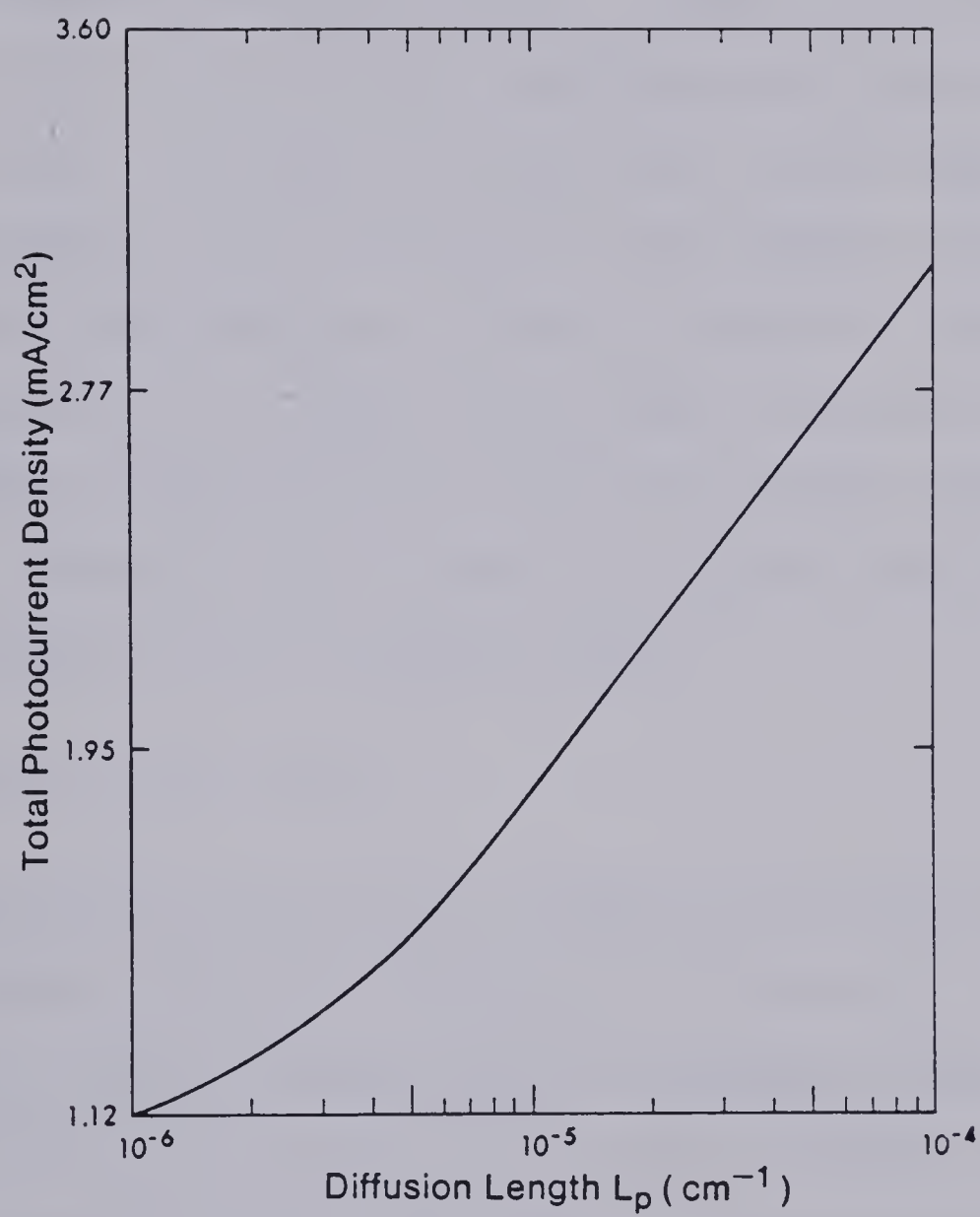


Fig. 5.5c Effect of the Diffusion Length L_p on the Total Photocurrent Density J_T .

In the long wavelength range, i.e., for penetrating radiation most of the carriers are generated outside the space charge region. Photo-generated holes will therefore move towards the depletion region edge, driven by the action of both the hole concentration gradient and the drift field caused by nonuniform doping. Current in this range of the spectrum is mainly due to carriers generated outside the space charge region, and that is the reason for which the diffusion length shows a significant effect on cell performance in that range of wavelength. In Fig. 5.5c the total photocurrent density J_T (mA/cm²) is plotted versus L_p for the same set of parameters used in Figs. 5.5a and 5.5b. The total current density corresponding to a particular diffusion length was obtained by calculating the area under the curve for that particular diffusion length in Fig. 5.5a and the λ -axis.

5.6.3 Effect of Drift Field.

In Figs. 5.6a and 5.6b, the influence of the drift field on the spectral response and quantum efficiency are illustrated. Similar to the effect of diffusion length, the cell performance is relatively independent of the drift factor β in the short wavelength range, but is significant in the long wavelength range. This can be explained as follows. According to Eqn. 5.22, the depletion region width w , decreases with increasing β (with V , N_0 kept constant). In the short wavelength range this decrease in the depletion region width has almost no significance, due to the fact that the quantity $(1 - e^{-\alpha w})$ approaches zero, and the contribution of carriers generated in the depletion region to the total current is negligible. Current will therefore be mainly due to

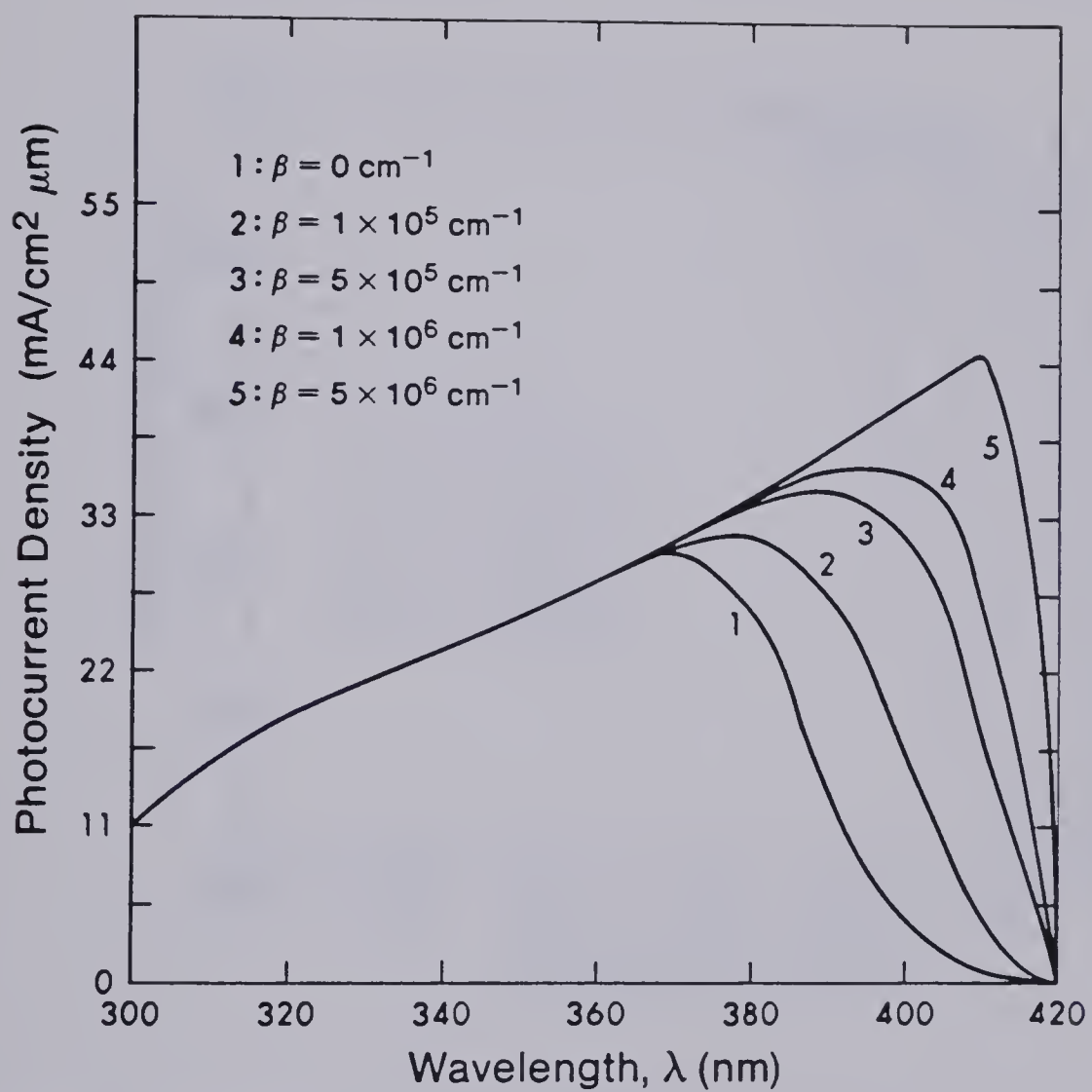


Fig. 5.6a Spectral Response of a TiO_2 Photoelectrolysis Cell, β as a Parameter.

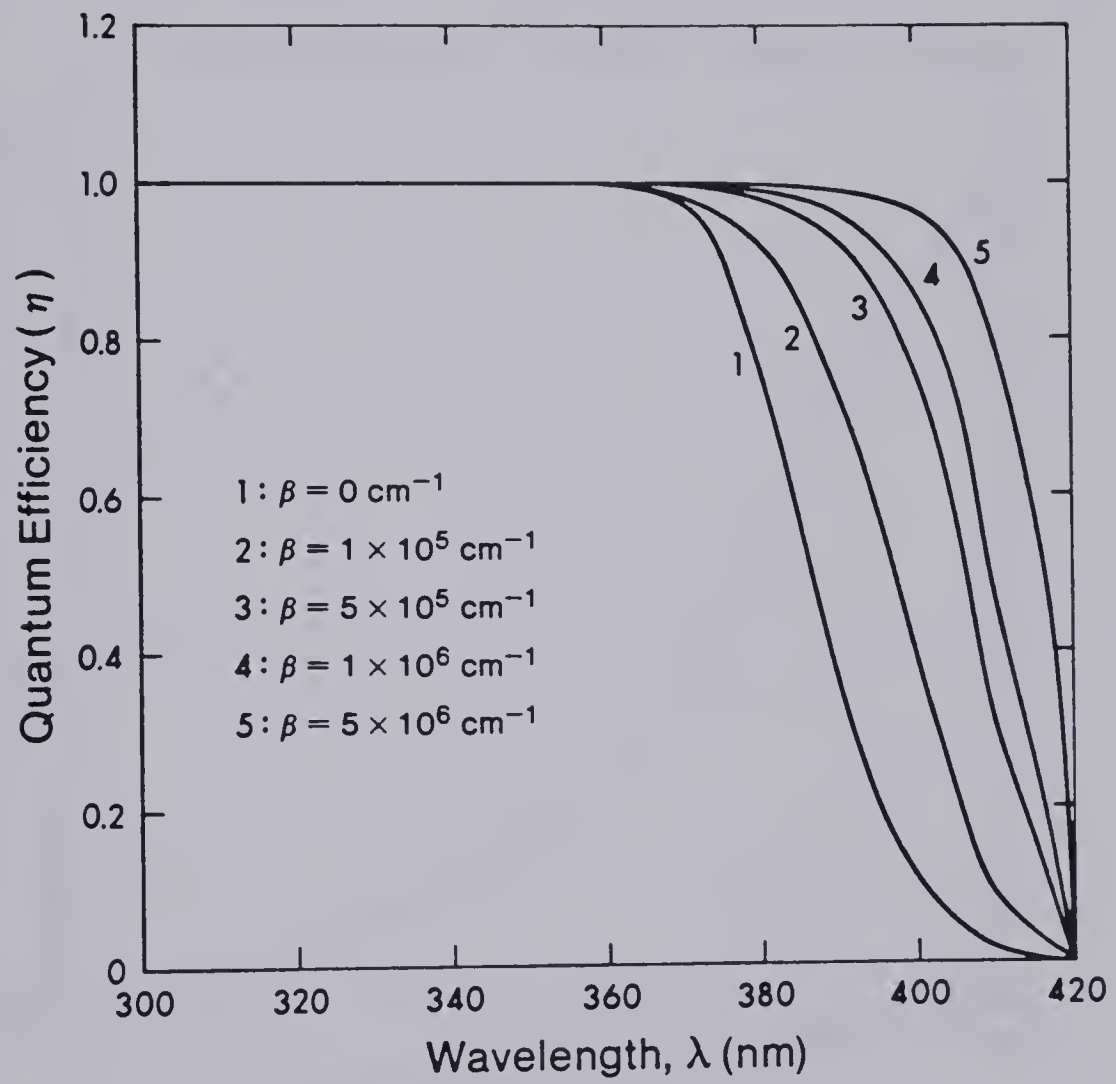


Fig. 5.6b Variation of Quantum Efficiency with λ , β as a Parameter.

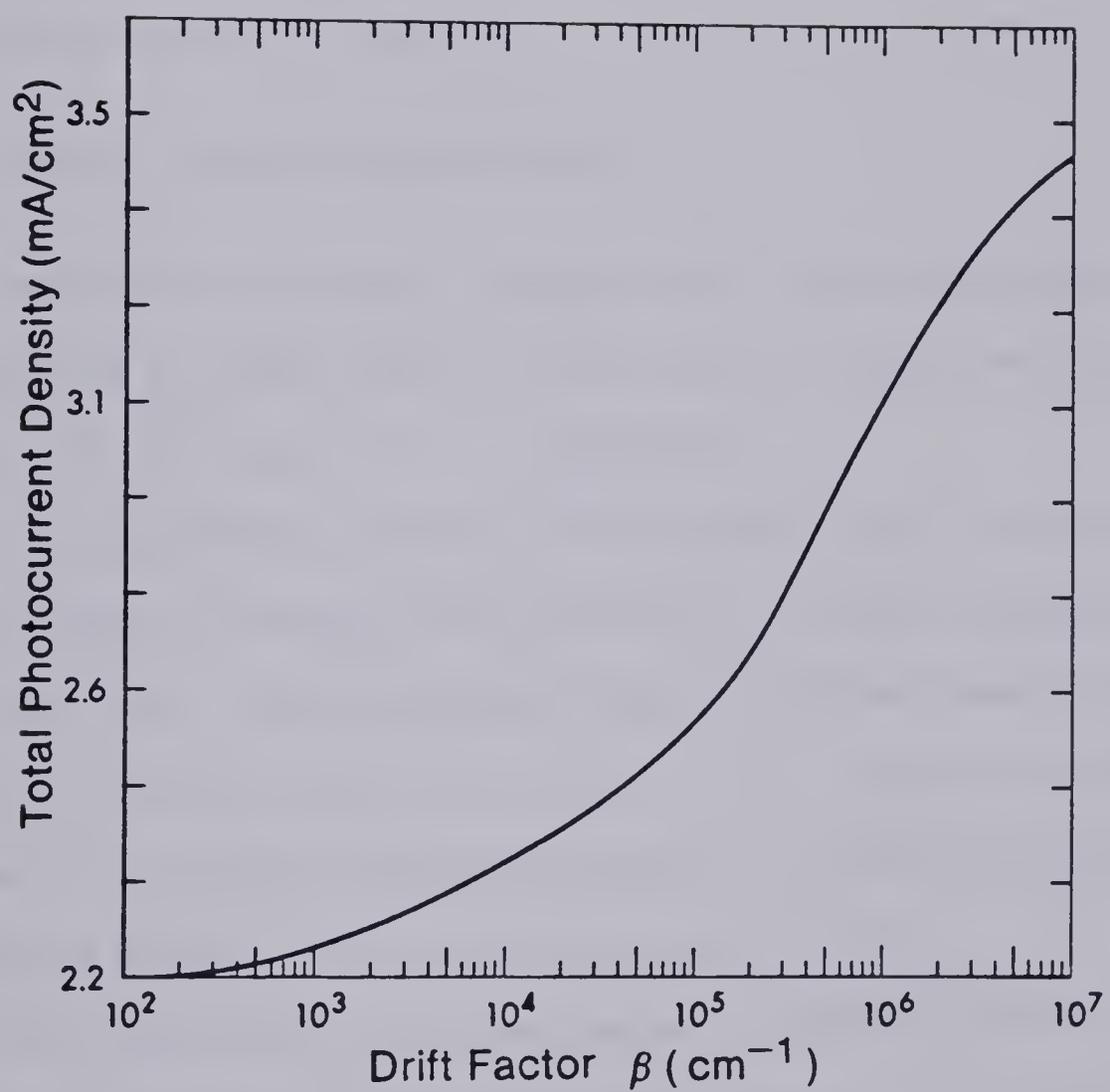


Fig. 5.6c Effect of the Drift Field β on the Total Photocurrent Density J_T .

carriers photogenerated in the semiconductor bulk. Since these photo-generated carriers are driven to the interface by diffusion and are acted upon by the built-in drift field, the increase in the cell response due to an increase in the drift factor β (and accordingly the drift field) is expected. In Fig. 5.6c, the total photocurrent density J_T is plotted versus the drift factor β .

5.6.4 Effect of Donor Concentration, N_0 .

The effect of the donor concentration N_0 was investigated for uniform doping profiles (with $\beta = 0$) as well as nonuniform doping profiles (for the case of $\beta = 1 \times 10^6(\text{cm}^{-1})$).

Our calculations show that for uniformly doped structures the cell performance increases with decreasing N_0 in the long wavelength range, Fig. 5.7a. For nonuniformly doped structures however, the response is totally insensitive to N_0 . Also at longer wavelengths the response of the impurity graded structures is significantly higher than the response obtained for a uniformly doped material.

The above results can be explained by the use of Eqn. 5.23 for w_0 and Eqn. 5.15 for current as follows. From Eqn. 5.15 the depletion region width determines the quantum efficiency in the long wavelength region. Consequently, the quantum efficiency will increase with increasing w . From Eqn. 5.23 it is also noted that the depletion region width is inversely proportional to the square root of the doping density. As a result the quantum yield is expected to decrease with increasing doping density in the long wavelength range, where more

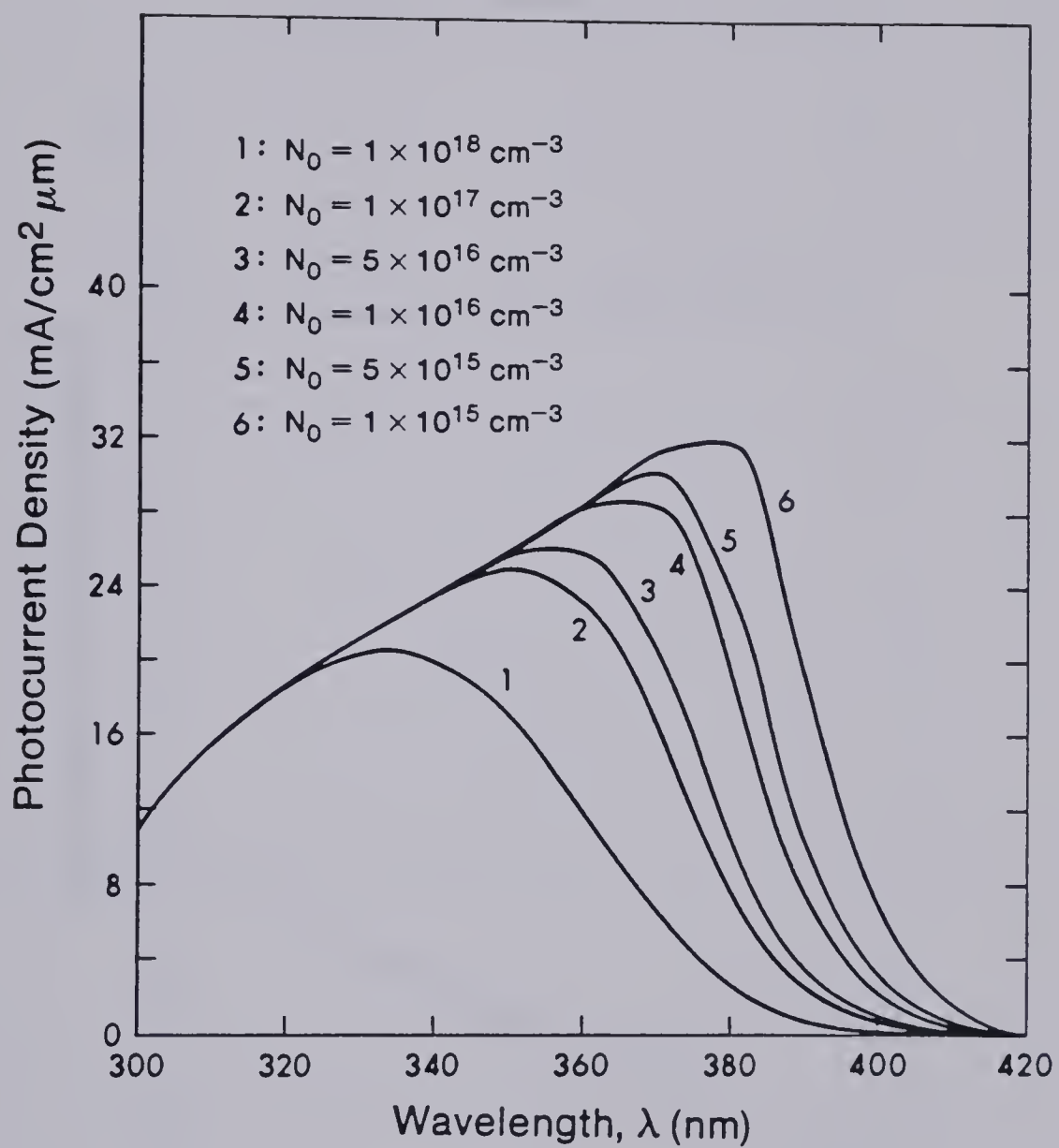


Fig. 5.7a Spectral Response of a TiO_2 Photoelectrolysis Cell, N_0 as a Parameter.

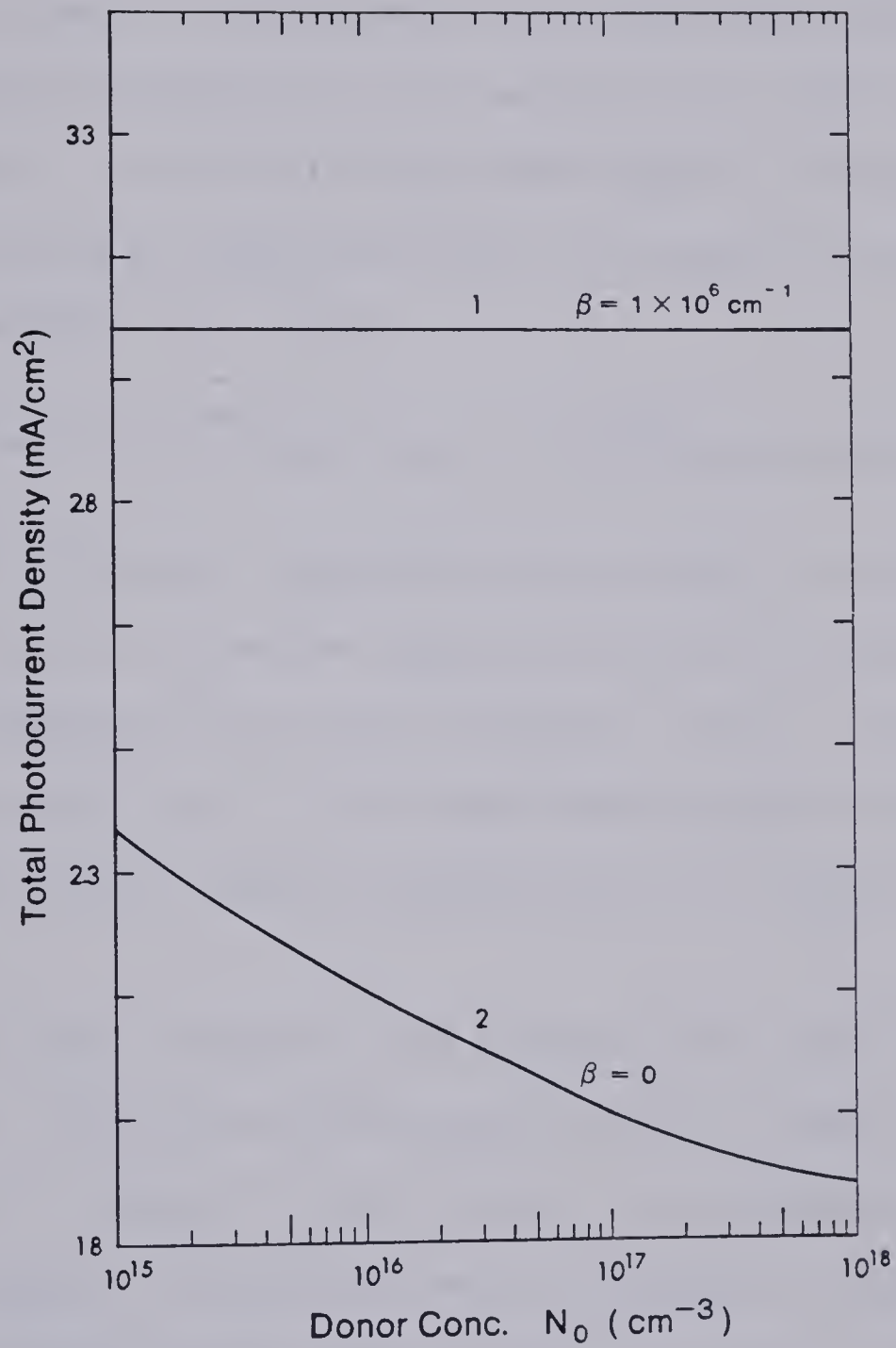


Fig. 5.7b Effect of Surface Donor Concentration N_0 on the Total Photocurrent Density J_T .

carriers are generated outside the space charge region. In Fig. 5.7b the total current is plotted versus N_0 .

For nonuniformly doped structures the situation is different. Our calculations of the depletion region width, given by Eqn. 5.22, indicate that the increase in the depletion region width due to the decrease of N_0 , is negligible compared to its decrease due to the inclusion of the drift factor β . The effect of the drift factor β will therefore be dominant, and as was explained before, an increase in the response at longer wavelengths will result.

5.6.5 Effect of the Voltage Drop, V , across the Depletion Region.

This effect was studied for uniform as well as for nonuniform doping profiles. For uniform doping profiles ($\beta = 0$), the cell performance increases slightly with increasing V (for $V > 0$) in the long wavelength range, Fig. 5.8. For nonuniformly doped structures the cell performance does not show any variation with V for the value of β chosen.

The slight variation of the response with V , for $\beta = 0$, is easily understood. Since the depletion region width w_0 is proportional to $(V)^{\frac{1}{2}}$, an increase in V means that more carriers are photogenerated in the depletion region. On the other hand, for the case of nonuniform doping, our calculations show that the variation in w , with V , is negligible compared to the variation with β . Therefore, a variation in V has almost no effect on the cell performance.

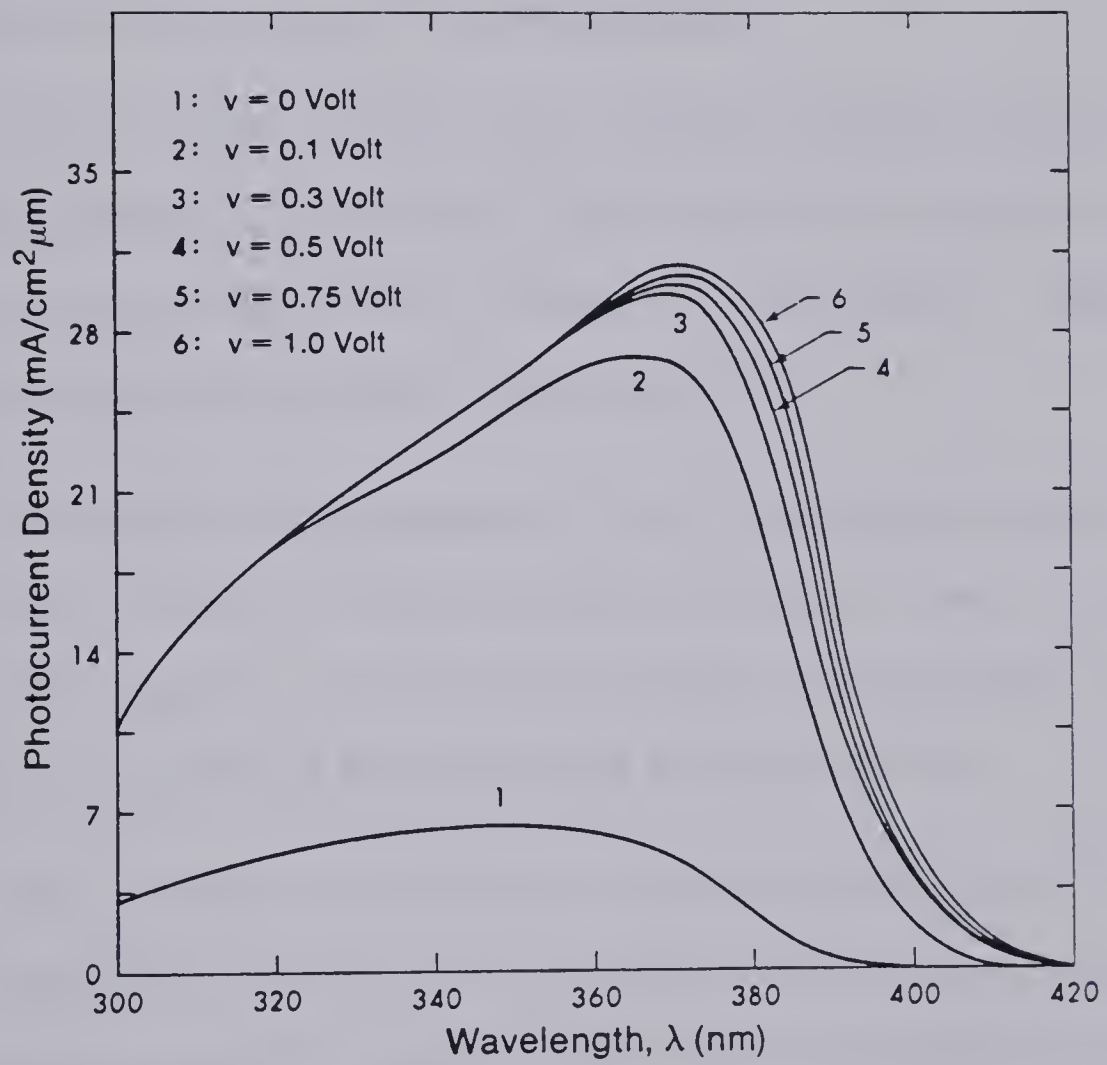


Fig. 5.8 Spectral Response of a TiO_2 Photoelectrolysis Cell, V as a Parameter.

5.7 LIMITATIONS OF THE MODEL

1. The model was developed on the basis of a depletion region approximation, therefore it is not adequate for the case when an inversion layer is formed at the semiconductor/electrolyte interface. Consequently, the model is appropriate only for the case of $V < E_g/2$, where E_g is the energy gap of the semiconductor.

2. Since little is known about surface reaction rates at semiconductor/electrolyte interfaces, only approximate expressions for surface reaction parameters were included in the analysis. Additional work is required to improve these approximations.

3. The extent of enhancement of cell performance by inclusion of a drift field is subject to the constraints that, the lower limit of impurity concentration is that of the intrinsic semiconductor, while the higher limit is specified by the maximum solid solubility.

4. The effects of variations in doping on mobility and lifetime were not included in the analysis simply because such data are not available for the materials used in these photoelectrochemical cells.

5.8 CONCLUSION

A theoretical model for the photoexcited semiconductor electrode predicting its behavior in terms of various physical parameters has been developed.

The model successfully includes the effect of the built-in drift field caused by an exponential impurity doping profile.

The effect of surface reaction rates at the semiconductor/electrolyte interface was also considered. In addition, an expression for the depletion region width that takes into account the influence of the drift field was derived.

The mathematical treatment was further simplified through solution of the continuity equation (for minority carriers generated outside the space charge region) in terms of the relative excess density of minority carriers, $\delta P/P_0$. This approach, which clearly showed that current is proportional to the relative excess density, provided a compact form for the current density that combined both drift and diffusion effects.

Curves illustrating the effects of different physical parameters on cell performance for a typical TiO_2 electrode were given.

The main conclusions drawn from the theoretical investigations are as follows:

- i) It seems unlikely that recombination at the semiconductor/electrolyte interface plays any important role in cell performance, especially if a voltage drop across the depletion region is essential for cell operation.
- ii) The cell performance is insensitive to variations in the hole diffusion length in the short wavelength range ($\lambda < \sim 330$ nm). The response however, increases significantly with increasing diffusion length at longer wavelengths.
- iii) For uniformly doped semiconductors the donor concentration greatly affects the overall response of the cell. For impurity graded structures, however, the response is independent of surface donor concentrations (which is limited by the carrier concentration of the intrinsic semiconductor).

iv) The built-in drift field caused by an impurity gradient always enhances the component of photocurrent which is due to absorption of light outside the space charge region. However, an increase in the drift field also results in a decrease in the depletion region width. This means that incorporation of a drift field into a semiconductor electrode will decrease somewhat the current component for carriers generated inside the space charge region but at the same time will significantly increase the current component for carriers generated outside the depletion region. The cumulative result is that the net current is enhanced, thereby, leading to an increase in overall cell response.

v) It should be noted here that although the analysis was presented for the case of a semiconductor/electrolyte interface, the model should be equally applicable to any Schottky barrier solar device.

vi) Experimental verification of the model and further theoretical investigations for other doping profiles are needed.

CHAPTER 6

AN INVESTIGATION OF THE POSSIBILITY FOR IMPROVEMENT OF THE PHOTORESPONSE OF A TiO_2 ELECTRODE

6.1 EFFICIENCY CONSIDERATIONS

Direct converters of solar energy can transduce only a fraction of incident broad band light to useful work because they can make use of only those photons with more energy than a minimum threshold value E_{th} . Photons of energy $E < E_{th}$ are generally not absorbed by the converter because, even if they are, they are not converted to useful work. Photons of energy $E < E_{th}$ are also not wholly and efficiently utilized. The fraction $(E - E_{th})/E_{th}$ of the photonic energy is dissipated as heat, therefore, only the fraction E_{th}/E is available for useful work (electrical or free energy).

For a semiconductor the threshold energy E_{th} corresponds to the energy gap E_g of the semiconductor. If it is assumed that the semiconductor has a steep absorption edge at the energy of the band gap E_g , all photons will be absorbed in a narrow depth beneath the surface.

According to this argument, if $f(E)$ is the power density per unit energy interval per second of the incident radiation, the useful power density at a certain energy E ($E > E_g$) will be given by $f(E)E_g/E$. A hypothetical conversion efficiency η_{hyp} for a semiconductor having an energy gap E_g , may be therefore written as

$$\eta_{hyp} = \frac{E_g \int_{E_g}^{\infty} f(E)/E dE}{\int_0^{\infty} f(E) dE} . \quad (6.1)$$

Numerical evaluation of this efficiency expression for the solar radiation spectrum reveals maximum solar conversion efficiency of the order of 47%. This occurs in a semiconductor with an energy gap of 1.2 eV [6.1, 6.2].

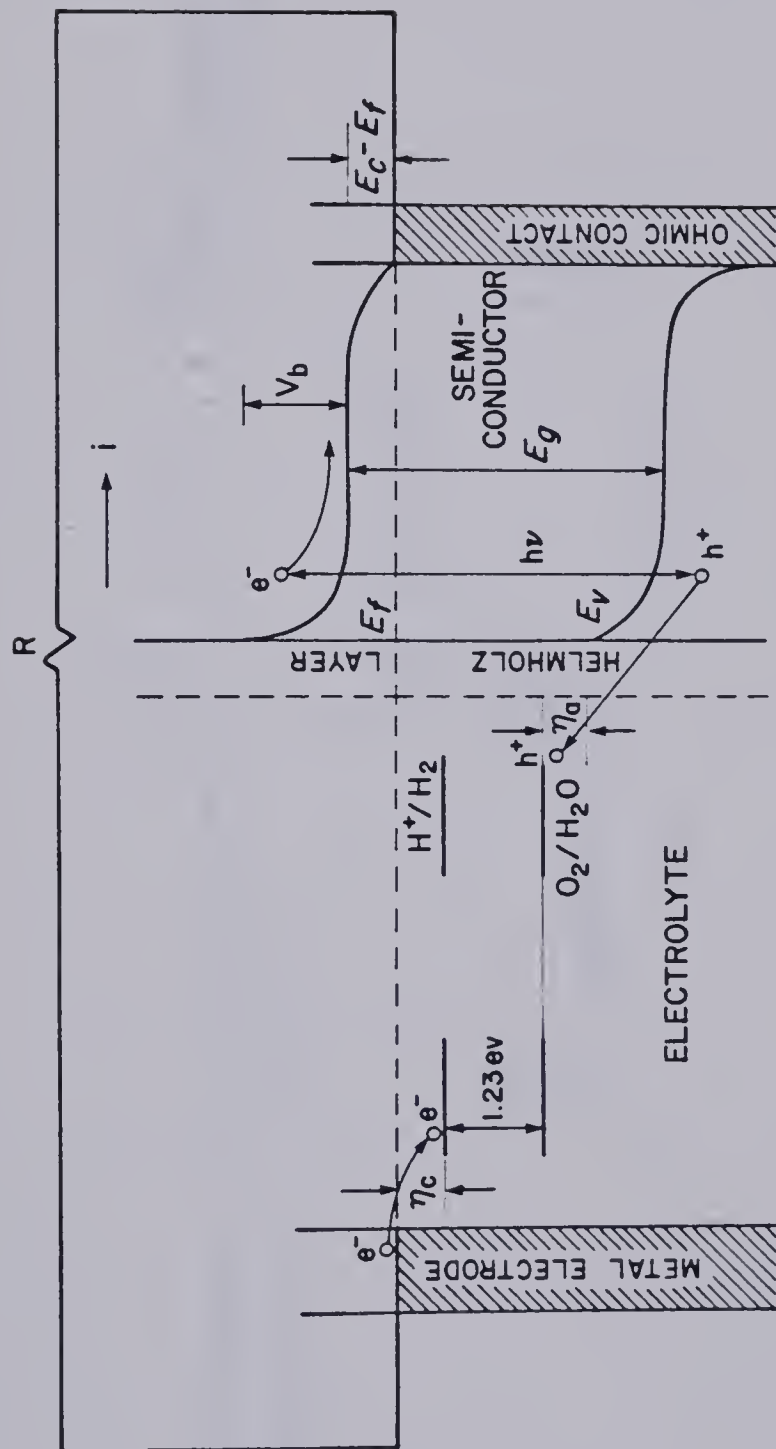
The real conversion efficiency into useful free energy is lower than that given by Eqn. 6.1 due to unavoidable energy dissipation mechanisms and free energy entropy production.

To get an estimate of the energy loss in a photoelectrolysis cell, an energy balance diagram needs to be considered [6.3]. According to the energy balance diagram, Fig. 6.1, one can write

$$h\nu = E_g = \frac{\Delta G}{nF} + iR + \eta_c + \eta_a + E_f - E_c + qV_b \quad (6.2)$$

where $h\nu$ is the energy of the incident radiation; $\frac{\Delta G}{nF}$ is the free energy for water oxidation and is equal to 1.23 eV; V_b is the band bending which is the difference between the redox potential of the electrolyte and the flat band potential; $E_c - E_f$ is the difference between the band edge for majority carriers and the Fermi level; η_c is the energy difference between the majority carrier quasi Fermi level and the water reduction level; η_a is the difference between the valence band edge at the semiconductor electrolyte/interface and the water oxidation level.

There are some serious problems to be solved before realizing the idea of the photoassisted electrolysis of water using a semiconducting TiO_2 electrode. One is that the band gap of TiO_2 is in the ultraviolet range of the solar spectrum. Consequently its poor response to visible light makes it of limited use. Another is that the energy levels of TiO_2 are not properly located w.r.t. the energy levels of the redox couples for water electrolysis, Fig. 6.2. The conduction band edge is



$$h\nu = E_g = \frac{\Delta G}{nF} + iR + \eta_c + \eta_a + E_f - E_c + qV_b$$

Fig. 6.1 An Energy Balance Diagram for a Water Photoelectrolysis Cell using an n -type Semiconductor.

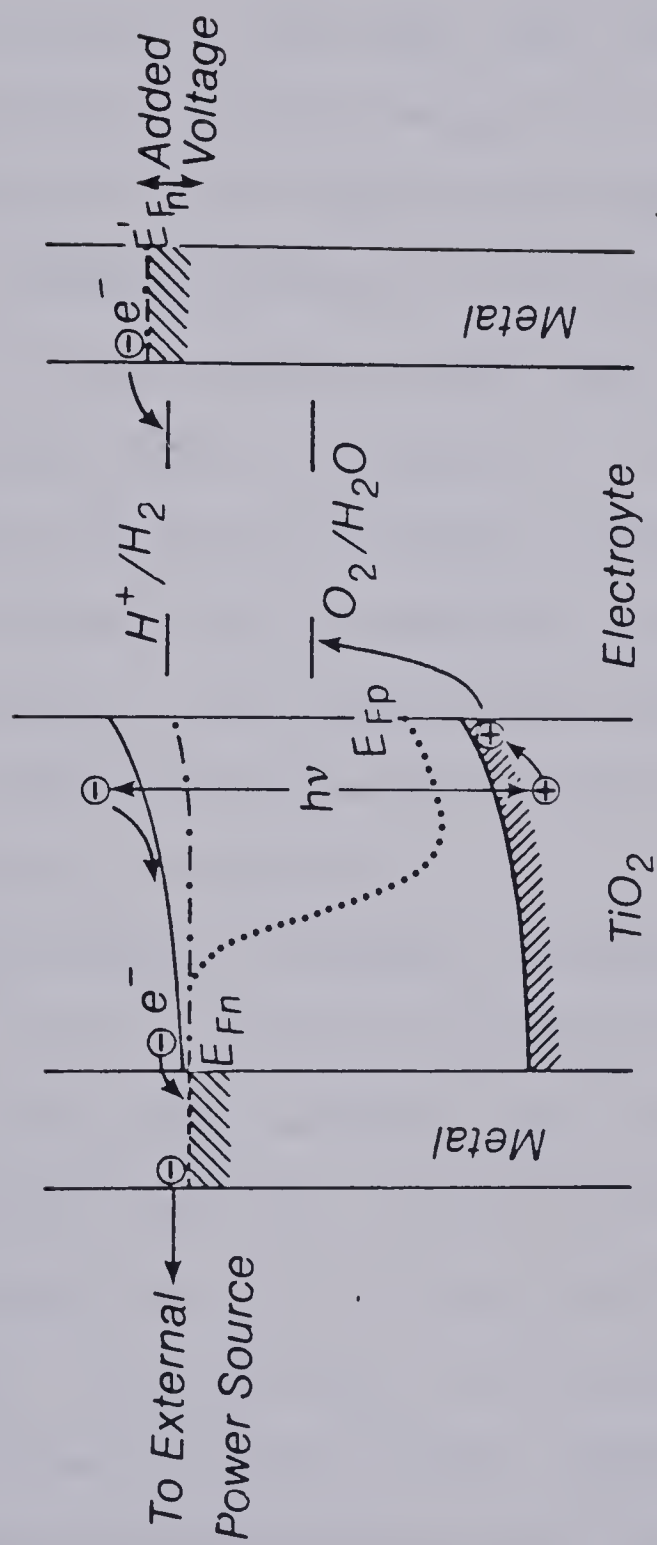


Fig. 6.2 Electron Energy Correlations in a Water Photoelectrolysis Cell with an n -type TiO_2 Photoelectrode.

slightly above the Fermi level for water reduction. The quasi Fermi level of the electrons cannot therefore reach a large enough driving force for hydrogen evolution. This requires an additional bias. On the other hand, the valence band edge of TiO_2 is far below the Fermi level for water oxidation. The quasi Fermi level of holes E_{fp} will therefore reach and surpass this energy at very weak illumination as long as the energy of light exceeds the band gap. The result is that, even at weak illumination intensity, this system has a much higher driving force for the oxidation of water than necessary, and thus considerable excess energy is dissipated.

A study of the physical processes involved in the photoassisted electrolysis of water using a semiconductor electrode reveal that the principal requirements that determine the suitability of such an electrode for water photoelectrolysis may be roughly divided into two classes: electronic and chemical.

From the electronic standpoint the energy band bending in the space charge region must be sufficient to separate the free charge carriers (especially for the case of uniformly doped semiconductors) and the relevant electronic levels must line up (the conduction band is above the water reduction level and the valence band is below the water oxidation level). In other words, the semiconductor must generate as large a photocurrent as possible without suffering appreciable loss.

From the chemical standpoint the main requirement is the chemical stability of the electrode against decomposition.

The possibility of using small band gap semiconductors has been investigated [6.4, 6.5]; only a few have been found to be adequately stable. However, the flat band potential for these stable small band

gap semiconductors indicate that a larger bias is required for their operation than for TiO_2 .

This being the case, it appears that an appropriate approach to overcome these problems may be to attempt to alter the properties of materials like TiO_2 and SrTiO_3 , which exhibit the best performance in such a way as to improve their photoresponse.

Towards this end, we have investigated the possibility of extending the spectral response of TiO_2 thin films into the visible portion of the solar spectrum using different doping techniques. In the forthcoming sections the rationale behind the approach is explained, laying particular emphasis on the effect of impurity doping on the optical properties of a semiconductor electrode.

6.2 IMPURITY CENTERS IN SEMICONDUCTORS

The presence of foreign atoms in crystals may lead to essential changes in their physical and chemical properties. These foreign atoms may act as electron donors or acceptors. Thus, the control of the physical and chemical properties of a crystal can be realized by introducing admixtures of either donor or acceptor characters. The problem is different in the case of oxides, which as a rule have a tendency to deviate from stoichiometry. The donors, acceptors and other impurity centers are provided by native defects. Therefore to obtain controlled properties, the relationship between the concentrations of native defects and foreign atoms in oxides must be known.

Crystal imperfections and foreign atoms in semiconductors introduce discrete energy levels in the forbidden energy gap. According

to a simple hydrogen model, the donor levels lie close to the conduction band edge, and the acceptor levels lie close to the valence band edge. Moreover, whenever an impurity atom can contribute more than one extra carrier (a multiple donor or a multiple acceptor) it introduces a state for each carrier that it contributes. The various impurity levels extend deeper from the band edges with the increase of the degree of ionization.

Some impurities, however, do not behave according to the above model, and form levels which lie deep within the band gap. These levels, which will be referred to as deep levels (or recombination centers) throughout this discussion, have a small probability for thermal ionization. It should be noted that transition elements seem to form deep levels such as these [6.6].

Deep impurity levels in semiconductors are of particular interest in this study, and the existence of such levels will be shown to govern several important physical properties of the semiconductor.

6.2.1 Impurity Absorption.

Illumination of the semiconductor not only changes the densities of free electrons and holes in the conduction and valence bands, but also changes the population of the local impurity levels in the forbidden energy gap. That is, as with thermal excitation, light may produce transitions between impurity levels and the allowed bands, as well as interband transitions. This can be explained with the help of Fig. 6.3 as follows:

i) The transition between the valence band and an ionized donor (it must be empty to allow the transition) or between an ionized

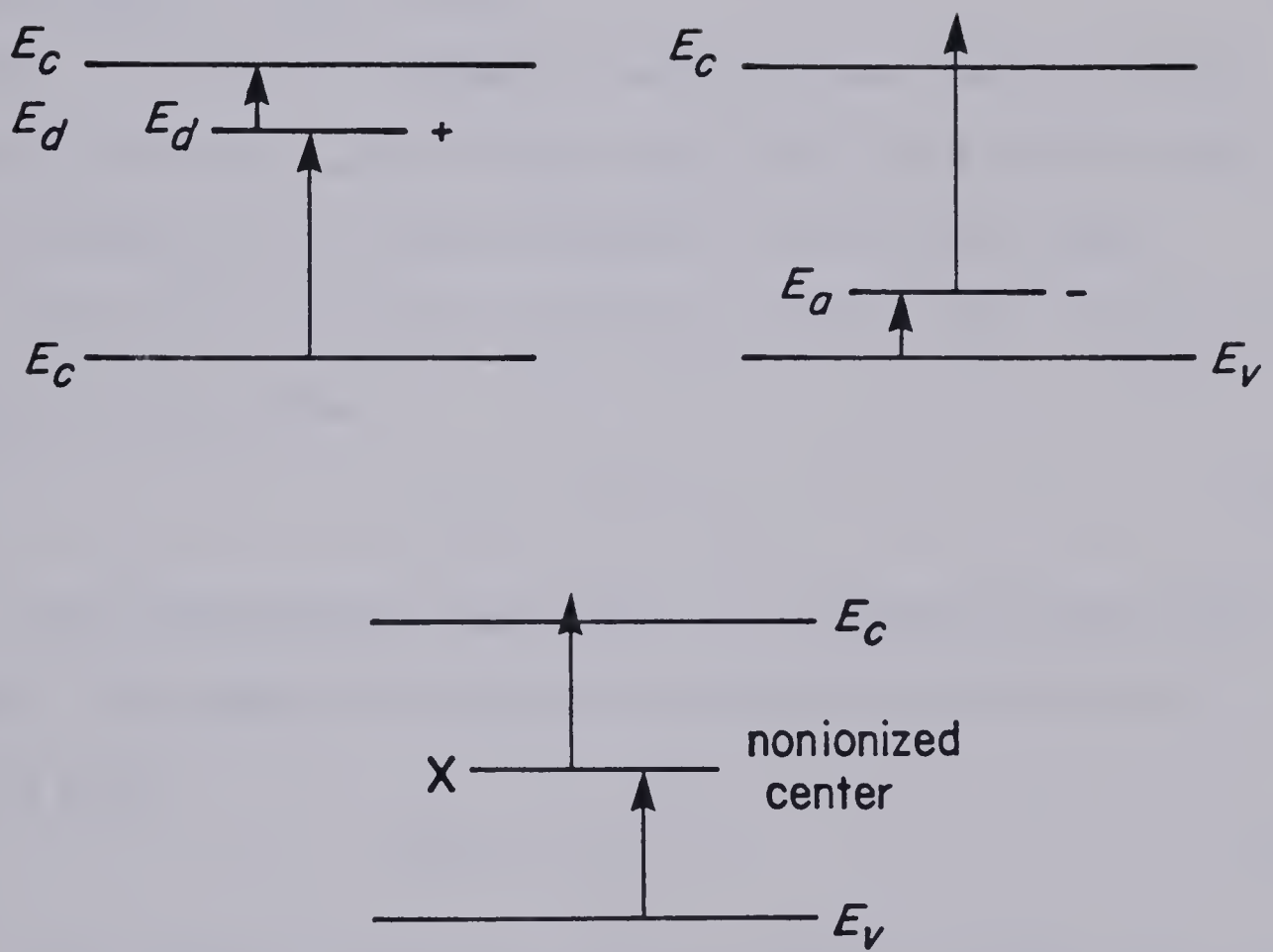


Fig. 6.3 Impurity Absorption in Semiconductors.

acceptor and the conduction band occurs at energies which are given by

$$h\nu > E_g - E_i ,$$

where E_i is the ionization energy.

ii) When both donors and acceptors are simultaneously present in the semiconductor, the acceptor states are at least partly empty. Then it is possible to absorb a photon by exciting an electron from an acceptor state to a donor state.

iii) The transition between a nonionized deep impurity center X and the conduction band or between the valence band and the center can occur by absorption of light according to the following scheme.

The initial excitation step of the impurity center results in ionization of the center



The ionized center is equivalent to a trapped hole and a free electron. The trapped hole can be ionized either thermally or by light to give



Since impurity absorption requires photons of lower energy than interband absorption, the main absorption edge will be shifted toward longer wavelengths. This is the working principle for extending the response of TiO_2 to the visible range of the spectrum in the approach under investigation here.

6.2.2 Impurity Sensitization.

Sensitizing a semiconductor means increasing the lifetime of a free carrier; lifetime here referring to the statistical lifetime of the photogenerated carrier. The lifetime of a carrier is terminated when it moves out of the space between electrodes without being replaced from the opposite electrode, or when it recombines with a deep lying impurity center from which it has to be re-excited by the incident radiation in order to appear as a free carrier again [6.7, 6.8].

In practice a semiconductor is sensitized by the addition of chemical impurities (deep impurity centers in this case). However, the introduction of deep impurity centers in the energy gap of a semiconductor does not necessarily mean that the lifetime is increased. Whether the lifetime of a free carrier will increase or decrease depends on the relations between the parameters of the impurity centers that already exist in the semiconductor (density of occupied and unoccupied states and capture cross sections for electrons and holes) and those of the added impurity centers. That is, if the parameters of the added and existing centers are the same, the lifetime of one or both carriers can only decrease. On the other hand, the addition of impurity centers of a second kind can increase the lifetime of one type of carrier.

Increasing the lifetime of one type of charge carrier by the addition of impurity centers is the model of sensitization. It requires an explanation to show how the addition of recombination centers might increase the lifetime of a free carrier. A simple quantitative example is given to illustrate this model. Consider a set of recombination centers lying near the intrinsic Fermi level of a semiconductor, Fig. 6.4a.

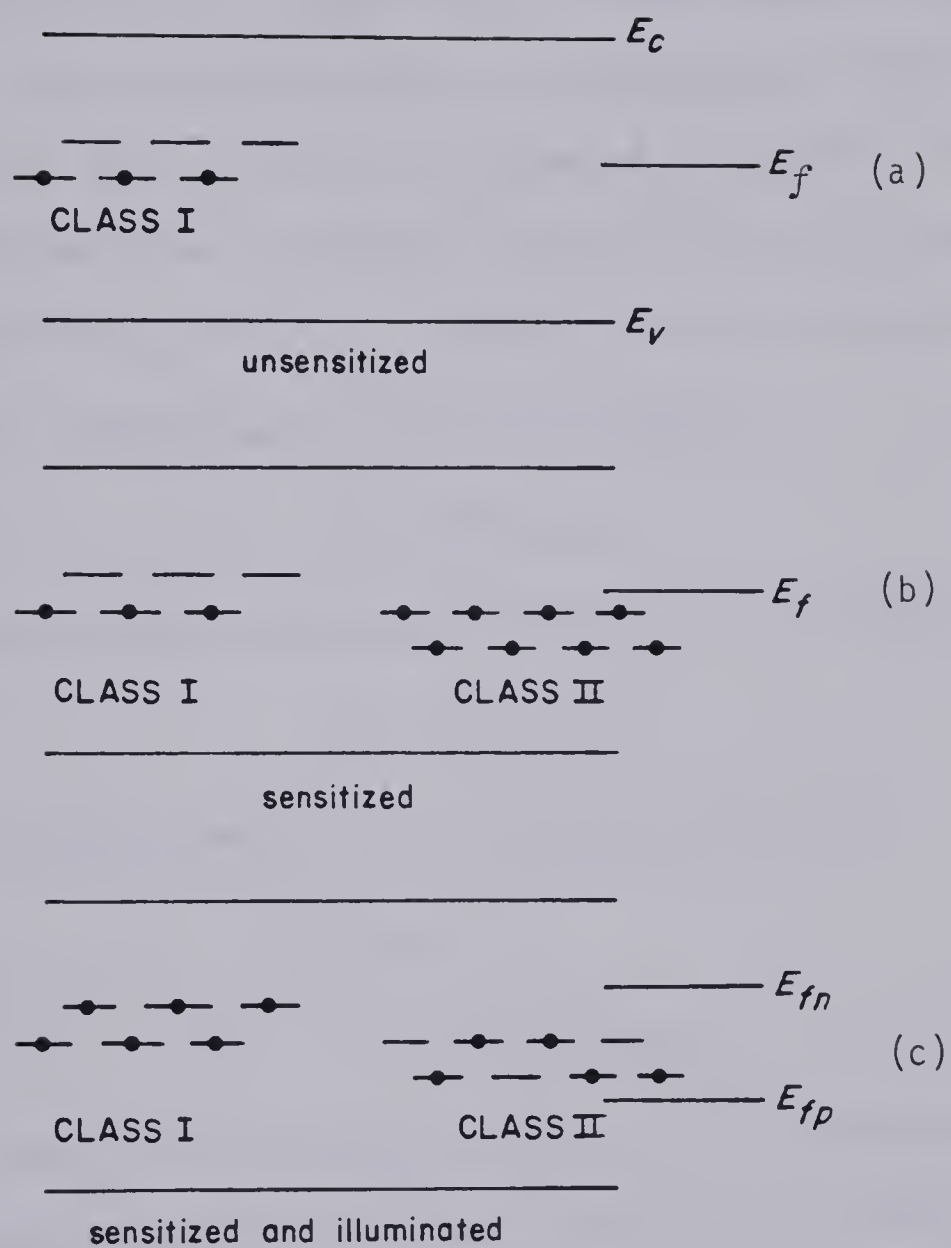


Fig. 6.4 Schematic Outline of Sensitization.

Let their density be N_{1r}/cm^3 and let p_{1r} be the density of centers unoccupied by electrons; n_{1r} being the density of centers occupied by electrons. Let s_{1n} be the capture cross section of an unoccupied center for free electrons, and s_{1p} be the capture cross section of an occupied center for free holes. Assume that the semiconductor material is exposed to light with energy greater than the energy gap. The volume rate of generation of free carriers is designated by G (cm^{-3}). We further assume that densities of excess carriers δn and δp are both small in comparison with n_{1r} and p_{1r} . According to these assumptions, the rate of electron recombination R_n may be written as

$$R_n = \delta n p_{1r} s_{1n} v_n .$$

Similarly, the hole recombination rate R_p can be written as

$$R_p = \delta p n_{1r} s_{1p} v_p ,$$

and the continuity equation for electrons will be

$$\begin{aligned} \frac{d\delta n}{dt} &= G - R_n \\ &= G - v_n p_{1r} \delta n s_{1n} , \end{aligned}$$

where v_n and v_p are the thermal velocities for electrons and holes respectively. Under steady state conditions, the continuity equation for electrons takes the form

$$G - v_n p_{1r} \delta n s_{1n} = 0$$

from which, after substituting for $\delta n = G\tau_n$ and $v_n = v_p = v$, electron life-time will be given by

$$\tau_{1n} = \frac{1}{v s_{1n} p_{1r}} . \quad (6.5)$$

Similarly,

$$\tau_{1p} = \frac{1}{v s_{1p} n_{1r}} . \quad (6.6)$$

In general electron and hole capture cross sections will be different. Similarly, the densities of electron occupied and hole occupied centers will be different. However, for simplicity, corresponding parameters of electrons and holes will be taken as equal. This assumption does not affect the principle of the discussion. That is, if $s_{1n} = s_{1p} = 10^{-15} \text{ cm}^2$, and $n_{1r} = p_{1r} = 10^{15} / \text{cm}^3$, then according to Eqns. 6.5 and 6.6 both electron and hole lifetime will assume the value

$$\tau_{1n} = \tau_{1p} = 10^{-7} \text{ sec} . \quad (6.7)$$

Assume now that additional impurity centers of density N_{2r} / cm^3 , all filled with electrons, have been introduced in the energy gap of the semiconductor (class II states in Fig. 6.4b). The class II impurity centers are assumed to have the same capture cross section for holes ($s_{1p} = s_{2p}$) and a very small cross section for electrons ($s_{2n} = 10^{-5} s_{1n}$). In addition the density of class II centers is assumed to be much higher than the density of class I centers ($N_{2r} \gg N_{1r}$).

Under illumination, steady state conditions must be rigorously satisfied. This specifies that the rate at which free electrons occupy the recombination centers (individually or collectively) must be equal to the rate at which free holes are being captured. That is,

$$\frac{\delta n}{\tau_{1n}} = \frac{\delta p}{\tau_{1p}}$$

or

$$\delta n p_{1r} v s_{1n} = \delta p n_{1r} v s_{1p} .$$

Similarly,

$$\delta n p_{2r} v s_{2n} = \delta p n_{2r} v s_{2p} ,$$

where p_{2r} and n_{2r} are respectively, the densities of occupied and unoccupied class II states. Therefore,

$$\frac{\delta n}{\delta P} = \frac{n_{1r} s_{1p}}{p_{1r} s_{1n}} = \frac{n_{2r} s_{2p}}{p_{2r} s_{2n}}$$

from which,

$$p_{1r} = p_{2r} \left(\frac{s_{2n}}{s_{1n}} \right) \left(\frac{s_{1p}}{s_{2p}} \right) \frac{n_{1r}}{n_{2r}} . \quad (6.8)$$

In addition, according to the particle conservation condition we have

$$n_{1r} + p_{1r} = N_{1r} ,$$

$$n_{2r} + p_{2r} = N_{2r} .$$

Under illumination, free carriers are generated and the occupation density of these impurity centers changes radically. Free electrons will be captured at about the same rate by both class I and class II states. But, whereas holes in class I states are rapidly captured by electrons, those in class II are not, owing to their small electron capture cross section. The net result is that the class I states tend to become filled with electrons; the electrons from class II being transferred to the class I states. This shift in occupancy can proceed to the point that a free hole will have difficulty in being captured by class I states because they are already nearly filled with electrons, thus, there are few empty states. Electrons will also have difficulty in being captured by class II states because they have a small capture cross section for electrons. Therefore, in the limiting case, one can write

$$p_{1r} \rightarrow N_{1r} ,$$

$$p_{2r} \rightarrow N_{1r} ,$$

and for $N_{2r} \gg N_{1r}$, one can write

$$n_{2r} \simeq N_{2r} .$$

With these approximations, Eqn. 6.7 becomes

$$p_{1r} \simeq N_{1r} \left(\frac{N_{1r}}{N_{2r}} \right) \left(\frac{s_{2n}}{s_{2p}} \right), \quad (6.9)$$

and the total rate at which electrons fall into the p_{1r} and p_{2r} states is

$$\frac{\delta n}{\tau_n} = \delta P p_{1r} v s_{1p} + \delta P p_{2r} v s_{2p}$$

$$\tau_n = \frac{1}{p_{1r} v s_{1n} + p_{2r} v s_{2n}},$$

where τ_n is the electron lifetime with both impurity centers present in the energy gap.

If p_{1r} is substituted for in Eqn. 6.9, and by putting $s_{2n} = 10^{-5} s_{1n}$, one gets

$$\tau_n = \frac{1}{v s_{1n} N_{1r} (N_{1r}/N_{2r}) \times 10^{-5} + N_{1r} v s_{2n}},$$

therefore,

$$\tau_n \simeq \frac{1}{N_{1r} v s_{2n}} \simeq 10^{-2} \text{ sec}. \quad (6.10)$$

Comparing the two values for the electron lifetime given by Eqns. 6.6 and 6.10, it is clear that the lifetime increased by a factor of 10^{-5} as a result of the addition of class II impurities.

The effect of the increase of carrier lifetime was theoretically investigated in Chapter 5. As was explained, an increase in lifetime and hence the diffusion length results in an increase in the cell response in the long wavelength range of the spectrum.

6.2.3 Electron Transfer via Impurity Centers.

It has been shown that impurity centers at the semiconductor/electrolyte interface (surface states) can contribute to electron exchange [6.9, 6.10]. This contribution will become much more important as the direct exchange with the energy bands decreases. This effect is therefore most likely to occur in semiconductors with wide band gaps such as TiO_2 . For such semiconductors, the energy level for water oxidation is in the range of the energy gap.

The diagram of charge transfer via surface states is represented in terms of the band model in Fig. 6.5. The mechanism of an *n*-type semiconductor/electrolyte interface can be briefly explained as follows [6.11, 6.12]. Illumination of the electrode with band gap light generates holes in the valence band which in turn can be filled by electrons from the intermediate level. The resulting hole at this intermediate level can then isoenergetically exchange electrons with the reduced species in the electrolyte.

6.3 IMPURITY CENTERS IN TiO_2

In this section a brief review of the recent investigations on the impurity and defect structure of TiO_2 is given.

Ghosh et al. [6.13] studied the photoelectronic processes in TiO_2 in a wide range of experiments and were able to detect large numbers of defect levels. The levels detected in their experiment were according to their definition: shallow traps (thermal ionization energy below 1 V) and deep levels (optical ionization energy greater than 1.5 V).

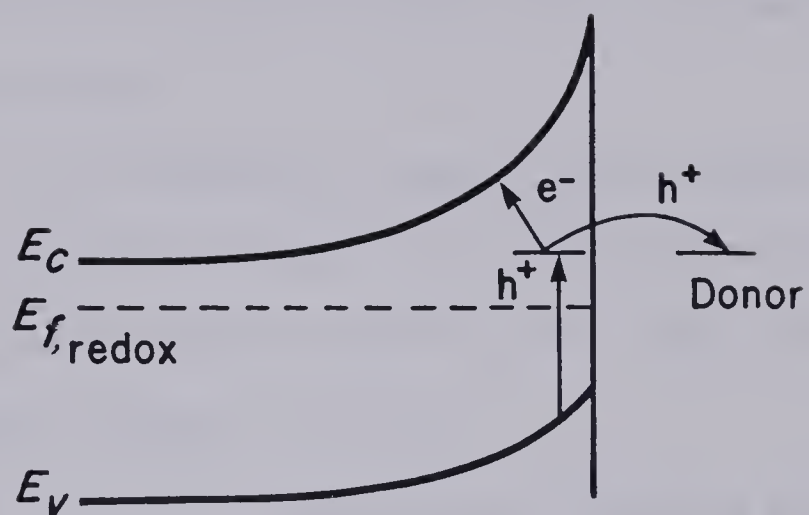


Fig. 6.5 Charge Transfer via Surface States at the Semiconductor/Electrolyte Interface.

Mirlin et al. [6.14] studied the optical absorption and electrical conductivity in chromium-doped reduced TiO_2 . They reported that the electrical conductivity of chromium-doped crystals was much lower than the undoped ones. These observations led them to conclude that chromium doping produces quite deep centers which capture electrons and they found that the absorption in chromium-doped crystals borders on the fundamental absorption edge.

Ghosh et al. [6.15] presented a model for the impurity centers in TiO_2 . They assumed that the presence of a luminescence center was due to Cr^{3+} ions being substituted for the Ti^{4+} ions, where the former was present as unintentional doping in rutile.

Morisaki, et. al. [6.16] reported on an anomalous photoresponse observed with a reduced n -type semiconductor TiO_2 electrode in a photo-electrochemical cell. The anomaly was that the photocurrent was induced by light of photon energy lower than the band gap. They speculated that the charge transfer process in the photoelectrolysis of water occurs via surface states quite efficiently.

The presence of an intermediate energy level in n -type semi-conducting TiO_2 was also confirmed by Frank et al. [6.12], who concluded that the existence of such levels is a general characteristic of n -type TiO_2 electrodes. However, it is possible that this impurity center is due to oxygen vacancies or Ti^{3+} in reduced TiO_2 samples.

Recently there have been some investigations directed towards extending the response of the TiO_2 electrode to visible light, utilizing different forms of impurity doping techniques [6.17, 6.18].

We have adopted a similar approach and concentrated our investigations primarily on the effect of doping on the optical absorption spectrum. Our approach differs from those referred to before in that we have devoted our investigations to the doping of sputtered thin film electrodes using a simple sputter doping technique.

6.4 EXPERIMENTAL

Three different doping techniques were tried in order to investigate the possibility of extending the absorption of TiO_2 to visible light. These include: 1. Sputtering from an Oxide-Doped TiO_2 (oxidized) Target; 2. Reactive Sputtering of a Metal-Doped Ti (metal) Target and; 3. Diffusion of a Predeposited Impurity Layer.

1. Sputtering of an Oxide-Doped TiO_2 Target: Doping was achieved by mixing (by weight) the desired proportions of the dopant oxide powder and TiO_2 powder. This process is characterized by the ease with which the oxides of the two powders can be obtained and proportioned, thus providing precise and easy control of the dopant content in the sputtered film. Hot pressed pellets of doped TiO_2 were prepared by the standard Ceramic technique. The two oxides were then slightly moistened with distilled water and thoroughly mixed in a motorized tumbler for ~ 2 hours. The mixed powder was then pressed at 8000 Psi into pellets with typical dimensions, 5 cm (diameter) \times 6 mm (thick). The pressed pellets were heated either in air at 1000°C for 4 hours or in vacuum at 1100°C for ~ 8 hours.

Films were then sputter deposited in an oxygen-argon plasma atmosphere at a pressure of $\sim 5 \times 10^{-4}$ Torr and an oxygen partial pressure of $\sim 5 \times 10^{-5}$.

2. Reactive Sputtering from a Metal-Doped Ti Metal Target: In a manner similar to that described previously, doping was achieved by mixing the desired proportions (by weight) of the dopant metal powder and titanium metal powder. To avoid oxidization of the pressed pellets, these pellets were heated in vacuum at 1100°C for ~ 6 hours.

Films were deposited in an oxygen-argon plasma atmosphere. The partial pressure of oxygen was $\sim 1 \times 10^{-4}$ Torr and the total sputtering pressure was $\sim 5 \times 10^{-4}$ Torr.

In both techniques discussed above films were deposited on quartz substrates 2.5×2.5 cm, and the substrate table was heated to 400°C

3. Diffusion of a Predeposited Impurity Layer: Solid state diffusion is most frequently employed in semiconductors to form diffused layers of impurities. Thus, if there is a concentrated region of atoms of material "A" imbedded in a crystal of material "B", atoms will eventually distribute themselves uniformly over the crystal if the entire assembly is held at a constant temperature for a long enough period of time.

We have adopted this principle of diffusion to fabricate doped thin TiO_2 films. These films were prepared as in Fig. 6.6 according to the following scheme:

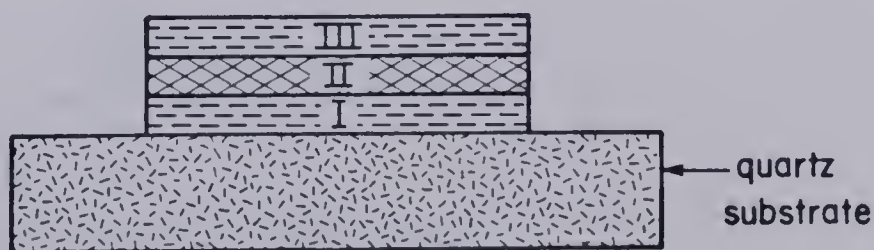


Fig. 6.6 Configuration of a TiO_2 Thin Film, Doped by Diffusion.

i) A titanium dioxide layer (layer I) was first deposited on a quartz substrate by reactive sputtering from a Ti metal target. Films were deposited at a high partial pressure of oxygen (1×10^{-4} Torr) at about 400°C for ~ 10 hours.

ii) Then, a very thin layer of the dopant oxide (layer II) was next deposited also by reactive sputtering from the dopant metal target, under the same conditions for ~ 3 minutes.

iii) Finally, a second layer of titanium dioxide (layer III) was deposited on the top of the dopant oxide layer for ~ 10 hours at 400°C .

iv) The whole assembly was then annealed at 400°C for \sim two hours.

6.5 MEASUREMENTS

Optical spectra in the UV and visible regions were determined using a PYE Unicam Spectrophotometer. Absorption (or transmission) versus wavelength, in the range from 250-700 nm, was recorded on a semilog scale. In the visible range, this record appeared as an oscillatory behavior, the amplitude of which was decreasing with wavelength. This was apparently caused by alternate reinforcement of the transmitted and reflected light beams (interference pattern) [6.19, 6.20]. The absorption coefficient for an oxide layer of thickness t and a refractive index n_1 , deposited on a quartz substrate having a refractive index n_2 , Fig. 6.7, was calculated as follows.

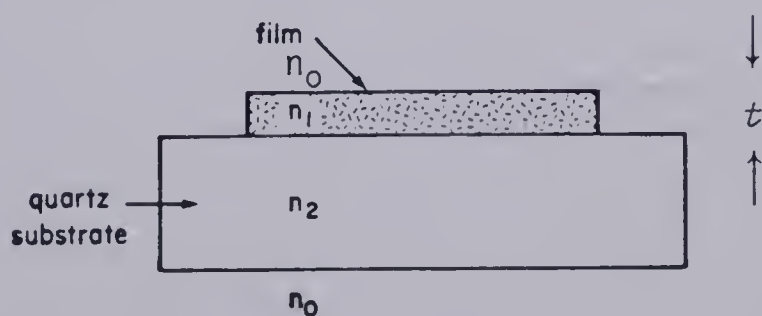


Fig. 6.7 A Thin Film/Quartz Interface.

If a beam of light is normally incident at the n_1/n_0 interface separating the media of refractive indices n_0 and n_2 , the amplitude of transmittance T (which is the ratio of the transmitted energy to the incident energy) at the n_2/n_0 interface is given by

$$T = T_1 \times T_2 \times T_3 ,$$

where

$$T_1 = (1-R_1)e^{-\alpha t}$$

$$T_2 = T_1(1-R_2)$$

$$T_3 = T_2(1-R_3) ,$$

in which R_1 , R_2 and R_3 are the reflectances (reflected energy/incident energy) at the n_0/n_1 , n_1/n_2 and n_2/n_0 interfaces respectively. R_1 , R_2 and R_3 are given by

$$R_1 = \left(\frac{n_1 - n_0}{n_1 + n_0} \right)^2$$

$$R_2 = \frac{(n_1 - n_2)^2}{(n_2 + n_1)^2}$$

and

$$R_3 = \left(\frac{n_2 - n_0}{n_2 + n_0} \right)^2 .$$

For $n_0 = 1$, $n_1 = 2.6$ [6.21] and $n_2 = 1.5$, the transmittance T is given by

$$T = 0.715e^{-\alpha t} . \quad (6.11)$$

6.5.1 Film Thickness Measurement.

Film thickness may be determined utilizing an interference pattern as follows.

If an m th order maximum occurs at a wavelength λ_1 , and the $(m+n)$ th order occurs at λ_2 , for normal incidence one can write

$$2n_1 t = m\lambda_1 = (m+n)\lambda_2$$

where it is assumed that the refractive index is the same at λ_1 and λ_2 . Therefore, the film thickness t can be written as

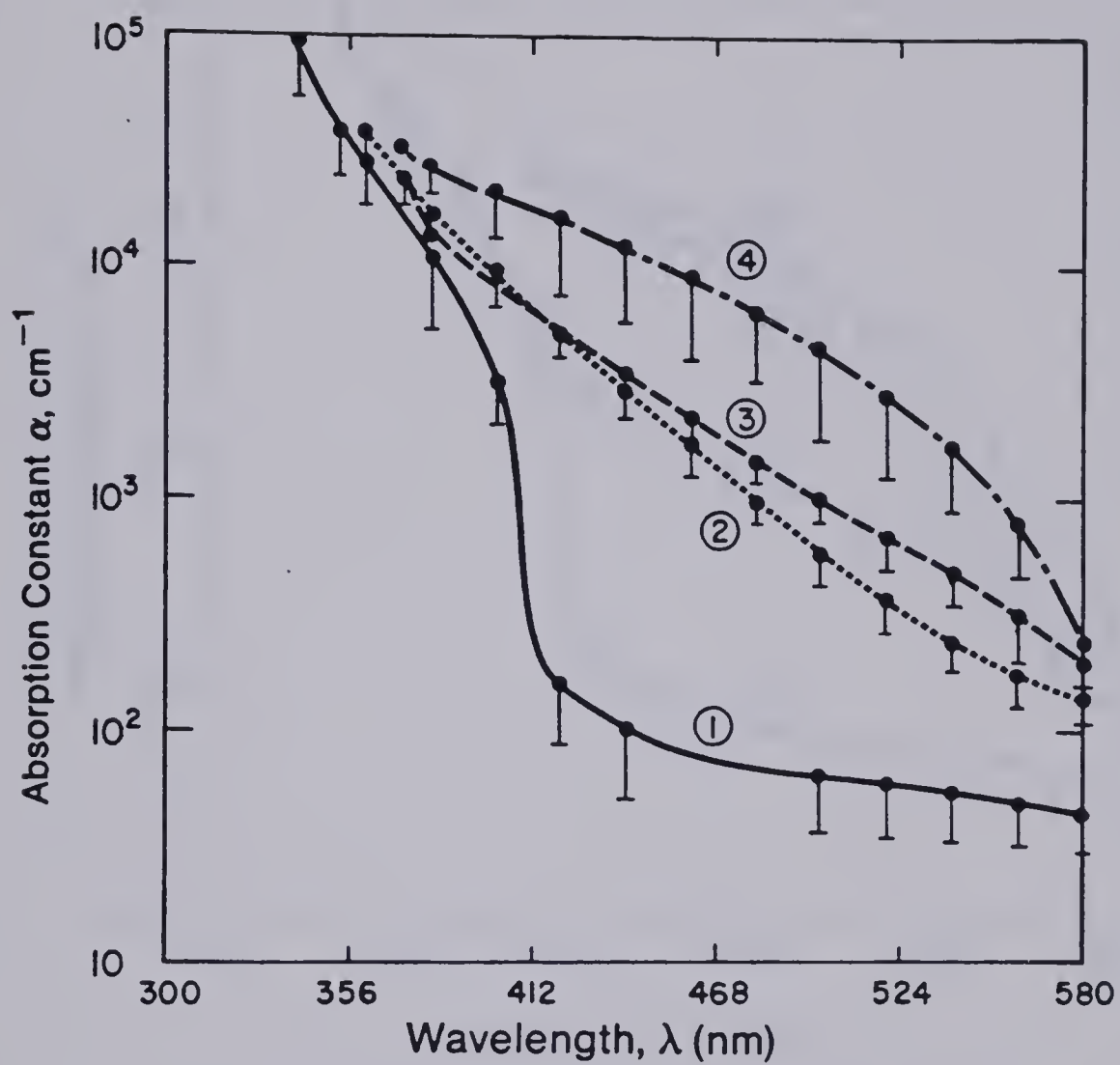
$$t = \frac{m}{2n_1} \frac{\lambda_1 \lambda_2}{\lambda_2 - \lambda_1} . \quad (6.12)$$

Thus, the film thickness can be determined if n_1 is known or vice versa, provided the index does not vary rapidly with wavelength.

A computer program was written to calculate t from Eqn. 6.12, and α from Eqn. 6.11 and to generate curves for the absorption coefficient versus wavelength.

6.6 RESULTS AND DISCUSSION

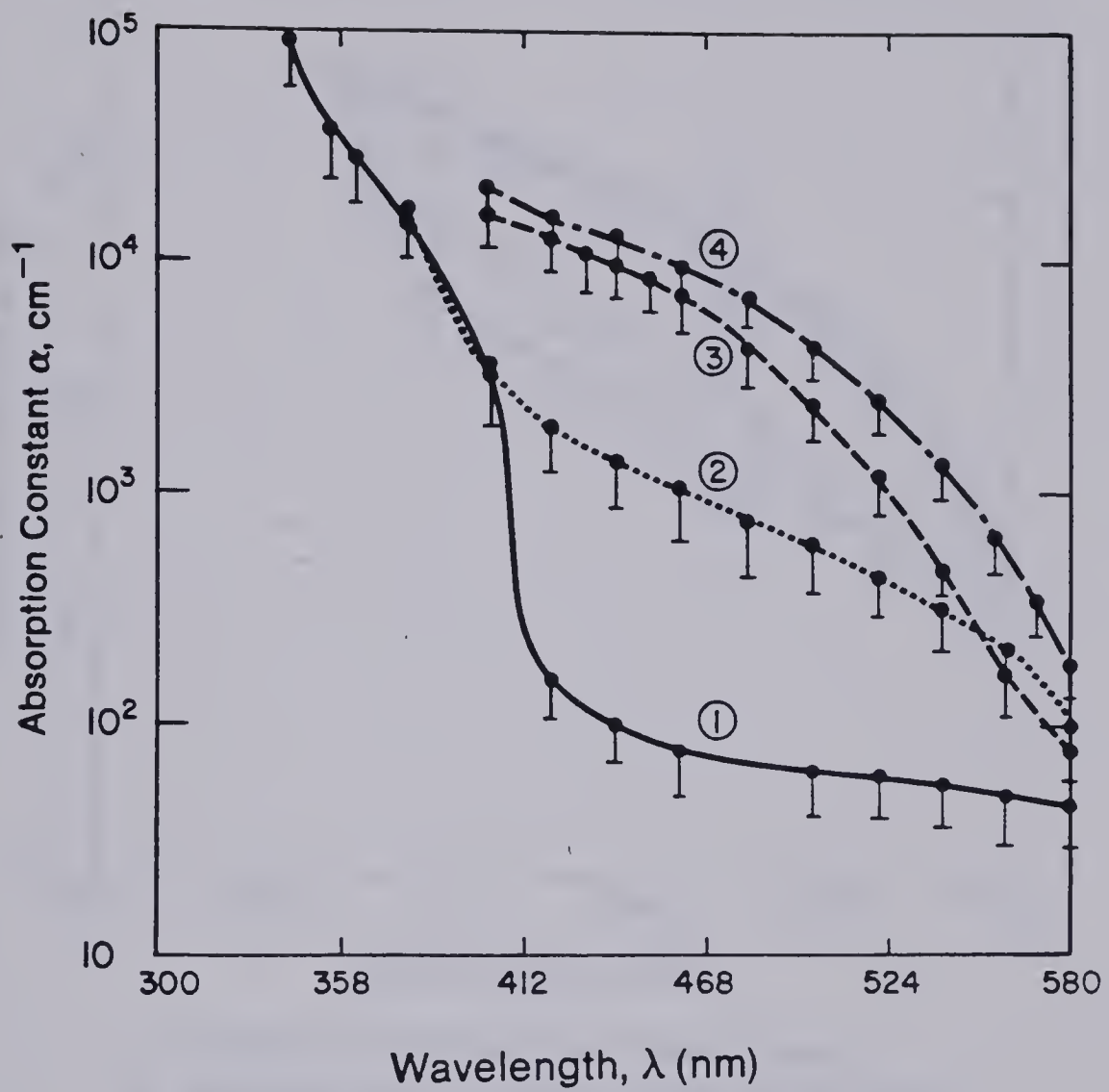
Examples of some of the results obtained for titanium dioxide films heavily doped with two different materials are given in Fig. 6.8. The choice of the dopant material and the doping technique utilized is given in the legend. As can be seen therein, the addition of cadmium or chromium dopants to TiO_2 (in the fully oxidized state) did indeed provide visible absorption.



- 1 Undoped TiO_2
- 2 Diffusion of a predeposited Chromium layer
- 3 Sputtered from a Chromium doped Ti metal target
- 4 Sputtered from a chromium oxide doped TiO_2 target

(a)

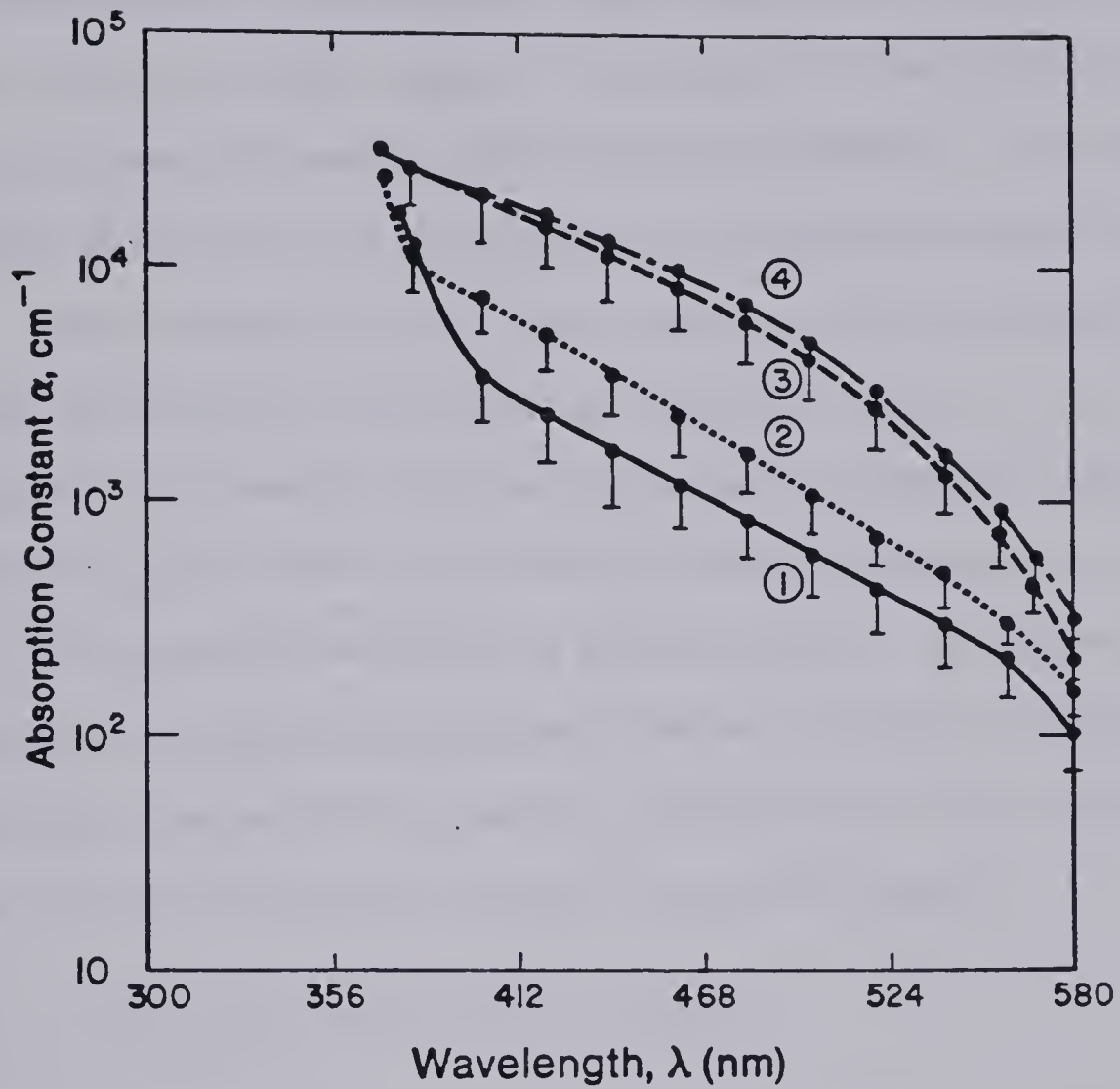
Fig. 6.8



- 1 Undoped TiO_2
- 2 Diffusion of a predeposited Cadmium layer
- 3 Sputtered from a Cadmium doped Ti metal target
- 4 Sputtered from a Cadmium oxide doped TiO_2 target

(b)

Fig. 6.8



- 1 Diffusion of a predeposited Cadmium layer
- 2 Sputtered from a Chromium doped Ti metal target
- 3 Sputtered from a Cadmium doped TiO_2 target
- 4 Sputtered from a chromium doped TiO_2 target

(c)

Fig. 6.8 Dependence of the Absorption Coefficient on Wavelengths for Different Doped TiO_2 Thin Films.

For undoped samples a main absorption edge at ~ 400 nm was obtained. For doped samples the absorption spectra extended from the main absorption edge across the visible range. The increase in the absorption coefficient was significant for wavelengths shorter than 580 nm. At wavelengths longer than 580 the increase in the absorption coefficient became less apparent.

When titanium dioxide films (doped as well as undoped) were reduced in hydrogen, they turned a blue black color, so that it was not possible to measure the absorption due to impurities after reduction. Undoped TiO_2 thin films in the fully oxidized state were transparent, while the doped ones exhibited a brownish color. To assure that the brownish color exhibited by doped films was not due to oxygen deficiency, sputtering from metallic as well as oxide targets was carried out in an argon plasma containing a partial pressure of oxygen.

6.6.1 Limitations and Sources of Errors.

1. The accuracy which may be obtained from the interference method utilized here for thickness measurement is a function of the number of peaks that are available in the useful scanning range. This limits the minimum thickness that can be measured using such a technique. This, however, did not represent any major problem since most of the samples investigated were at least 200 nm thick.

2. The refractive index n_1 of titanium dioxide varies with the wavelength of the incident light used, the purity of the oxide and the crystal structure. In the calculations made here it was assumed that the refractive index for the film is, the same for the bulk, independent of the wavelength and, the same for TiO_2 films doped with different

dopants. These assumptions might have been a source of error in calculating both film thickness t and transmittance T (and accordingly α).

3. Another source of error lies in the accuracy with which the wavelength, corresponding to a peak, was read from the transmission spectrum, since peaks were often broad or not defined in a smooth curve.

4. *The major source of error in the calculating procedure lies in the accuracy with which transmission values were read from a log scale, since any small error in the reading resulted in a very large error in the calculation.* This was more pronounced at wavelengths longer than 580 nm due to the slow variation of the transmittance T with wavelength in this range.

For these reasons it was difficult to compare the results obtained utilizing different doping techniques or different doping materials. The main conclusion derived from these investigations is that doping with transition metal dopants shifts the main absorption edge of TiO_2 towards longer wavelengths.

6.7 CONCLUSION

The effect of chromium and cadmium dopants on the absorption spectrum of polycrystalline TiO_2 thin films was investigated utilizing different simple doping approaches. Results indicate that both dopants do indeed provide visible light absorption in TiO_2 . Although investigations were carried out for fully oxidized TiO_2 thin films it is certainly possible that the absorption of doped films will be different in the oxidized and reduced states.

Shifting the main absorption edge to longer wavelengths by impurity doping should allow for the utilization of a greater portion of the solar

spectrum and as a result an increase in the overall conversion efficiency is expected. However this effect may not always be true, since there are some serious limitations to the possibility of improvement of the overall efficiency utilizing an impurity doping technique. That is, the introduction of impurity centers in the energy gap of a semiconductor could lead to the formation of recombination centers. The result would be a marked loss in the quantum efficiency. This effect would more than nullify the gain in overall optical to chemical conversion efficiency which would be expected from the extension of the photoresponse to the visible part of the solar spectrum.

In conclusion, it appears that further investigations directed to a large extent towards better understanding of impurities and defect structures in TiO_2 and SrTiO_3 , which are of interest for water photo-electrolysis cells, are essential. In addition, extensive work to ascertain if some combinations of dopants can be found which might allow for a better match to the solar spectrum is needed. Also, further studies on the effect of the different parameters involved in target as well as film fabrication techniques are required.

CHAPTER 7

CONCLUSION

The feasibility of fabricating an inexpensive and stable thin film semiconducting TiO_2 electrode has been demonstrated experimentally and theoretically. Three different sputtering approaches were utilized for the development of such electrodes; namely, plasma oxidation of a predeposited Ti metal film, dc sputtering from a reduced TiO_2 pellet and dc reactive sputtering from a Ti metal target.

Using the first approach it was found that oxidation of a predeposited Ti film resulted in a nonhomogeneous TiO_2 photoelectrode that developed a highly insulating region at the surface, rendering it unsatisfactory for electrochemical cell applications.

On the other hand semiconducting electrodes fabricated by dc sputtering from a reduced TiO_2 pellet and dc reactive sputtering from a Ti metal target were comparable. Reactive sputtering allowed for the possibility of controlling film properties during film deposition in ways that were not possible in sputtering from a TiO_2 target reduced to the desired conductivity prior to use.

A simple and attractive technique for forming an abrupt doping level change in a very thin region at the back surface of a sputter-deposited thin film electrode and hence the creation of a back surface electric field, BSF, was developed. This BSF enhances the charge carrier separation and tends to confine the holes towards the n -region from the ohmic contact. One main advantage of such a development lies in allowing for the possibility of depositing an n -type semiconductor

at a partial pressure of oxygen that makes it doped to a level that provides a reasonable space charge region width without paying the penalty of high resistive loss in the bulk. This will result in an increase in cell performance.

Investigations of the sputter kinetics of a Ti metal in an oxygen-argon plasma atmosphere indicate that the resistivity of reactively sputtered oxide films can be changed by many orders of magnitude simply by varying the partial pressure of oxygen in the sputtering atmosphere. That is, titanium metal films can be deposited by sputtering in an argon plasma, while TiO_2 films can be sputter-deposited at a high partial pressure of oxygen without precise control of the oxygen to argon ratio in the plasma. Further investigations on characterization of the film crystalline structure are needed.

Theoretical investigations of the photoexcited semiconductor electrode in a photoelectrochemical cell indicate that, while the depletion region in a uniformly doped semiconductor electrode is essential for the separation of photogenerated carriers, this layer does not play the same important role in nonuniformly doped profiles. In this latter case, a built-in drift field that favors the transport of minority carriers towards the semiconductor/electrolyte interface will result in a reduction of the depletion region width. This will lead to a decrease in the current component for carriers generated in the space charge region, but at the same time will lead to a significant increase in the current component for carriers generated outside the depletion region. The cumulative result is that the net current is enhanced, thereby leading to an increase in overall cell response. Further studies on

the effect of different doping profiles on both cell performance and the semiconductor physical parameters, along with experimental verification of the theoretical investigations, are needed.

The possibility of improving the photoresponse of a TiO_2 electrode was investigated utilizing an impurity doping approach. Preliminary results show that the concept of extending the absorption spectrum of wide band gap semiconductors by doping is feasible.

Due to the broad scope of the investigations described in this thesis, a thorough study of all aspects of the project was difficult to accomplish. There are therefore, in addition to those items mentioned before, many aspects which warrant further investigation. Some of these are:

- i) Kinetics of charge transfer at the semiconductor/electrolyte interface.
- ii) An understanding of impurity and defect structures of materials such as TiO_2 and SrTiO_3 , of interest in water photoelectrolysis.
- iii) The possibility of scaling the deposition system, in order to allow for practical device fabrication.
- iv) The effect of sputtering conditions such as target potential, substrate temperature, and substrate bias, on film properties.
- v) Effect of oxygen partial pressure on the flat band potential, the doping concentration and overall cell performance.
- vi) Influence of target fabrication conditions; namely, pressure of forming the pellet, temperature of reduction, reducing atmosphere, reducing period, doping level, dopant material, doping technique, etc.

Finally, it is worth re-emphasizing here that if water photoelectrolysis on a large scale, using a semiconductor electrode, is ultimately proven to be a practical process, then sputtering will certainly be a potentially viable technique for achieving the goal of inexpensive and efficient photoelectrode fabrication.

REFERENCES

CHAPTER 1

- 1.1 Archer, M., J. Appl. Electrochem. Vol. 5, p. 17, 1975.
- 1.2 Bolton, J., In "Solar Energy-Chemical Conversion and Storage", R. Hautala, R. King and C. Kotal (eds.), The Humana Press, N.J., p. 31, 1979.
- 1.3 Tien, H. and Verma, S., Nature, Vol. 227, p. 1232, 1970.
- 1.4 Calvin, M., Photochem. Photobiol., Vol. 24, p. 425, 1976.
- 1.5 Fujishima, A. and Honda, K., Bull. Chem. Soc. Japan, No. 44, p. 1148, 1971.
- 1.6 Nozik, J., Nature, Vol. 275, p. 383, Oct. 1975.
- 1.7 Gerischer, H., In "Physical Chemistry, an Advanced Treatise", L. Eyring, D. Henderson and W. Jost (eds.), Vol. 9A, Academic Press, N.Y., p. 463, 1970.
- 1.8 Myamlin, V. and Pleskov, Y., "Electrochemistry of Semiconductors", Plenum Press, N.Y., 1967.
- 1.9 Gerischer, H., In "Advances in Electrochemistry and Electrochemical Engineering", P. Delhay (ed.), Vol. 1, Interscience Publishers, N.Y., London, p. 139, 1961.
- 1.10 Gerischer, H., In "Solar Power and Fuel", J. Bolton (ed.), Academic Press, Inc., p. 74, 1977.
- 1.11 Lowman, F., Z.F. Naturforschung, Vol. 22a, p. 843, 1967.
- 1.12 Maruska, H. and Ghosh, K., Solar Energy, Vol. 20, p. 443, 1978.
- 1.13 Spaarnay, M., "The Electrical Double Layer", Pergamon, Oxford, 1972.
- 1.14 Pleskov, V., In "Progress on Surface and Membrane Science", J. Danielli, M. Rosenberg and C. Cadenhead (eds.), Vol. 7, Academic Press, N.Y., p. 57, 1973.
- 1.15 Dewald, F., J. Bell Systems Technology, Vol. 39, p. 615, 1960.
- 1.16 Gerischer, H., In "Special Topics in Electrochemistry", P. Rock (ed.), Elsevier Scientific Publ., N.Y., p. 35, 1977.

- 1.17 Nozik, A., Proceedings of a Conference on Electrochemistry and Physics of Semiconductor Liquid Interfaces, Vol. 77-3, p. 272, 1977.
- 1.18 Tomkiewicz, M. and Fay, H., Appl. Phys., Vol. 18, p. 1, 1979.
- 1.19 Gerischer, H., In "Topics in Applied Physics-Solar Energy Conversion", B. Seraphin (ed.), Springer-Verlag Publishers, p. 113, 1979.
- 1.20 Gerischer, H., Electroanal. Chem., Vol. 82, p. 133, 1977.
- 1.21 Wrighton, M., Ginley, D., Wolczanski, P., Ellis, A., Morse, D. and Linz, A., Proc. Nat. Acad. Sci. U.S.A., Vol. 72, p. 4, 1975.
- 1.22 Mavroides, J., Tchernev, D., Kafalas, J., and Kolesar, D., Mat. Res. Bull., Vol. 10, p. 241, 1976.
- 1.23 Mavroides, J., Kafalas, J. and Kolesar, D., Appl. Phys. Lett., Vol. 28, p. 241, 1976.
- 1.24 Watanabe, T., Fujishama, A. and Honda, K., Bull. Chem. Soc. Japan, Vol. 49, p. 355, 1976.
- 1.25 Nasby, R. and Quin, R., Mat. Res. Bull., Vol. 11, p. 985, 1976.
- 1.26 Ellis, A., Kaiser, E. and Wrighton, M., J. Phys. Chem., Vol. 80, p. 1325, 1976.
- 1.27 Clechet, P., Martin, J., Oliver, R. and Vallony, C., Acad. Sci. Ser. C282, p. 887, 1976.
- 1.28 Wrighton, M., Morse, D., Ellis, A., Ginley, D. and Abrahamson, H., J. Am. Chem. Soc., Vol. 98, p. 44, 1976.
- 1.29 Kung, H., Jarret, M., Sleight, A. and Ferreti, A., J. Appl. Phys., Vol. 48, p. 2463, 1977.
- 1.30 Butler, M., Nasby, R. and Quin, R., Sol. St. Com. p. 1011, 1976.
- 1.31 Gissler, W., Memming, R., in [Ref. 1.17, p. 241].
- 1.32 Hardee, K. and Bard, A., J. Electrochem. Soc., Vol. 124, p. 215, 1977.
- 1.33 Butler, M., Ginley, D. and Eibschutz, M., J. Appl. Phys., Vol. 48, p. 3070, 1977.
- 1.34 Quin, R., Nasby, R. and Baughman, R., Mat. Res. Bull., Vol. 11, p. 1011, 1976.

- 1.35 Kennedy, J. and Freese, K., J. Electrochem. Soc., Vol. 125, p. 709, 1978.
- 1.36 Nozik, A., J. Appl. Phys., Vol. 29, No. 3, p. 150, 1976.
- 1.37 Nozik, A., Appl. Phys. Lett., Vol. 30, No. 11, p. 567, 1977.
- 1.38 Wagner, S. and Shay, J., Appl. Phys. Lett., Vol. 31, p. 446, 1977 and in [Ref. 1.17, p. 231].

CHAPTER 2

- 2.1 Berry, R., Hall, P. and Harris, M., "Thin Film Technology", D. Van Nostrand Company, Inc., Princeton, 1968.
- 2.2 Chapman, B., Trans. of Conference and School on Sputtering Technology, p. 28, June, 1973.
- 2.3 Chopra, K., "Thin Film Phenomena", McGraw Hill Book Co., 1969.
- 2.4 Cambey, L., in [Ref. 2.2, p. 129].
- 2.5 Maissel, L., In "Handbook of Thin Film Technology", L. Maissel and R. Glang (eds.), McGraw Hill Book Co., Chapt. 4, 1970.
- 2.6 Jazebksi, Z., "Oxide Semiconductors", Pergamon Press, Inc., 1973.
- 2.7 Loeb, L., "Basic Processes in Gaseous Electronics", University of California Press, Berkeley, p. 329, 1961.
- 2.8 Nickerson, J. and Mosesno, R., Res. Devel., Vol. 3, p. 53, 1965.
- 2.9 Vossen, J. and Kern, W., "Thin Film Processes", Academic Press, N.Y., p. 31, 1978.
- 2.10 Azaroff, L., "Elements of X-ray Crystallography", McGraw Hill Book Co., 1968.
- 2.11 Lipson, H. and Steeple, H., "Interpretation of X-ray Powder Diffraction Patterns", MacMillan and Co. Ltd., London, 1970.

CHAPTER 3

- 3.1 Miles, J. and Smith, P., J. Electrochem. Soc., Vol. 110, p. 1240, 1963.
- 3.2 Kerksen, J. and Volger, J., Physica, Vol. 69, p. 535, 1973.

- 3.3 Gronemeyer, D., Phys. Rev., Vol. 87, p. 876, 1952.
- 3.4 Hippel, A., Kalnjs, J. and Westphal, W., J. Phys. Chem. Solids, Vol. 23, p. 779, 1962.
- 3.5 Hurlen, T., Acta Chem. Scand., Vol. 13, p. 365, 1959.
- 3.6 Kofstad, P., J. Less Common Metals, Vol. 13, p. 635, 1967.
- 3.7 Iguchi, E. and Tajima, K., J. Phys. Soc., Japan, Vol. 32, p. 1415, 1972.
- 3.8 Maissel, L. and Schaible, P., J. Appl. Phys., Vol. 36, No. 1, p. 237, 1965.
- 3.9 Chopra, K., "Thin Film Phenomena", McGraw Hill Book Co., 1969.
- 3.10 Wrighton, M., Ginley, D., Woloanski, P., Ellis, A., Morse, D. and Linz, A., Proc. Nat. Acad. Sci. U.S.A., Vol. 72, No. 4, p. 1518, 1975.
- 3.11 Hovel, H., "Semiconductors and Semimetals", A. Beer (ed.), Vol. 11, Academic Press, 1975.
- 3.12 Soliman, A. and Seguin, H., Solar Energy Mat., (to be published).
- 3.13 Mavroides, J., Techernev, D., Kafalas, J. and Kolesar, D., Mat. Res. Bull., Vol. 10, p. 1023, 1975.
- 3.14 Butler, M., Nasby, R. and Quin, R., Sol. St. Com., Vol. 49, p. 1011, 1976.
- 3.15 Gerischer, H., In "Advances in Electrochemistry and Electrochemical Engineering", P. Delhay (ed.), Vol. 1, Interscience Publ., N.Y., p. 139, 1961.
- 3.16 Tomkiwicz, M., and Fay, H., Appl. Phys., Vol. 18, p. 1, 1979.
- 3.17 Maruska, H. and Ghosh, A., Solar Energy, Vol. 20, p. 443, 1978.

CHAPTER 4

- 4.1 Geraghty, K. and Donaghey, L., J. Electrochem. Soc., Vol. 123, No. 8, p. 1201, 1976.
- 4.2 Berry, R., Hall, P. and Harris, M., "Thin Film Technology", D. Van Nostrand Company, Inc., Princeton, N.J., 1968.
- 4.3 Holland, E. and Campbell, D., J. Mat. Sc., Vol. 3, p. 544, 1968.

- 4.4 Donaghey, L. and Geraghty, K., "Thin Solid Films", Vol. 38, p. 271, 1976.
- 4.5 Heller, J., "Thin Solid Films", Vol. 17, p. 63, 1973.
- 4.6 Abe, Y. and Yamashina, T., "Thin Solid Films", Vol. 30, p. 19, 1975.
- 4.7 Goldlewski, M., Baraona, C. and Brandhorst, H., I.E.E.E. Photo. Spec. Conf., 10th, Palo Alto, p. 212, 1976.
- 4.8 Noufi, R. and Tench, D., J. Electrochem. Soc., Vol. 127, No. 1, p. 188, 1980.
- 4.9 Soliman, A. and Seguin, H., Can. J. of Physics (to be published).
- 4.10 Monnier, M. and Augustynski, J., J. Electrochem. Soc., Vol. 127, No. 7, p. 1576, 1980.
- 4.11 Subbarao, S., Tun, T., Kershaw, R., Dwight, K. and Wold, A., Mat. Res. Bull. Vol. 13, p. 1461, 1978.
- 4.12 Gerischer, H., In "Special Topics in Electrochemistry", P. Rock (ed.), Elsevier Sci. Publ. Comp., N.Y., p. 35, 1977.

CHAPTER 5

- 5.1 Jordan, A. and Milnes, A., I.R.E. Trans., Vol. ED. 7, p. 242, Oct. 1960.
- 5.2 Wolf, M., Proc. I.R.E., Vol. 15, p. 674, May, 1963.
- 5.3 Ellis, B. and Moss, T., Sol. St. Elect. Vol. 13, p. 1, 1970.
- 5.4 Tyagai, V., J. Phys. Chem., Vol. 38, No. 10, p. 1335, 1964.
- 5.5 Myamlin, V. and Pleskov, Y., "Electrochemistry of Semiconductors", Plenum Press, N.Y., 1967.
- 5.6 Wilson, R., J. Appl. Phys., Vol. 48, No. 10, p. 4292, Oct. 1977.
- 5.7 Grove, A., "Physics and Technology of Semiconductor Devices", John Wiley and Sons, Inc., N.Y., 1967.
- 5.8 Kennedy, D., Murley, P. and Kleinfelder, W., I.B.M. J., Res. Develop., p. 399, Sept. 1968.
- 5.9 "Handbook of Chemistry and Physics", R. Weast (ed.), Chemical Rubber, 1971.

- 5.10 Ghosh, A. and Maruska, H., J. Electrochem. Soc., Vol. 124, p. 1516, 1977.
- 5.11 Eagles, D., J. Phys. Chem. Solids, Vol. 25, p. 1243, 1964.
- 5.12 Munoz, C., Electronic Lett., Vol. 11, No. 16, p. 365, 1975.
- 5.13 Moon, P., J. Frank. Inst., Vol. 230, No. 1375, p. 583, 1940.

CHAPTER 6

- 6.1 Wolf, M., Proc. I.R.E., Vol. No. 7, p. 1246, 1960.
- 6.2 Shockley, W. and Queisser, H., J. Appl. Phys., Vol. 32, No. 3, p. 510, 1961.
- 6.3 Nozik, J., Nature, Vol. 275, p. 383, Oct. 1975.
- 6.4 Butler, M., Nasby, R. and Quin, R., Sol. St. Com., Vol. 49, p. 1011, 1976.
- 6.5 Ginley, D. and Butler, M., J. Appl. Phys., Vol. 48, No. 5, p. 2019, 1977.
- 6.6 Pankove, J., In "Optical Processes in Semiconductors", N. Holonyak (ed.), Prentice-Hall, 1971.
- 6.7 Rose, A., Proc. I.R.E., Vol. 43, p. 1850, Dec. 1955.
- 6.8 Rose, A., "Progress in Semiconductors", Vol. 2, John Wiley and Sons, Inc., N.Y., p. 109, 1957.
- 6.9 Gleria, M. and Memming, R., J. Electroanal. Chem., Vol. 65, p. 163, 1975.
- 6.10 Morisaki, H. and Yazawak, K., Appl. Phys. Lett., Vol. 30, No. 1, p. 7, 1977.
- 6.11 Gerischer, H., J. Electrochem. Soc. Vol. 97, p. 2180, 1978.
- 6.12 Frank, S. and Bard, A., J. Am. Chem. Soc., Vol. 97, p. 7472, 1975.
- 6.13 Ghosh, A., Wakim, F. and Addiss, R., Phys. Rev., Vol. 184, No. 8, p. 979, 1969.
- 6.14 Mirlin, D., Reshina, I. and Sochava, L., Sov. Phys. Sol. St., Vol. 11, No. 9, p. 1995, 1970.
- 6.15 Ghosh, A., Laver, R. and Addiss, R., Phys. Rev. B., Vol. 8, No. 11, p. 4842, Nov. 1973.

- 6.16 Morisaki, H., Hariya, M. and Yazawa, K., Appl. Phys. Lett., Vol. 33, No. 12, p. 1013, 1978.
- 6.17 Ghosh, A. and Maruska, P., J. Elect. Chem. Soc., Vol. 124, No. 10, p. 1517, 1977.
- 6.18 Salvador, P., Sol. En. Mat., Vol. 2, p. 413, 1980.
- 6.19 Jenkins, F. and White, H., "Fundamentals of Optics", Fourth Ed., McGraw Hill, N.Y., p. 286, 1976.
- 6.20 Carl, E. and Wimpheimer, H., Sol. St. Elect. Vol. 7, p. 755, 1964.
- 6.21 Heavens, O., "Optical Properties of Thin Solid Film", Dover Publ. Inc., N.Y., 1969.

B30329